The Dissertation Committee for Leonardo Andres Ramirez

certifies that this is the approved version of the following dissertation:

Models for Estimating VOC Emissions from Latex Paints

Committee:

Howard M. Liljestrand, Supervisor

Richard L. Corsi

Benny D. Freeman

Atila Novoselac

Danny D. Reible

Models for Estimating VOC Emissions from Latex Paints

by

Leonardo Andres Ramirez, M.S.E., M.S., B.E.

Dissertation

Presented to the Faculty of the Graduate School of

The University of Texas at Austin

in Partial Fulfillment

of the Requirements

for the Degree of

Doctor of Philosophy

The University of Texas at Austin

December 2009

This thesis is dedicated to my family,

Pa, Ma, Abue, Laura, Carol and Lisita

You are the most important people in my life

I could not have come this far

without all the support and love that you have given me.

I love y'all

Acknowledgments

This research was possible thanks to the continuous support of my advisor and mentor Dr. Howard M. Liljestrand. His invaluable help, funding and support through my graduate studies, as well as his patience with the many questions I always came to ask. I would also like to thank Dr. Richard L. Corsi for all his input and guidance in my research, and for his comments and revisions of this manuscript. I would also like to express my appreciation to my committee members, Dr. Danny D. Reible for the modeling discussions we had, Dr. Atila Novoselac for his early help with Airpak modeling, and to Dr. Benny Freeman for discussions about polymer diffusion coefficients.

I want to thank Dr. Neil Crain for our very instructive discussions related to small-scale chamber results, and GC experiments. I would also like to acknowledge the support gained trough my affiliation with the IGERT program at the University of Texas at Austin "Indoor Environmental Science and Engineering -An Emerging Frontier" (NSF grant # DGE-0549428). Funding from the IGERT were used for presenting research findings at international conferences.

I would like to thank Dori Eubank, for her encouragement words and always positive attitude. I would also want to express my gratitude to my long time friend Ivan Castillo. His emotional support and help were instrumental in the pursuit of my doctoral degree. Finally, I would like to thank my soul mate and beloved Lisa. This would not have been finished without you.

There were many individuals who contributed to my life in many different ways during the writing of this dissertation. And for that, many thanks also go to you.

Leonardo Andres Ramirez

The University of Texas at Austin

December 2009

Models for Estimating VOC Emissions from Latex Paints

Publication No. _____

Leonardo Andres Ramirez, Ph.D.

The University of Texas at Austin, 2009

Supervisor: Howard M. Liljestrand

Many models for predicting volatile organic compounds (VOC) emissions from latex paints have been developed. Earlier models were developed for solvent-borne paints, particularly since these paints evaporate rapidly and can be modeled with simple decay models. However, paint has changed in the past fifty years, and a transition has been made towards water-borne paints. These paints were introduced for indoor applications because they lacked the health hazards and odors of their solvent-borne counterparts. These paints also have organic modifiers, therefore it is very important to predict how these modifiers evaporate from the coated material. New mechanistic models that can predict slow emitting VOCs over long periods of time are not available. An improved ability to predict VOC emissions from latex paints could lead to improved understanding, better policy-making and promotion of environmen-

tal regulations that benefit both the consumer and producers of architectural coatings.

This research improves on existing models used to estimate VOC emissions off-gassed from latex paints. The developed two layer model (2LM) has a layer for paint and substrate material, and accounts for mass transfer at the paint layer, and diffusion transport between paint and material layers. The model provides a semi-mechanistic way to predict paint drying and VOC emissions from coatings on a variety of substrates. The model only requires the estimation of one parameter (the paint layer diffusion coefficient), unlike other models available that require multiple parameter estimations. This model is robust in the sense that it could be used to predict VOC emissions from paint, as well as predicting the variation of the internal VOC distribution on both paint and material layers with time. The model was tested and validated with empirical data collected from previous controlled chamber experiments, and also with data collected from short evaporation experiments. Critical paint components like polymer and pigment composition and its relation to VOC fate and transport after paint application, both initially and over long periods of time, were explored.

Modeling results indicated that the diffusion coefficient of 2,2,4-trimethyl-1,3-pentadediol monoisobutyrate (TMPD-MIB) in the paint layer does not depend on the thickness of the wet paint film, but it depends on the pigment volume concentration (PVC) of the paint. Additionally, a constant diffusion coefficient used in the 2LM was successful for modeling emissions of TMPD-MIB from low pigment volume concentration (LPVC) paints, but it failed to capture the physical mechanisms of the drying film for high pigment volume concentration (HPVC) paints. A major finding from this research was that a detailed gas phase analysis of mass transport for TMPD-MIB would have negligible effects on the predicted overall evaporation rate. Therefore, the entire wet and dry emissions processes are likely dominated by diffusion processes.

Contents

List of Tables

List of Figures

Chapter 1

Introduction

The overall goal of this research was to better understand the relationship between paint components and transport mechanisms of volatile organic compounds (VOCs) released after paint application. This goal was achieved through the development of a model that works for porous and non-porous substrate materials, that is physically based and that can be used for prediction of emissions over the short term as well as for longer periods of time after paint application. The remaining sections of this chapter include: the motivation (Section 1.1), the research objectives (Section 1.2), the hypotheses (Section 1.3), a summary flow chart of the research activities (Section 1.4), and the organization of the dissertation (Section 1.5).

1.1 Motivation

Most manufactured materials are coated to either provide surface protection or to embellish a finished product. Indoor environments are surrounded by finished, coated materials; walls and ceilings are just examples of large coated surface areas.

The indispensable component of a coating material that does not evaporate is the binder or film-forming agent (Goldschmidt and Streitberger 2003). This component solidifies as a result of physical-chemical processes. On the contrary, solvents, co-solvents and rheology modifiers account for the volatile part of the paint that evaporates over time and can affect human health or comfort, e.g. cause eye or skin irritation (Decopaint 2000).

More than 670 million gallons of architectural coatings are used in the U.S per year (Census-Bureau 2008). While the 9 billion dollar architectural coatings industry is highly dependent on the global economy, this industry has seen an increase of 124 million of gallons or (20%) in the past ten years. Water-based latex coatings were introduced for indoor application because they are easy to use and have reduced health hazards and odors compared to their solvent-borne counterparts. Government agencies worldwide are limiting the amount of VOCs permitted in coatings, because of concerns about environmental and health effects primarily due to ground level ozone formation. Therefore, waterborne coatings are currently being developed to comply with stricter environmental regulations as well as to reduce the use of costly petroleum-based solvents.

For interior coatings, the clarity and protection offered by water-based paints approaches that of solvent-based paints, and water-based paints are currently the dominant choice for interior paint selection. However, rheology modifiers, coalescing aid agents, and other additives are required in the paint formulation, to achieve the equivalent properties of solvent-based paints (Hester and Squire 1997). Due to the relatively low evaporation rate of these additives, dramatic peak exposure concen-

trations are less likely to occur. However, long term exposure to these chemicals is more likely to increase as the continuous growth in the use of water-based coatings increases the demand for paint additives and particularly of coalescing aid agents. Although coalescing aid agents are typically of low volatility, they do evaporate out of the drying paint film, can persist in substrate materials, and be measured even many months after paint application (Lin and Corsi 2007).

Previous attempts to model VOC emissions have been highly empirical, (e.g., models using one or two pseudo first order decay constants) and fail to capture the fundamental physical-chemical behavior of such emissions. Some of the more mechanistic emission models are specifically for dry building materials, but there is not a published model that can predict the emissions over a continuous time frame after a paint event especially after the paint layer has dried and adsorbed VOCs from the substrate layer are released. The model developed for this dissertation provides a semi-mechanistic way to predict paint drying and VOC emission from coatings on a variety of substrates provided sufficient experimental data for parameter estimation. The model was tested and validated using previous small chamber experiments completed at the University of Texas (Lin and Corsi 2007). Additional validation of the model was obtained from controlled Thermogravimetric Analyzer (TGA) experiments, where the focus of the experiments was to estimate VOC parameters (evaporation rate, mass transfer coefficient) and VOC distribution inside the material after paint application. Comparative results of changes in paint composition as well as thickness were explored in order to determine critical paint and material characteristics that affect VOC emissions initially and over long periods of time.

1.2 Research objectives

The main objective of this research was to develop a model to predict VOC emissions after latex paint application. In order to accomplish this task, a coalescing aid agent was selected as the VOC to predict due to the availability of experimental data to validate the model. In particular, emissions of 2,2,4 trimethyl, 1-3 pentanediol monoisobutyrate or (TMPD-MIB), more often known by its trade name Texanol®, were used to validate the proposed two layer diffusion model for architectural coatings.

Other objectives of this dissertation were:

(A) To determine under what circumstances VOC diffusion through the paint layer is a significant mechanism of mass transfer for the overall emission estimation.

(B) To determine the significance of water content of latex paints with respect to VOC emissions, and if there is a diffusivity dependence (for porous materials) on moisture content.

(C) To determine under what conditions VOC sorption to internal pore surface is a significant mass transfer process for porous materials such as gypsum board.

1.3 Research hypotheses

The research hypotheses for this study are:

(H1) Polymer volume content of a paint is a significant parameter that affects VOC

emissions from latex paints.

(H2) VOC Diffusion in the paint layer is a significant process that continues to affect VOC emissions after thousands of hours of the paint event.

(H3) Initial water content of the paint retards emissions of VOCs in latex paints.

The proposed two layer diffusion model was used in conjunction with latex paint experiments in order to test these hypotheses. Paints with different pigment volume content were analyzed, and the resulting variations in their emissions were established. After the model was validated with experimental data, a parametric analysis followed in order to assess the importance of diffusivity of the paint layer and material layers. Finally, the internal material VOC concentration profile model prediction was compared with experimental data from sectioned gypsum board core samples analyzed with a TGA.

1.4 Summary of research components

A summary of the different activities accomplished in order to fulfill the objectives of this dissertation is summarized in a flow chart provided in Figure 1.1. Initially, a literature review was conducted to evaluate existing models and review experimental data and parameter ranges. To further understand the short term and long term VOC emissions, experiments were conducted. Additional experiments were conducted to understand the accumulation of VOCs within the material. The experimental data collected was then used to determine parameters and validate the model results.

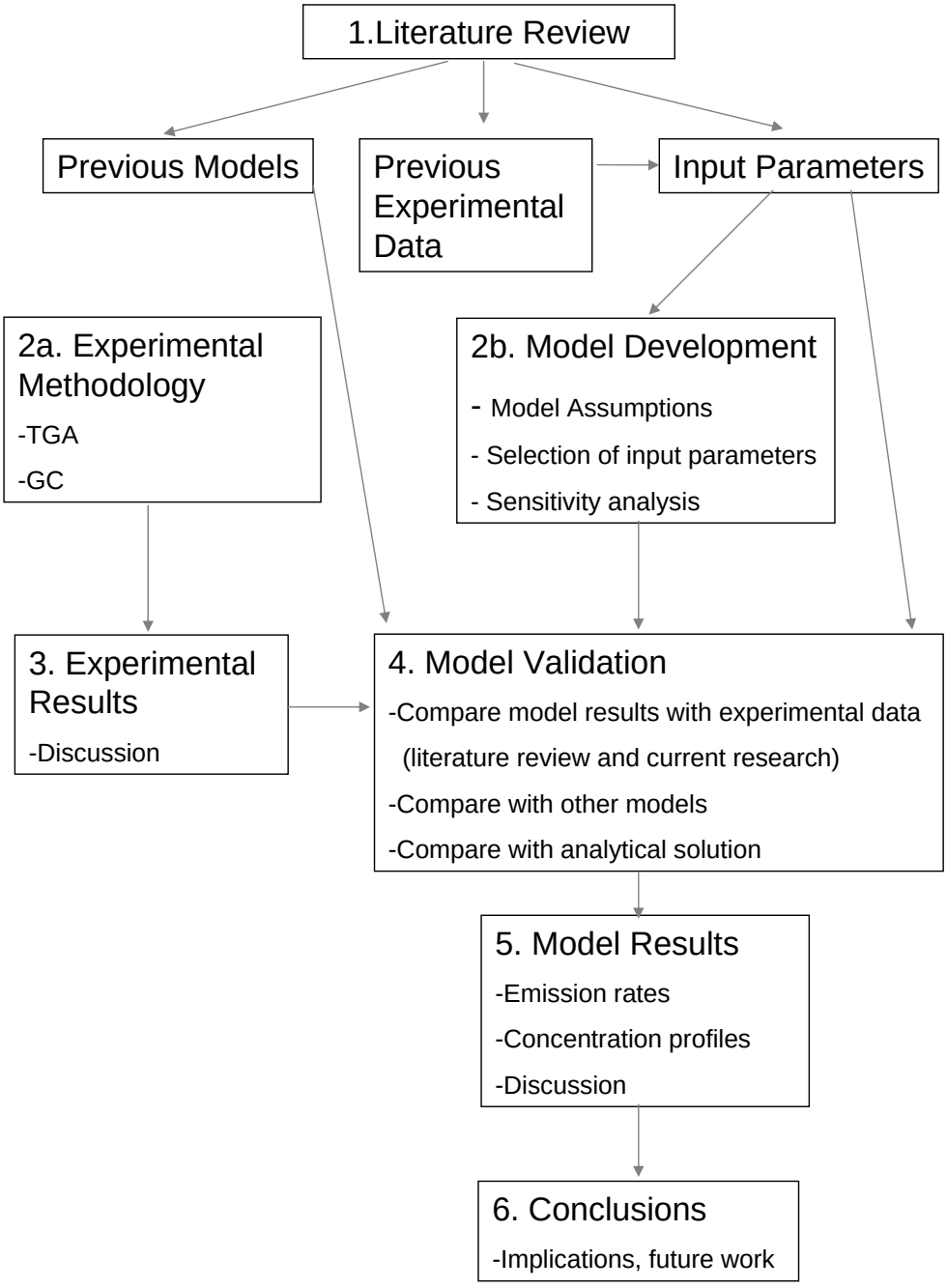

Figure 1.1: Flow chart of major research components.

The semi-mechanistic model was developed to capture the behavior of VOC emissions based on a known paint diffusion coefficient. The model was evaluated by comparing its predictions with experimental data collected by Lin and Corsi (2007). The model predictions were compared to existing models, and the model was shown to accurately predict both short and long term emissions. Finally, the model was used to assess critical parameters for emissions and obtain a better understanding of TMPD-MIB fate after latex paint application.

1.5 Organization of the dissertation

Background and literature review of previous models to predict emissions from paint are covered in Chapter 2. The proposed model to predict VOC emissions after latex paint applications and model sensitivity analysis are presented in Chapter 3, followed by experimental methods and quality assurance and control activities in Chapter 4. Experimental data for parameter estimation, emission rates and differences of paint drying are presented in Chapter 5. Model validation with experimental data and comparison with different models is covered in Chapter 6. Results and predictive capabilities of the model are presented in Chapter 7. Conclusions, research implications and future work are discussed in Chapter 8.

Chapter 2

Literature Review

2.1 Introduction

Coating materials are used mainly with the purpose of providing surface protection. Coating materials are typically formed in the following manner: wetting of substrate, transforming into a closed film, flowing and then solidifying so that a desired mechanical and chemical protection of the object is achieved. Depending on the type of solvent used, two main classes of paints can be distinguished: solventborne paints when the solvent is organic/mineral spirits, and waterborne, when the solvent is water. The focus of the present research was placed on the later ones, particularly on latex paints.

In Section 2.2, basic definitions used in coating technology are covered. Paint drying modeling and some of the processes occurring after paint application are described in Section 2.3, porous transport processes and definitions are explained in Section 2.4. Finally, previous attempts to model the complex physical-chemical processes of VOC emission after paint application on porous and non-porous materials

are presented in Section 2.5.

2.2 Coating materials and definitions

Paints are coating materials featuring particular or desired properties (Goldschmidt and Streitberger 2003). Some of these properties are opacity, decoration, and protection. Typical components of latex paints are: water, defoamer, thickener, co-solvent, pigment dispersant, wetting agents, preservatives, pigment, extender/filler, coalescing agent, binder, rheology modifiers. However, as shown in Figure 2.1, these components can be grouped in four main categories: pigment, additives, binder and solvent.

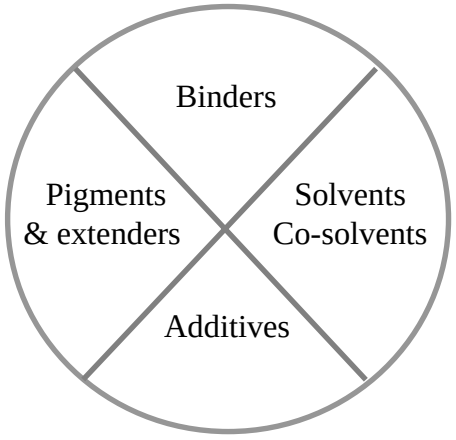

Figure 2.1: Typical composition of coatings.

2.2.1 Pigment and extenders

An important paint component is the pigment, which is usually titanium dioxide, and is the responsible for providing hiding properties. Titanium dioxide is the most widely used white pigment because of its brightness and very high refractive index.

Homogeneous pigment distribution is desired in order to obtain adequate opacity. Some paints also contain fillers and extenders which are use either to modify the rheological properties or to reduce the productions costs of the paint.

2.2.2 Additives

Additives are used in to change physical and chemical characteristics. For example, the flow and leveling in waterborne coatings tends to be less satisfactory than for solventborne compositions, and the use of additives such as rheology modifiers are needed in order to produce a required stability and pigment dispersion, thus obtaining an acceptable coating (Kirsch et al. 2001). Anti-foaming agents are additives used to counteract the foaming effect produced by emulsifiers in paints. Moreover, waterborne paints are susceptible to tainting thus may require a biocide. Depending on the technical demands of the paint, other additives may be added, such as wetting agents, pigment dispersants, thickeners, anti-cratering agents, thixotropic agents, dryers, curing agents, anti-skinning agents, stabilizers and corrosion inhibitors (Decopaint 2000).

2.2.3 Binders

An indispensable component of a coating material is the binder, which solidifies as a result of physical-chemical processes. The binder is formed from a water dispersion of polymer particles in the range of 0.1-0.8 μm. Water-based paints are usually manufactured using a process known as emulsion polymerization, where the water-insoluble monomers form an emulsion with the aqueous phase by addition of a surfactant. The final polymer dispersion is often described as latex. This polymerization technique allows for the formation of copolymers in which the addition of relatively small

quantities of co-monomer may have a significant effect on the final properties of the polymer and ultimately on the performance of water-based coating.

Polymers are large molecules that consist of many individual monomer units that have been covalently bonded to each other to form a single molecule. The polymer is composed of structural or repeat units that are duplicated along the polymer chain. Step-growth and chain-growth polymerizations are by far the two most important general processes used to make polymers and resins for paintings and coatings (Walker 2001).

When the main chain of the polymer is composed of carbon-carbon bonded atoms, the polymer is referred to as a chain-growth polymer. In contrast, when carbon-oxygen bonds are part of the linkage, the polymer is referred to as a step growth polymer if an appropriate catalyst is present to facilitate a reaction. Styrene-acrylic polymer is an example of a chain-growth polymer with a random polymer structure, and it is one of the most commonly used copolymers employed as a coating binder (Walker 2001). Figure 2.2 shows the structure of a polymer made of a mixture of monomers A and B, that have polymerized in a random fashion.

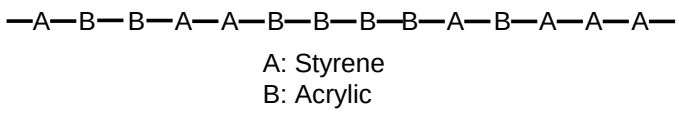

Figure 2.2: Random copolymer structure.

2.2.3.1 Pigment volume concentration

Paints are sometimes classified by their pigment volume concentration or PVC, which is the ratio between the pigment (and extender) volume, to the combined pigment and binder volume. The PVC typically ranges from 10-15 for high gloss paints to 65-85 for flat paints. This number is related to the polymer content of the paint. The higher the PVC, the lower is the amount of polymeric binder within the paint and the greater the portion of pigment and filler particles. PVC has been recognized as a key-parameter adjusting the desired application properties of the paint that strongly determines application properties such as gloss, scrub resistance, tensile strength, and hiding power as it can be seen in Figure 2.3. For example in high-gloss paints, a low PVC (LPVC) is required to accommodate the proper surface roughness to achieve a high gloss, therefore requiring a high concentration of titanium dioxide to obtain good hiding power at the same time.

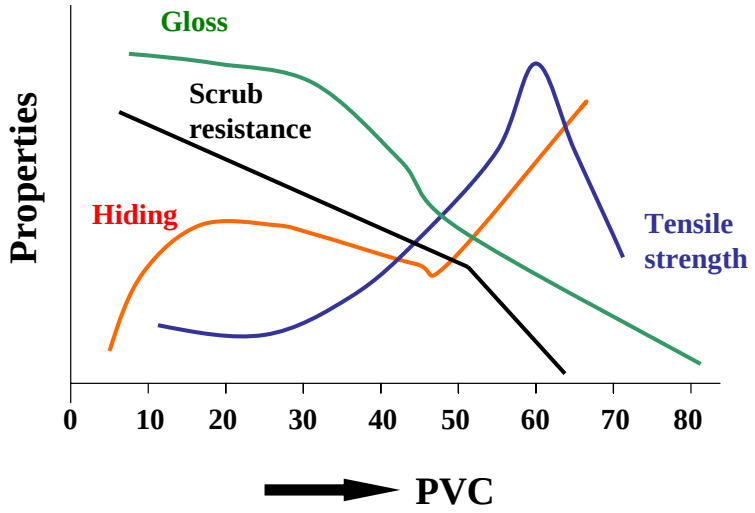

Figure 2.3: Pain characteristics and PVC (Adapted from Tiarks et al. 2003).

On the other hand, flat paints typically contain high PVC (LPVC), and fillers due to cost reasons. These paints typically use a $CaCO_3$ filler, therefore increasing

the pigment binding capacity of the paint (Tiarks et al. 2003). The PVC of a paint can be estimated using Equation 2.1.

$$PVC = \frac{V_p}{V_p + V_b} \times 100 \tag{2.1}$$

Where
Vp is the pigment volume,
Vb is the non-volatile binder (polymer) volume.

2.2.4 Solvent and co-solvents

Solvents are the liquid part of paint that suspends the pigment and resins and transports them from the paint brush to the wall. Since the solvent in latex paints is water, these paints are said to contain zero or very small amounts of VOCs. Co-solvents are often added to latex and water-soluble systems for different purposes but must be accounted when calculating the VOC amount of waterborne paints.

2.2.4.1 Solvent

The solvent discussion in this section will be limited to water-borne paints. Water is a very important component of latex paint, but its role for film formation is still not thoroughly understood. Water has been attributed as the fundamental factor in promoting polymer particle deformation, and also as being a convenient vehicle to maintain polymers dispersed at ambient temperatures prior to film formation. An uniformly accepted mechanism the film formation process has yet to be found. Experimental results that support various theories (dry and wet sintering, capillary theory, inter-particle cohesion, to name a few) can be found in the literature (Steward et al. 2000).

2.2.4.2 Cosolvent

Cosolvents are used to adjust paint properties like flow, leveling, freeze-thaw stability, and coalescence (Marrion 2004). Coalescence includes the process of compaction, deformation, cohesion and polymer chain inter-diffusion of the individual latex particles (Steward et al. 2000). The discussion in this section will be focused on co-solvents that help improve the coalescing properties of the paint.

An important parameter related to coalescence is the glass transition temperature (T_g) of a polymeric material. At the glass transition temperature, a shift occurs from a brittle, glassy solid to a rubber for any material. When the T_g of the paint polymer is too high, insufficient inter-diffusion of polymer chains can occur. The lack of polymer chain mobility results in a weak film. In architectural paints, T_g largely determines the minimum film formation temperature. The coalescing aid agent added to the paint results in a reduction of the glass transition temperature, therefore allowing an appropriate film formation at ambient conditions.

Co-solvents like TMPD-MIB ($C_{12}H_{24}O_3$), more commonly known by its trade name Texanol®, are typically used in latex paints. TMPD-MIB is a widely used coalescing agent that acts as a temporary plasticizer for the polymer particles, allowing particles to fuse together into one coherent film free from distinct physical boundaries, and improving the film formation properties of the binder (Swan 2005). TMPD-MIB is a mixture of two isomers, and the structure of each isomer is shown in Figure 2.4.

The improvements in the binder results in a high pigment-binding capacity that has relatively strong adhesion at the surface of pigments, is less deformable, and

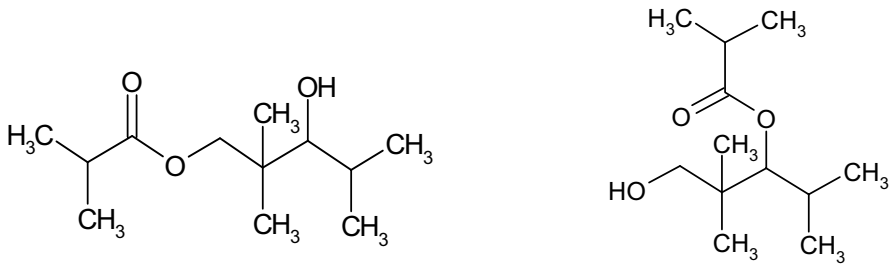

Primary isomer- 65%

Secondary isomer- 35%

Figure 2.4: TMPD-MIB isomers' structure formula.

exhibits higher mechanical stability.

2.3 Drying of water-borne coatings

Drying of paint is a mechanism that involves the loss of solvent via evaporation and the formation of a solid film that depends on the properties of the paint formulation used. Paint systems may be considered to be a combination of small number of constituents in a continuous or discontinuous phase.

Key components of the continuous phase are the polymer and surfactant (vehicle), while pigment, extender and additives belong to the discontinuous phase (Davison and Skuse 1999). Paints can be characterized depending on their drying characteristics as either thermoplastic or thermosetting, the former being the most common for indoor finishing coatings which can be air dried, while the latter needs to be heat dried. To be able to accurately predict the emissions of VOCs from latex paints it is necessary to describe the generally accepted stages that paint drying undergo particularly in the initial 50 hours or during the "wet phase". This transition period will

be critical for the further study of VOC emissions, since the properties (i.e. scrub resistance, opacity) of the coalesced film will be determined by the paint formulation (water, PVC) and will therefore affect the VOC mobility from the coalesced paint.

2.3.1 Paint drying modeling

The latex film formation occurs as the continuous phase from changes in composition primarily from water to primarily organic through water evaporation. This is followed by a continuous solid film of latex particles. Latex film formation is a step in paint drying that has been overlooked in many of the VOC emission models. When the substrate gains contact with the aqueous film (wet paint), the discrete polymer particles remain dispersed in the paint, and the system is stabilized by the surfactant at the water-particle interface (Kiil 2006). The general mechanism for latex film formation includes three phases of drying (Eckersley and Rudin 1994). The first drying period is characterized by rapid water evaporation and latex particle compaction, with water still filling the interstices among particles. The latex particles are spherical, with an average diameter of 0.1-0.2 μm. The second drying period is the final water evaporation, where particles deform and contact each other. At the end of this stage, the system is practically dry, and the paint film resembles a honey-comb like structure as shown in Figure 2.5. In this figure, the initial paint layer applied had a wet film thickness of 100 μm, and it was later reduced to 50 μm at the end of phase II.

In the third drying period, residual water diffuses across the particle-particle boundary, and a homogeneous film is formed. For a latex paint with a T_g much lower than the film formation temperature, this last stage may be very fast and begin to occur before evaporation of all the bulk water is complete (Dewhurst et al. 2001).

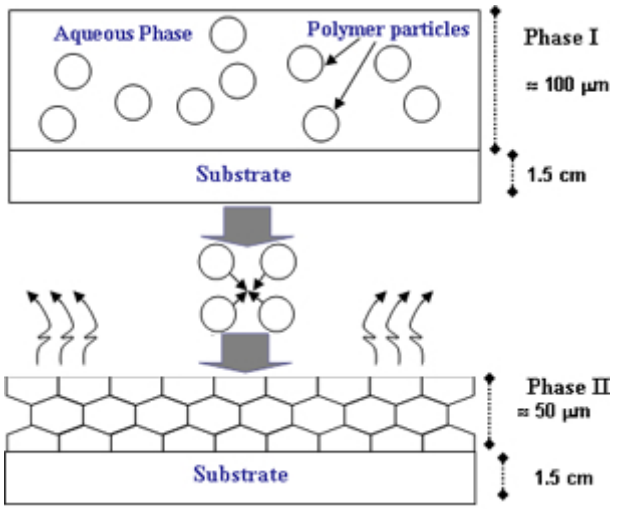

Figure 2.5: Paint drying processes.

The water closest to the coating surface evaporates faster. If the last stage is rapid, a continuous film may be formed at the surface with a small amount of water trapped inside the coating as isolated dispersed domains. Thus the final water loss will occur by diffusion through the solid phase instead of evaporating from particle-particle interstices.

2.4 Porous solids transport processes

Diffusion transport within porous solids involves a complex variety of processes including surface diffusion due to concentration gradient in the pores, molecular diffusion in the larger pores, and Knudsen diffusion in the smaller pores (when the mean free path is relatively long compared to the pore size). Molecular and Knudsen diffusion are processes that occur in series, so if one rate is very large compared to the other over a given time period, then the larger one becomes the dominant process. On the other hand, surface diffusion, involving the motion of the diffusing species along the pore wall surfaces, occurs in parallel to the molecular and Knudsen diffusion processes

(Axley 1995) and is recognized as important in porous materials provided that both concentration gradients and surface area are high.

At the molecular level, the thermal motions of atoms and molecules are random, thus transport of heat or mass is generally defined as a process caused by random molecular interactions. Mass transport by diffusion as described by Fick's law for an isotropic medium in the z direction can be expressed as:

$$j_A = -D_A \frac{\partial C_A}{\partial z} \tag{2.2}$$

where,

j_A is the rate of mass transfer per unit area $\left[\frac{kg}{m^2 s}\right]$,
C_A is the concentration of diffusing substance $\left[\frac{kg}{m^3}\right]$,
z is the diffusion coefficient $[m]$,
D_A is the diffusion coefficient $\left[\frac{m^2}{s}\right]$

while the diffusion coefficient for dilute solutions can be taken as constant, it can also be concentration dependent, for example for diffusion in polymers with high concentration gradients as described by Crank and Park (1951). Additionally, Vahdat (1991) found a linear decrease (on a log-log scale) of the diffusion coefficient with viscosity of the liquid. He also suggested that for a given polymer, the diffusion coefficient is mainly a function of viscosity and specific volume of pure solvent. However, evaluating these concentration dependent expressions for the diffusion coefficient is complex and requires physical property data that are generally not available.

2.4.1 Effective diffusion coefficient, porosity and tortuosity

Values for effective diffusion coefficients for chemical species in air and water can be obtained from experiments or from correlations. An effective diffusion coefficient in a porous medium is function of the free air diffusivity and the physical properties of the material. The mass transport inside the material will occur along an irregular and tortuous path as it is depicted in Figure 2.6. For the present study, the approach used by Currie (1970), considering a material volume element of length l and cross sectional area A in which there is a tortuous channel of length l_i with cross sectional area A_i, can be adopted. An expression for D_{eff}/D_i is obtained to describe the effects of tortuosity and porosity on diffusion as shown in the following equation:

$$D_{eff} = D_i \epsilon_a \tau \tag{2.3}$$

where, ϵ_a is the fluid-filled porosity and τ is the tortuosity defined as:

$$\epsilon_a = \frac{V_i}{V} = \frac{A_i l_i}{A l} \tag{2.4}$$

$$\tau = \left(\frac{l}{l_i}\right)^2 \tag{2.5}$$

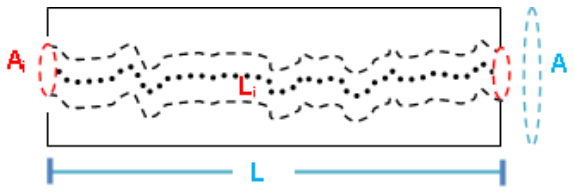

Figure 2.6: Diffusion tortuosity model.

2.4.2 Partition coefficients

In general, the partitioning of an organic compound i between two bulk phases 1 and 2 at equilibrium can be expressed as the ratio of concentrations between the two different phases. For an organic compound in the painted film, K_{pa} can be calculated by:

$$K_{pa} = \frac{C_{i_0}}{C_{a_0}} \tag{2.6}$$

where, C_{i_0} is the mole per volume of the saturated liquid at temperature tested, and C_{a_0} is the equilibrium vapor phase concentration of the organic compound.

In order to evaluate the degree to which a compound is attached to the solid phase in a given system at equilibrium, the solid-water partitioning coefficient (K_{id}) is used, and it is calculated as a ratio of the compound's total equilibrium concentrations in the solid and in the aqueous solution.

$$K_{id} = \frac{C_{is}}{C_{iw}} \tag{2.7}$$

where, C_{is} is the total sorbate concentration (e.g., $\frac{mol}{kg}$), and C_{iw} is the chemical's concentration in the solution (e.g., $\frac{mol}{L}$). For a system containing water, VOC and solids, the fraction of the compound dissolved in water f_{iw} is:

$$f_{iw} = \frac{C_{iw}}{C_{iw}V_{iw} + C_{is}M_s} \tag{2.8}$$

using Equations (2.6) and (2.7) then,

$$f_{iw} = \frac{C_{iw}V_w}{C_{iw}V_w + K_{id}C_{iw}M_s}$$

finally canceling C_{iw}, f_{iw} becomes:

$$f_{iw} = \frac{V_w}{V_w + K_{id}M_s} \tag{2.9}$$

where, V_w is the volume of water (e.g., L) in the total volume, M_s is the mass of solids (e.g., kg) and K_{id} is the solid water partition coefficient (e.g., $\frac{L}{kg}$). The retardation factor, R_f is equal to the reciprocal of the fraction of molecules capable of transport with the mobile phase at any instant, $\frac{1}{f_{iw}}$.

Making use of the retardation factor and the differential equation of transport (Choy and Reible 2000), the final form of the equation that describes the dynamics of a contaminant species for diffusion in one dimension for the mobile phase of a species reduces to:

$$R_f \cdot \frac{\partial C_A}{\partial t} = D_{eff}\frac{\partial^2 C_A}{\partial z^2} \tag{2.10}$$

2.5 Review of VOC emission models

Three distinct drying models (acting separately, successively or together) can be defined (Holl et al. 2001). The first one assumes drying is homogeneous. In this

approach, the water concentration remains uniform in the system throughout the film during the initial part of the drying process. The second one assumes drying is normal to the surface. In this approach,the heterogeneity in the distribution of water is characterized by a top dry region on the air side and a bottom wet region on the substrate side. The third one assumes drying occurs laterally. In this approach, the drying front propagates in a lateral direction parallel to the substrate, starting inward from the outer edges and ending with the center as the last portion to dry.

For the purposes of the present research, drying will be assumed to be normal to the surface and lateral drying effects will not be considered. Traditional models for normal drying have been developed by others (Sheetz 1965, Vanderhoff et al. 1966, Croll 1986). For these models, the drying process is based on water loss measurements from latex dispersions. These models are characterized by an initial constant rate of water loss followed by a decay of this rate until complete water evaporation.

Previous studies on VOC emissions from latex paints have used models that do not account for substrate effects or are fitted empirical models to single or double exponential decay models. For example, a pioneering study by Hansen (1968), used a mass transfer model for lacquer films. In this study, he found that solvent evaporation occurs in two distinct phases, the first one controlled by surface resistance to solvent loss and the second one controlled by internal diffusion resistance, and argued that this second phase may last for years. However, this model did not account for porous effects of the material. Other mass transfer models like the proposed by Tichenor et al. (1993) theorize transport occurring by molecular diffusion across a laminar boundary layer, but also fail to account for material properties. In a similar approach,

Guo et al. (1998) included vapor pressure and boundary layer theory to model the emission of individual VOCs from a coating, but did not account for substrate effects.

Another modeling approach has been to develop double exponential decay models, like the one proposed by Chang and Guo (1992). This model describe the process of mass transfer for wood stain applied on a wood material, can be adapted to obtain VOC concentrations, but it is empirical by nature and does not capture the physical transport mechanisms particularly for continuous emissions for long times. It has been the simplicity of this models what have made them popular among the scientific community. For example, Silva et al. (2003), used these decay models to compare emission results from different substrates like aluminum, gypsum and concrete. More sophisticated models like the one by Sparks et al. (1999) use a mass transfer model that has three components, one for the initial (short term) emissions, one for long term emissions, and one transitional term, but the are several model parameters that have to be fitted to experimental data, and lacks a mechanistic approach for the VOC emission problem.

Recent published literature has focused on mass transfer models, but in some cases the validation of the models has been performed at conditions that differ from typical indoor conditions and the use of empirical models developed from polynomial fitting using controlled chamber experiments. For example, Yang et al. (2001) developed a comprehensive emission numerical model that considers VOC mass transfer in the air and material-air interface, diffusion in the material film, and also diffusion in the substrate. However, this model uses a third power empirical equation to describe the dependence of the diffusion coefficient on VOC concentration in the material

film. The model only works for emissions during the wet stage of the paint event and assumes that all the liquids of the coating material were quickly absorbed by the porous substrate. This later assumption was also made in the model developed by Zhang and Niu (2003) which proposed a modified version of Yang et al. (2001) that included flow geometry of the cavity used in their experiments, and the corresponding convective surface mass transfer coefficients. However, their model that uses an Arrhenius equation for the diffusion coefficient, focused on emissions of wet paintings in a FLEC, and therefore was only validated for periods of 24 hours. Additionaly, Li et al. (2006) developed a physically based model for short-term predictions of VOCs. This model was validated using results from FLEC experiments for aluminum, but no actual validation were made for porous materials.

Alternative efforts have been made for modeling VOC emissions from dry materials. For example, Huang and Haghighat (2002), introduced a model to predict VOC emissions from dryied materials, using transport processes description at the macroscopic level, mainly assuming that the dry material behaves as a single homogeneous medium. In a different study, Xu and Zhang (2003a), also studied emissions from dry materials. They found that the dimensionless emission rate of VOC was a function of the partition coefficient and the Fourier number for mass transfer. The problem with these "dry models" is the accurate estimation of VOC amount at the initial time of application. A more detailed review for dry emission models can be found in Haghighat et al. (2005). A summary table with some of the key characteristics from previous published VOC emission models is shown in Table 2.1.

Extensive research has been done for paint drying models where the focus is

solely on drying of the film. Mechanisms described in section 2.3.1 have been modeled by many researchers. Additionally, VOC emission models from paint have also been used, but none of these models relate the water loss with the VOC emissions from the paint film. More importantly, the lack of a single model that can predict both short and long term VOC emissions was filled by the semi-mechanistic model developed in this research. The two layer model has improved the way to predict paint drying and VOC emissions from latex paints applied on a variety of substrates provided sufficient experimental data for parameter estimation. Details on the model and and validation can be found in Chapter 3.

Table 2.1: Literature summary of VOC emission models.

Author	**Model Type/Details**	**Substrate Type**	**Duration (h)**	**Chemical Measured**	**Disadvantage**
Hansen (1968)	Mass transfer model, No substrate effects (Wet model). Ingredients are evaporating independently of each other	Aluminum	100 h.	Glycol, Coalescent solvent	Internal diffusion was not found to be the controlling factor. (No substrate effects.) Surface resistance controls the loss of volatile material even at very long times.
Tichenor et al. (1993)	Mass transfer model, no substrate effects (Wet model). Double exponential model.	Oak boards	25 h.	Wood stain Floor wax Polyurethane	Ingredients in the formulated product are evaporating largely independently of each other. Good fit for only wet phase.
Chang et al. (1998)	Sink strength of carpet and gypsum board. Chamber Experiments.	Carpet Gypsum board	150-300 h.	Prop. glycol. Eth. glycol BEE Texanol	Sink model based on surface adsorption and desorption failed to predict longterm reemission process. Ads/Des of VOC controlled by chemisorption and or diffusion related processes.
Sparks et al. (1999)	Empirical and mass transfer models. (Wet model)	Gypsum board Stainless steel	100-300 h.	Paint Eth. glycol. Prop. glycol. BTEX Texanol	Contains empirical values obtained from fitting experimental data. Mass transfer model requires 8 days of small chamber data of small chamber data to estimate the parameters req. for the model. Model has 3 components, (Short, long and intermediate)
Yang et al. (2001)	Numerical model to simulate VOC emissions from dry materials. (Dry model). Multilayer model. Numerical Simulation	Particle board	60-70 h.	TVOC Hexanal α-Pinene	Uses 4 parameters:(kma, AGE,Dm, Co). The AGE of the material may be difficult to determine. Model for emission of dry materials only, does not account for paint layer/drying.
Yang et al. (2001)	Numerical model to simulate VOC emissions from wet materials. (Wet model). Numerical Simulation	Wood stain applied on oak substrates	24 h.	Wood stain.	Model uses a third power empirical equation to describe the dependence of the diffusion coefficient on VOC concentration in the material film. All the liquids of the coating material are assumed to be absorbed by the permeable material. Experimental data used "wind tunnel" type air velocities.
Huang and Haghighat (2002)	Mass diffusion within the material and mass convection and diffusion processes in the boundary layer. (Dry model). Numerical and Analytical. Validated with experiments and CFD model	Particle board	100-800 h.	TVOC Hexanal α-Pinene	Model does not account for wet phase of the paint, assuming homogeneous distribution of the VOC inside the porous material
Xu and Zhang (2003b)	Diffusion out of Bld. Material from a uniform layer . (Dry model).Analytical solution	Particle board	100-1000 h.	TVOC Hexanal	Model for diffusion out of dry materials, no drying of paint or paint film is taken into account. Validated with literature experiments.
Li et al. (2006)	Numerical Solution Model considers Air, film and substrate mass transfer.(Wet model). Numerical solution	Aluminum Particle board	7 h.	TVOC	Model assumes VOC concentration within the applied paint film is always uniform (internal difussion is neglected). Experimental data used "wind tunnel" type air velocities.
Zhang and Niu (2003)	Numerical Solution, CFD calculation.(Wet model).Cylindrical coordinates	Flec Cell	24 h.	TVOC, 23 VOCs quantified	Model does not account for water evaporation. No substrate diffusion (used aluminum). The model assume that the amount of coating material is so small that it is quickly absorbed by the porous substrate after the application.

Chapter 3

Model Development

3.1 Introduction

In this chapter, details of the model development and sensitivity analysis of the numerical solution are given. Additionally, experimental data that was used to validate the model is analyzed and methods for experiments is also presented in this chapter. This chapter starts with the model description, mechanics and details of the two layer diffusion model in Section 3.2, followed by details of the model's numerical solution in Section 3.3, the model sensitivity analysis in Section 3.4 and a brief discussion about the developed model in Section 3.5.

3.2 Model description

Given the complexity of paint systems described in Chapter 2, it was assumed that water-borne paints are composed of water, solids (TiO_2 pigment and polymer), and coalescing aid. Furthermore, the following assumptions were made:

1. The model is applicable for thermoplastic paints.

2. Paint drying is normal to the surface and no lateral drying effects are present.

3. Water is lost from the paint with a constant rate of evaporation.

4. The dried skin layer formed shortly after paint application is assumed to be porous enough to allow for transport of water or other chemicals.

5. Fick's law in one-dimension applies to mass transfer in both material film and substrate.

6. The material is homogeneous and the diffusion coefficient for the VOC in the material is constant.

7. There are no chemical reactions inside the paint or material that generate or consume the VOC.

8. Temperature effects are negligible.

9. No swelling occurs in the latex.

Shortly after initial application of the paint to the material, there is an initial thin layer of coating that will be referred to as layer L_1. This initial layer has a thickness that decreases with time. An additional layer L_2 was added to account for transport in the material. The key transport phenomena considered in the model are: transport of VOC between the interface and the bulk air, transport from the paint to the air and from the paint to the material, and transport in and out of the porous material for a system like the one shown in Figure 3.1, where a is the thickness of the material, and b-a is the thickness of the paint. The following sections will give details of the general two layer model proposed to explain the VOC transport for thermoplastic paints used in indoor architectural finishings by first using a constant paint film thickness L_1 (b-a is kept constant), and second by adjusting the model for

the rate of water loss as the water evaporates from L_1 (b-a variable).

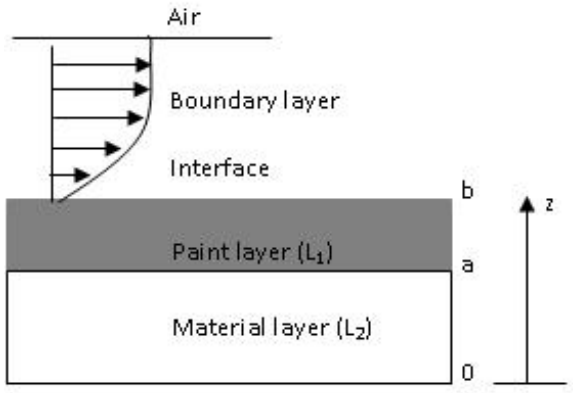

Figure 3.1: Physical phenomena during material coating.

3.2.1 Constant paint film thickness (Case I)

Choy and Reible (2000) gave the analytical solution for a two-layer composite system for the mobile phase concentration that can be assumed to be the VOC in this case. This analytical solution was used to initially calibrate the numerical solution of the proposed two-layer model for a constant paint film L_1, omitting the effect of water evaporation from the receding paint film.

Once the appropriate fate and transport mechanisms are chosen the equations for the VOC flux and reactions are combined in a mass balance equation. The rate of change of VOC for the particular boundary conditions is thus described by the following set of equations:

$$\frac{\partial C_{L_1}}{\partial t} = \left(\frac{D_{L_1}}{R_1}\right) \frac{\partial^2 C_{L_1}}{\partial z^2} \tag{3.1}$$

$$\frac{\partial C_{L_2}}{\partial t} = \left(\frac{D_{L_2}}{R_2}\right) \frac{\partial^2 C_{L_2}}{\partial z^2} \tag{3.2}$$

with boundary conditions[1]:

$$\left(\frac{D_{L_1}}{R_1}\right) \frac{\partial C_{L_1}}{\partial z}\Big|_{z=b} = -k_a \cdot C_{L_1}\Big|_{z=b} \qquad t > 0 \tag{3.3}$$

$$\left(\frac{D_{L_1}}{R_1}\right) \frac{\partial C_{L_1}}{\partial z}\Big|_{z=a} = \left(\frac{D_{L_2}}{R_2}\right) \frac{\partial C_{L_2}}{\partial z}\Big|_{z=a} \qquad t > 0 \tag{3.4}$$

$$\frac{\partial C_{L_2}}{\partial z}\Big|_{z=0} = 0 \qquad t > 0 \tag{3.5}$$

$$\frac{C_{L_1}}{R_1}|_{z=a} = \frac{C_{L_2}}{R_2}|_{z=a} \qquad t > 0 \tag{3.6}$$

The following initial conditions were employed:

$$C_{L_2}(z,t)\Big|_{t=0} = C^0_{L_2}(z) \qquad z \in [0,a) \tag{3.7}$$

$$C_{L_1}(z,t)\Big|_{t=0} = C^0_{L_1}(z) \qquad z \in (a,b] \tag{3.8}$$

$$C^0_{L_2}(z) = C^0_{L_1}(z) \qquad z = a \tag{3.9}$$

where,

[1]The paint air boundary condition (Equation 3.3) assumes that: $E = -k_a(C_{liq} - \frac{C_{gas}}{k})$, where $\frac{C_{gas}}{k} << C_{liq}$. C_{gas} and C_{liq} are the VOC gas and liquid phase concentrations respectively.

C_{L_1}, C_{L_2}	are the mobile compound concentration in layers 1 and 2 $\left[\frac{mg}{m^3}\right]$,
D_{L_1}, D_{L_2}	are the diffusion coefficient in layers 1 and 2 $\left[\frac{m^2}{h}\right]$,
R_1, R_2	are the retardation factor that account for layer adsorption$[-]$,
ka	is the VOC mass transfer coefficient $\left[\frac{m}{h}\right]$
z	is the space coordinate measured normal to the section $[m]$,
a	is the material thickness $[m]$,
b	is the location of the paint-air boundary $[m]$.

3.2.2 Variable paint film thickness (Case II)

In order to adjust for water evaporation and thickness reduction of the paint film, the previously proposed model can be further modified to allow for more complex boundary conditions (i.e variable film thickness). Kiil (2006) found a linear relationship for water evaporation from paint films under 400 μm, which is the typical range of wet film thickness application of indoor architectural coatings. To estimate the water evaporation from the paint formulation, an expression for the time-dependent evaporation rate in a multi-component liquid system was derived. The equations that describe the water flux or rate of water depletion (N) from the liquid paint are:

$$N = k_c \cdot (C_{surf} - C_{Bulk}) \tag{3.10}$$

$$\frac{dM}{dt} = -N \cdot A \tag{3.11}$$

where,

N is water flux or the rate of evaporation of water per area $\left[\frac{kg}{m^2 s}\right]$,

k_c is the water mass transfer coefficient $\left[\frac{m}{s}\right]$,

C_{Surf} is the saturation vapor density at the surface $\left[\frac{kg}{m^3}\right]$,

C_{Bulk} is the vapor density of the room in the bulk air $\left[\frac{kg}{m^3}\right]$,

M is the mass of water on the substrate $[kg]$,

A is the area of paint applied $[m^2]$

The rate of change of mass in a water film, can be written as:

$$\frac{dM}{dt} = \frac{d}{dt}\rho V = \rho \cdot \frac{dV}{dt} \tag{3.12}$$

where,

ρ is water density $\left[\frac{kg}{m^3}\right]$,

V is water volume content of the paint $[m^3]$

By combining Equations (3.10)-(3.12), the following relation is obtained:

$$\frac{k_c}{\rho} \cdot (C_{Surf} - C_{Bulk}) = \frac{1}{A} \cdot \frac{dV}{dt} \tag{3.13}$$

The quantity on the right hand side of Equation (3.13) is the rate of change of the thickness in the paint film.

$$\frac{k_c}{\rho} \cdot (C_{Surf} - C_{Bulk}) = \frac{\Delta\delta}{\Delta t} \tag{3.14}$$

The right hand side of Equation (3.13) has been approximated as $\frac{\Delta\delta}{\Delta t}$, where δ is the initial thickness of the paint (m), and t is time (s). The vapor density in the

room can be defined as:

$$C_{Bulk} = \frac{RH \cdot C_{Sat}}{100} \tag{3.15}$$

Solving for time[2], using $C_{Surf} = C_w$ and replacing $C_{Bulk-air}$ in Equation (3.14) follows:

$$t_{evap} = \frac{\Delta\delta}{\frac{k_c}{\rho} \cdot C_w \left(1 - \frac{RH}{100}\right)} \tag{3.16}$$

The experimental time for paint drying can be obtained using the rate of water loss by evaporation estimated by a gravimetric method to calculate evaporation rates of pure liquids. The mass transfer coefficient for water at 20°C has been found to be in the range from 0.001 to 0.035 $\frac{m}{s}$ for pure water measured using a gravimetric technique (Beverley et al. 1999). In buildings, this number will be much slower in practice due to various resistances or barriers to the evaporation process; this mass transfer coefficient is an upper limit for the values that should be used for k_c. If a lower limit for k_c is taken as 0.0002 $\frac{m}{s}$ as calculated by Lin (2006), then the time required for evaporation of water will change from 49 min to 10.2 hours, so the actual total water evaporation will occur between these two time intervals. See Appendix A.1 for example calculations of this time using Equation 3.16.

Once the final thickness of the film is reached, the driving force for mass transfer will be mainly due to molecular diffusion, and the material as a source can be used

[2]This expression is obtained assuming that the wall temperature is equal to temperature in the room air, which will not always be the case.

to predict emissions over longer periods of time. The rate of water depletion from the liquid paint is used to develop an estimate of the water evaporation time t_{evap}, in conjunction with a linear function that represents the dynamic behavior of the diffusion coefficient as shown in Equation 3.17 and 3.18.

$$\frac{D_{final} - D_{initial}}{t_{evap}} \cdot t + D_{initial} \quad t \leq t_{evap} \tag{3.17}$$

$$D_{final} \quad t > t_{evap} \tag{3.18}$$

3.3 Numerical solution

In order to have more flexibility with the model, an implicit finite volume method approach was employed to solve Equations 3.1-3.9. Figure 3.2 shows the grid for such two layer system, and Figure 3.3 shows the resulting system of equations arranged in matrix form. The grid used for the paint layer included a variable number (P) of nodes for the paint layer and a variable number (M) of nodes for the material layer. A greater number of nodes were used for the paint layer, and this number of nodes was automatically adjusted during each simulation to obtain a grid independent solution.

A series of three coefficients per node can be calculated when discretizing Equations 3.1-3.9, obtaining the coefficients a_i, b_i and c_i that correspond to the terms in brackets from Equations 3.19-3.24. The C_{iLi} terms correspond to the chemical concentration values from each node at time t, and the superscript 0 denotes the concentration values from the previous time step. The equations for the interfaces, paint-air (S1) and paint-material (S2) can be substituted in neighboring nodes, affecting nodes

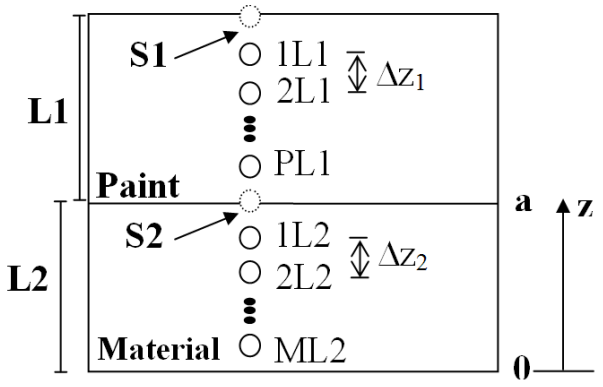

Figure 3.2: Node distribution of the two layer model.

$$\begin{bmatrix} b_1 & c_1 & 0 & 0 & 0 & 0 & \cdots & 0 \\ a_2 & b_2 & c_2 & 0 & 0 & 0 & \cdots & 0 \\ 0 & \vdots & \vdots & \vdots & 0 & 0 & \cdots & 0 \\ \vdots & a_P & b_P & c_P & \vdots & 0 & \cdots & 0 \\ 0 & \vdots & a_{P+1} & b_{P+1} & c_{P+1} & \vdots & \cdots & 0 \\ 0 & 0 & \vdots & a_{P+2} & b_{P+2} & c_{P+2} & \cdots & 0 \\ 0 & 0 & 0 & \vdots & \vdots & \vdots & \cdots & 0 \\ 0 & 0 & 0 & 0 & 0 & 0 & a_{P+M} & b_{P+M} \end{bmatrix} \cdot \begin{bmatrix} C_{1L1} \\ C_{2L1} \\ C_{3L1} \\ \vdots \\ C_{PL1} \\ C_{1L2} \\ \vdots \\ C_{(P+M)L2} \end{bmatrix} = \begin{bmatrix} C_{1L1}^{\,0} \\ C_{2L1}^{\,0} \\ C_{3L1}^{\,0} \\ \vdots \\ C_{PL1}^{\,0} \\ C_{L2}^{\,0} \\ \vdots \\ C_{(P+M)L2}^{\,0} \end{bmatrix}$$

Figure 3.3: System of equations for numerical solution.

1L1, pL1, and 1L2, obtaining Equations 3.19-3.22. Inner layer nodes for paint and material have the same coefficients as Equations 3.20 and 3.23 respectively. These equations were implicitly solved using a tridiagonal matrix algorithm. Derivation steps for the estimation of the coefficients for each node is provided in more detail in Appendix C.

$$C_{1L1}\left[-3\alpha_1 - 1 + 2\alpha_1 k_{cs}\right] + C_{2L1}\left[\alpha_1\right] = -C^0_{1L1} \tag{3.19}$$

$$C_{1L1}\left[\alpha_1\right] + C_{2L1}\left[-1 - 2\alpha_1\right] + C_{3L1}\left[\alpha_1\right] = -C^0_{2L1} \tag{3.20}$$

$$C_{(P-1)L1}\left[\alpha_1\right] + C_{PL1}\left[-1 - 3\alpha_1 + 2\alpha_1 m_1\right] + C_{(P+1)L1}\left[2\alpha_1 m_2\right] = -C^0_{PL1} \tag{3.21}$$

$$C_{PL1}\left[2\alpha_2 m_1\right] + C_{1L2}\left[-1 - 3\alpha_2 + 2\alpha_2 m_2\right] + C_{2L2}\left[\alpha_2\right] = -C^0_{1L2} \tag{3.22}$$

$$C_{1L2}\left[\alpha_2\right] + C_{2L2}\left[-1 - 2\alpha_2\right] + C_{3L2}\left[\alpha_2\right] = -C^0_{2L2} \tag{3.23}$$

$$C_{(M-1)L2}\left[\alpha_2\right] + C_{ML2}\left[-1 - \alpha_2\right] = -C^0_{ML2} \tag{3.24}$$

where,

$$\alpha_i = \frac{\Delta t}{(\Delta z_i)^2}\frac{D_{A_{L_i}}}{R_i},$$

$$k_{cs} = \frac{2\frac{D_{A_{L_i}}}{R_i}}{2\frac{D_{A_{L_i}}}{R_i} + k_a \Delta z_1},$$

$$m_1 = \frac{\frac{D_{A_{L_1}}}{R_1}\Delta z_2}{\frac{D_{A_{L_1}}}{R_1}\Delta z_1 + \frac{D_{A_{L_2}}}{R_2}\Delta z_1}, and$$

$$m_2 = \frac{\frac{D_{A_{L_2}}}{R_2}\Delta z_1}{\frac{D_{A_{L_1}}}{R_1}\Delta z_1 + \frac{D_{A_{L_2}}}{R_2}\Delta z_1}$$

Once the system of equation is solved for each time step, the concentration on

each node allows to calculate the mass of VOC remaining in the paint and material layers. The emission of VOC normalized by initial amount of VOC applied in grams for each time step can be obtained using the following approximation:

$$F\left[\frac{mg}{hg_{voc}}\right] = \frac{-D_{Aeff,L1}(C_{s1L1} - C_{1L1})}{\Delta z_1/2} \cdot \left(\frac{A}{M_{paint} \cdot f_{voc}}\right) \tag{3.25}$$

where,

M_{paint}	is the initial mass of paint applied [g],
f_{voc}	is the fraction of the compound present in the paint [-],
Δz_1	is the distance between nodes of layer 1 [m],
C_{S1L1}	is the VOC concentration in the surface of layer 1 $\left[\frac{mg}{m^3}\right]$,
C_{1L1}	is the VOC concentration in node 1 of layer 1 $\left[\frac{mg}{m^3}\right]$,
A	is the area over which the paint is applied $[m^2]$

3.4 Sensitivity analysis

In order to validate the two layer model, the proper selection of time step for the numerical solution, and choice of number of nodes in each layer is needed to obtain a parameter independent solution.

3.4.1 Time step

The time step Δt was initially set at 10 hours and decreased on powers of 10 down to 0.001 hours. Further comparisons of the results at t=10 hours revealed a variation in

the emission values of nearly 4% when reducing the Δt from 1h to 0.1h. Subsequent reductions in the Δt yielded emission value differences of less than 1% but significantly increase the computation time. At simulation time of t=1 hour, the emission trends for the different selected time steps was whithin 1% difference. Results of simulations for different time step selections can be seen in Figure 3.4.

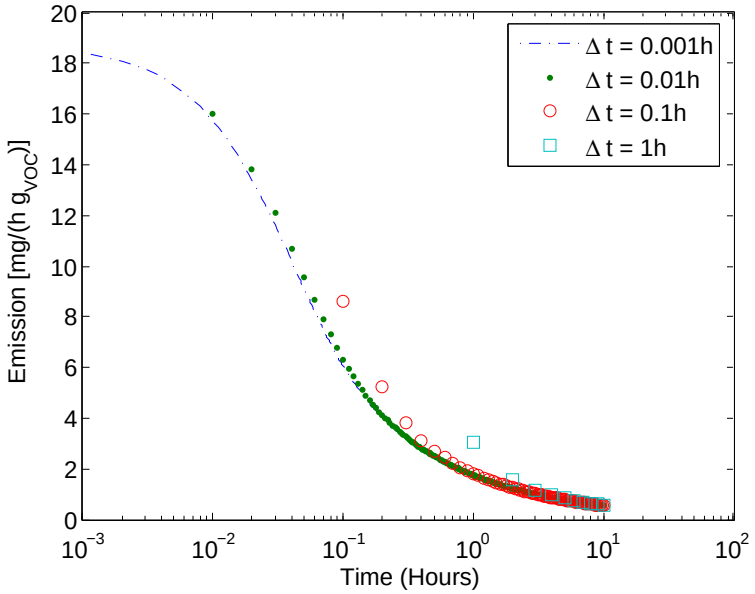

Figure 3.4: Time step variation.

The results of the emission profile obtained for the two smaller time steps coincide very well, even during times less than one hour. An optimal time step of Δt=0.1h was selected to reduce computation time without losing accuracy in the simulation results, since the simulation expands over long periods of time (hundreds or thousands of hours), and the time resolution for the experimental data was only available for unevenly spaced samples with time given in hours.

3.4.2 Nodes

Node increments in the material layer did not have an effect on the numerical solution, contrary to increments in the paint layer. Variation in the number of nodes of the paint layer affected both the paint and the material layers mass accumulation, but more significantly affected accumulation in the material layer. The change in total VOC mass in the paint and material layers with respect to number of nodes used inside the paint layer can be seen in Figures 3.5 and 3.6 respectively. Incrementing the number of paint layer nodes from 20 to 780 in this simulation, resulted in a variation of the total mass accumulated for paint and material. While the differences in the paint and material were inversely proportional, the largest changes occurred for the material layer where the mass changed from 0.0042 mg to 0.066 mg or 93% increment, while for the paint layer the mass changed from 34.23 mg to 34.10 mg or 0.4%. This result highlights the importance of selecting the proper number of nodes in order to establish a node independent solution for the system of equations.

Since the node selection was critical in the 2LM, a subroutine was implemented to automatically adjust the number of nodes per layer. This automatic selection of nodes guarantees that changes in the thickness of the paint or material layers will not affect the solution. To obtain the number of nodes, the subroutine starts with ten nodes on each layer and increases the number of nodes with increments in the layer until further increases do not change the solution. Therefore the automatic node selection guarantees the placement of the minimum amount of nodes in each layer required for a node independent solution.

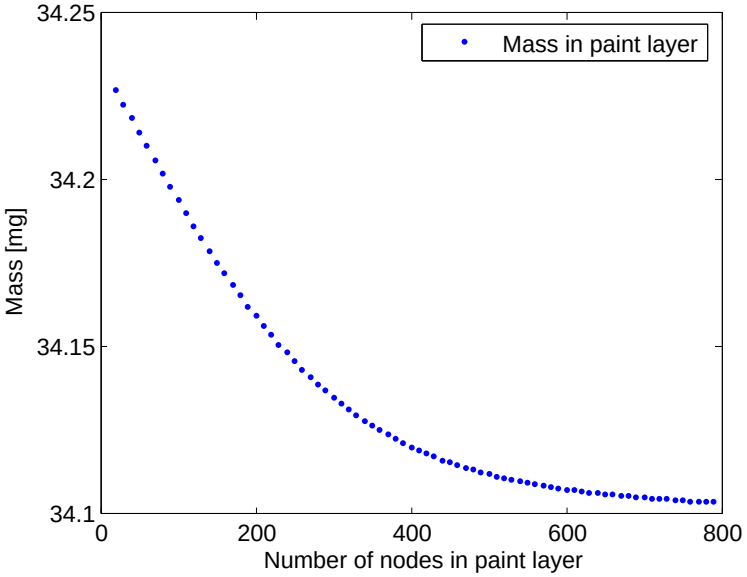

Figure 3.5: Solution variation in paint layer.

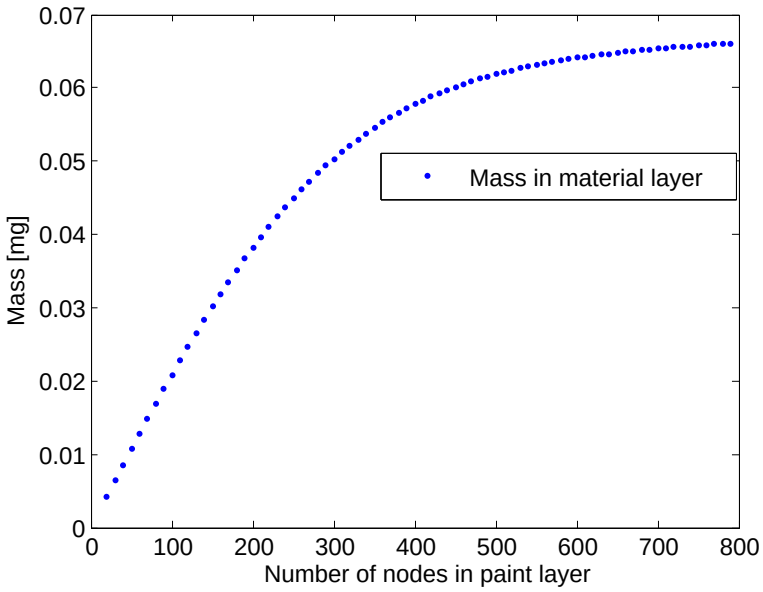

Figure 3.6: Solution variation in material layer.

Table 3.1: Paint diffusion coefficient values found in published literature $\left[\frac{m^2}{h}\right]$.

Value	Notes	Reference
3.6×10^{-15}	Solvent applied to polyvinil acetate	(Hansen 1968)
3.6×10^{-8}	Model used VOC substrate diffusivity value of 3.6×10^{-11} $\frac{m^2}{h}$	(Yang et al. 2001)
2.8×10^{-7}	VOC applied to particle board	(Xu and Zhang 2003b)
7.2×10^{-3}	Paint applied to aluminum plate	(Zhang and Niu 2003)

3.4.3 Paint diffusion coefficient

A key parameter for the model is the paint layer diffusion coefficient. Paint layer diffusion coefficients for different published models ranges anywhere from 10^{-3} to 10^{-15} $\frac{m^2}{h}$. A summary of different reported paint diffusion coefficients can be found in Table 3.1. The great differences in the numerical value of the diffusion coefficients found in the published literature is due to differences in the models used to estimate different model parameters. However, for the present model, the values of the diffusion coefficient are expected to be in the range of 1×10^{-11} to 1×10^{-13} $\frac{m^2}{h}$. Therefore, a sensitivity assessment of the 2LM to the diffusion coefficient was obtained by changing this parameter in a range spanning three orders of magnitude from 1×10^{-11} to 1×10^{-13} $\frac{m^2}{h}$. Figures 3.7- 3.9 show the results of the simulations for up to 10,000 hours as the paint diffusion coefficient is increased. The colors red and blue represent high and low VOC concentration distribution along the paint thickness respectively.

Additionally, the variation of this concentration with time is displayed in these 3D figures. VOC mobility highly depends on the diffusion coefficient value, for example Figure 3.7 shows a fast VOC mobility from the paint layer, since after 2,000 hours, the peak concentration of VOC in the paint layer was significantly reduced compared to the its initial value. Effects of the reduction of the diffusion coefficient are shown in

Figure 3.8. This figure shows the results after a 10 fold decrease in the paint diffusion coefficient. In this case, the peak VOC concentration remaining after 10,000 hours is 25% of its initial value, but it is much larger than the peak concentration from the previous case as seen in Figure 3.7. Furthermore, if the diffusion coefficient is reduced even more, the VOC mobility is significantly diminished, as shown in Figure 3.9. In this case, the distribution profile in the paint layer remains mostly uniform throughout the whole simulation period well beyond 10,000 hours.

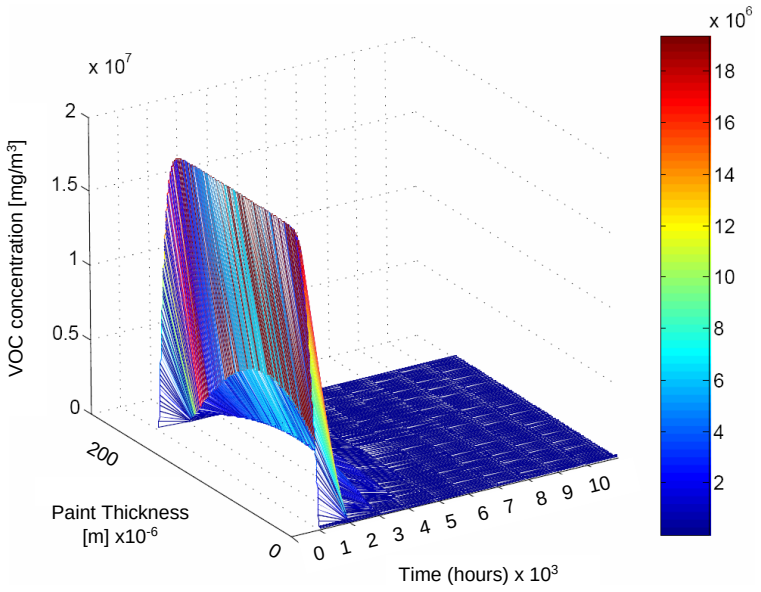

Figure 3.7: VOC distribution variation with time (D=$1\times10^{-11}\frac{m^2}{h}$).

The paint diffusion coefficient is a critical parameter for this model to capture the different effects of paint composition on VOC transport. Paints that have a more cohesive film that could be described by a small diffusion coefficient such as LPVC paints that present a similar behavior to the one shown in the simulation of Figure 3.9. The more fillers and pigments are added into a paint such as with HPVC paints, the more voids it will have, and the VOC mobility will likely be greater as in the case

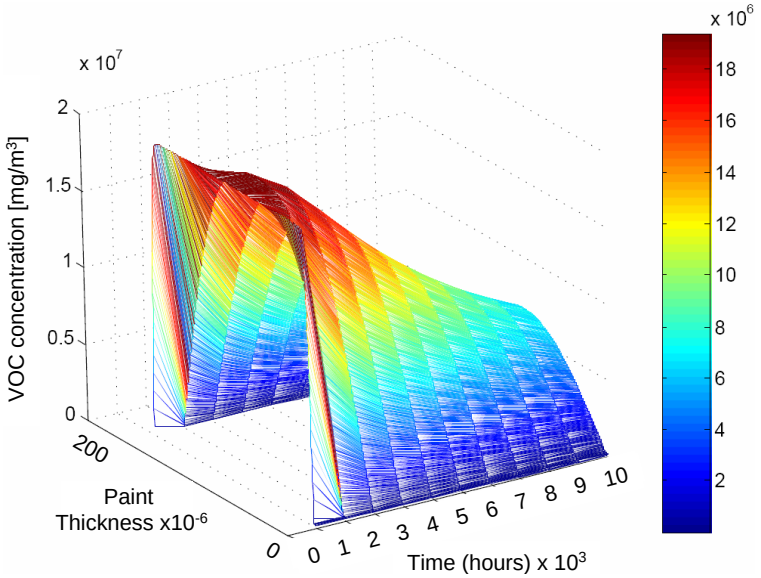

Figure 3.8: VOC distribution variation with time (D=$1\times10^{-12}\frac{m^2}{h}$).

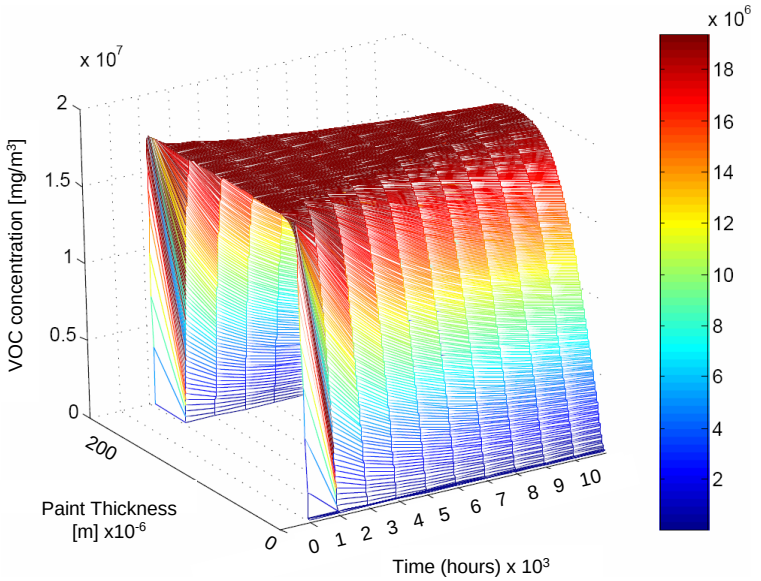

Figure 3.9: VOC distribution variation with time (D=$1\times10^{-13}\frac{m^2}{h}$).

shown of Figure 3.7. This rapid decay in VOC concentration is a characteristic of HPVC paints which contain a less homogeneous film, therefore having more hiding power but less retention of VOC mass.

3.5 Discussion

Changing the layer thickness and the diffusion coefficient of the two layers in the proposed model can lead to alternative modeling scenarios. For example, an impermeable materials could be simulated by shrinking the size of the material layer, and decreasing its diffusion coefficient. However, these variations to the modeling parameters were not studied under the scope of this research. It is important to highlight that during the development of the two layer model, addition of a third layer for simulation of paper backing did not have effects in the results. This behavior can be explained due to the differences of several order of magnitude in the VOC diffusion coefficient of paint and material (gypsum and paper backing). Gypsum board as used in real applications contains a paper backing layer. In order to account for this paper layer, the paper was assumed to be part of the paint layer when painted, and it was assumed to be part of the gypsum layer when unpainted (opposite side of painted gypsum). The no-flux boundary condition from Equation 3.6 does not always satisfy for real applications. If the gypsum wall is arranged in such a way that the back side is not attached to any other material, a different boundary condition should be used. If a stirred tank is assumed at the back, then a constant boundary condition can be assumed.

Chapter 4

Experimental Methods

4.1 Introduction

Experiments using Thermal Gravimetric Analysis (TGA) and gas chromatography (GC) were designed in order to further validate the 2LM and to gain a better understanding of paint composition effects in the fate and transport of TMPD-MIB. Methods used for estimation of TMPD-MIB evaporation rates and mass transfer coefficients after application of TMPD-MIB alone and after paint application are covered in Section 4.2. An additional method designed to explore effects in the mobility of TMPD-MIB caused by differences in polymer content is presented in Section 4.3. Section 4.4 explains the quality assurance and quality control activities performed to enhance the quality of the experimental data obtained.

4.2 Method for Thermal Gravimetric Analysis(TGA)

4.2.1 Pure substance application (mass transfer coefficient estimation)

A solution of 20% by weight of TMPD-MIB in methanol (hereafter referred to as TexM) was applied onto six-millimeter round material samples. The materials used were gypsum with and without paper backing and aluminum. These materials were chosen to establish emission differences between sorptive and non-sorptive materials. The samples were weighed before TexM application and then placed in the TGA Q-500 (TA Instruments company) auto sampler, that loaded individual samples inside the furnace as shown in Figure 4.1. The size and texture of the gypsum, paper backing and aluminum samples can be seen in Figure4.2.

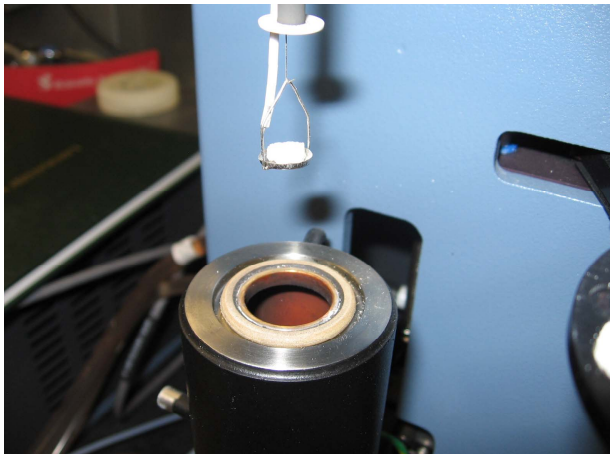

Figure 4.1: Gypsum sample being loaded into the TGA furnace.

The TGA recorded the amount and rate of change of the material weight as a function of time in a controlled atmosphere. The samples were maintained inside the standard furnace under isothermal conditions at 28 °C, and this temperature was held for up to ten hours. The sample weight was measured continuously over time.

Compressed air (Praxair) was used with purge and flow rates of 20 $\frac{ml}{min}$. The small furnace volume (V= 30x10^{-6} m^3) was operated with a total flow rate of 40 $\frac{ml}{min}$, results in an air exchange rate (ACH) of 65 h^{-1} and a calculated air velocity of 0.034 $\frac{m}{s}$. These parameters lie within the air speed comfort zone for indoor environments. The instrument has a weighing capacity of up to 1.0 g with a resolution of 0.1 μg with an accuracy of $\leq \pm 0.1\%$.

Figure 4.2: Six-millimeter material samples.

4.2.2 Paint application on impermeable substrate

These experiments investigated the paint evaporation rates from different latex paints. Six-millimeter aluminum samples were coated with paints that contained 45-65% of water by mass and different amounts of PVC. The paints used in this experiment were: a flat paint, an eggshell paint, and a high gloss paint. A summary of paint composition for each paint can be found in Table 4.1. The aluminum samples were weighed before paint application and then loaded in the TGA autosampler. The thickness of the paint layer was estimated gravimetrically. A temperature ramp was programmed to increase the furnace temperature to 28 °C and to hold this temperature for 24 hours, while continuously recording the sample weight.

Table 4.1: Paints' compositions

Component	High Gloss[a]	Semi-gloss[b]	Eggshell[c]	Flat[d]
	(% by weight)	(% by weight)	(% by weight)	(% by weight)
Pigment[e]	3	25	18	33
Water	65	16	65	45
Polymer	28	57	15	23
TMPD-MIB [f]	3	2	3	3
PVC	10	30	55	60

[a] Glidden paint EM7112.
[b] Simplified paint prepared by Eastman.
[c] Glidden paint EM6012.
[d] Glidden paint EM9012.
[e] Pigment includes limestone,clay,TiO_2 and silica.
[f] PVC was estimated using Equation 2.1

4.3 Method for concentration profile in porous substrate (TGA and GC)

These experiments investigated the TMPD-MIB fate after paint application on a porous substrate. Squared gypsum board samples of 5 cm by 5 cm and 1.2 cm in thickness were coated and sealed with sodium silicate on back and sides and air dried for one day. Two sets of gypsum samples were painted with a semi-gloss paint and a flat paint that contained high and low PVC, respectively, as shown in Table 4.1. The first set of coated gypsum samples was stored at room temperature and allowed to air dry for one week, prior to TMPD-MIB solid phase extraction. The second set of samples was painted with a thicker paint layer than the first, and allowed to air dry for a period of two weeks. A digital image of the gypsum board samples after the paint film dried is shown in Figure 4.3. The semi-gloss paint had a vivid white color, while the flat paint appeared to be more opaque.

The paint and underlying paper were carefully removed from the gypsum samples using a razor blade. Three cores of 6 mm diameter by 1.2 cm thickness were extracted from the bare gypsum. The samples were further processed following the steps described in the following sections. The process for estimating TMPD-MIB remaining in the material is detailed in Section 4.3.1, and the process to determine the profile of the TMPD-MIB concentration inside the material is detailed in Section 4.3.2.

4.3.1 TMPD-MIB remaining in paint and material layers

The gypsum was crushed with a pestle in a ceramic mortar, weighed and placed in a 250 mL glass bottle. The dried paint and paper were cut into transects and stored in a second glass bottle. Both bottles were filled with methanol, weighed and sealed with a silicon septa cap. The bottles were sonicated for 24 hours prior to injection into a GC/FID (Agilent 6890) equipped with an HP-1 capillary column (60 m x 0.32 mm; 1 μm film thickness).

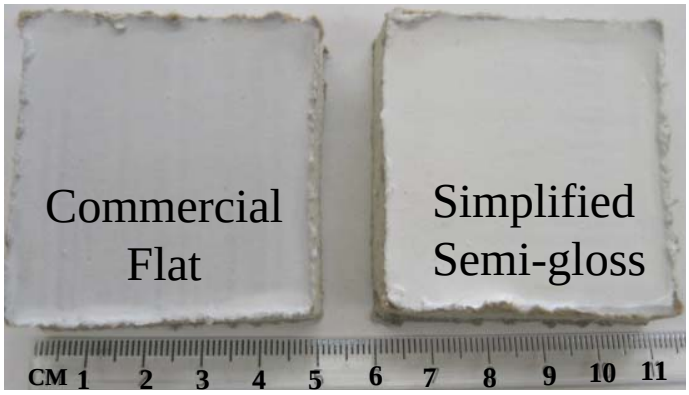

Figure 4.3: Gypsum board after being painted with latex paints.

A volume of 5 to 10 mL of methanol solution was transferred by syringe into Tenax-TA tubes, which was purged with helium at 25 $\frac{mL}{min}$ for 20 minutes to remove methanol, the remainder was re-dissolved in to a known volume and then analyzed by gas chromatography. The injector temperature of the GC/FID was increased at a rate of 10 $^{\circ}\frac{C}{s}$ from 60 $^{\circ}C$ to 280 $^{\circ}C$. The oven temperature started with an initial temperature of 100 $^{\circ}C$ for 1 minute, ramped at 30 $\frac{^{\circ}C}{min}$ to 200 $^{\circ}C$, ramped at 5 $\frac{^{\circ}C}{min}$ to 280 $^{\circ}C$ and a temperature hold for 1 minute at 280 $^{\circ}C$. A detector temperature of 300 $^{\circ}C$ was used. The mass of TMPD-MIB on each sample was quantified using a six-point external calibration curve with minimum correlation coefficients (R^2) of greater than 0.995 over the course of the experiments.

4.3.2 Concentration profile

Six-millimeter cores from the bare gypsum board samples were removed prior to pulverization and GC/FID analysis by method 4.3.1. The process for sample preparation and loading into the instrument is shown in Figure 4.4.

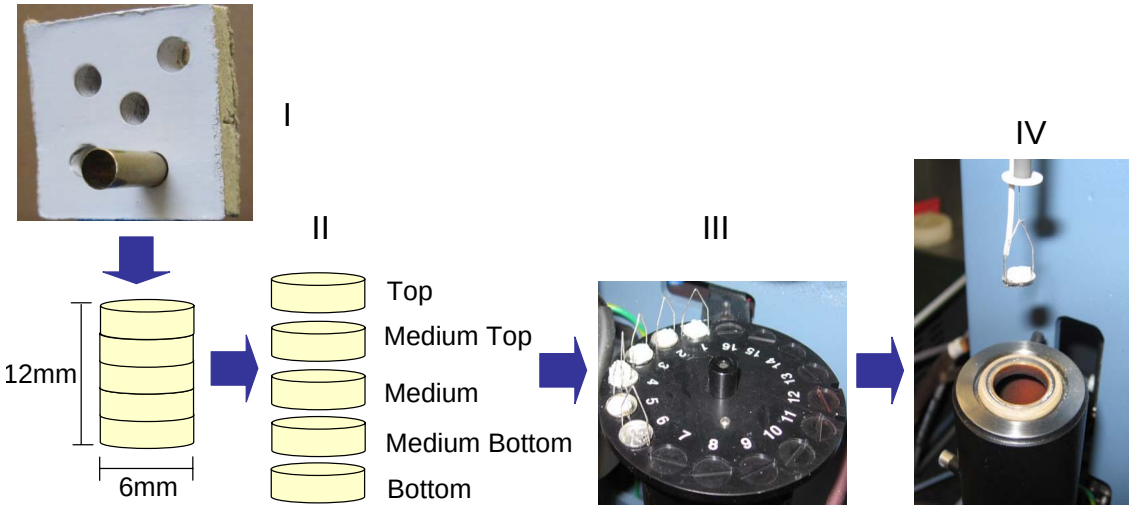

Figure 4.4: Method procedure for estimation of distribution profile inside material.

The different steps for sample preparation were as follows: first, a core was extracted from the gypsum with a brass tube. Then the gypsum core was sectioned in 5 different places in order to determine possible differences of TMPD-MIB concentration at different depths inside the material. And finally, each sectioned core was placed in the TGA auto-sampler tray. The samples were automatically loaded inside the TGA furnace that was configured with the following temperature program: a five minute temperature hold at 28 °C, followed by a ramp of 20 °C/min to 260 °C and a temperature hold for 10 minutes.

4.4 Quality assurance and quality control

4.4.1 TGA weekly calibration

Mass calibration of the TGA was performed at least once a week, using the recommended manufacturer's procedure using the TGA weight calibration routine to tare and mass calibrate the equipment using two calibration weights. The two point mass adjustment was weekly performed for the 100 mg and the 1000 mg scales.

After every sample was unloaded from the furnace, the temperature ramp was set for a cleaning mode. The temperature was increased at a rate of 50 $\frac{\circ C}{min}$ until 500°C was reached, and then the temperature was held constant for 20 minutes. This last step was used to evaporate any VOC remaining and therefore clean the furnace and sample pan.

4.4.2 Beginning and end of run

Before the start of every run, an electronic tare of the sample pan was initiated before loading a new sample, to ensure an accurate reading of the balance. These quality assurance and control procedures were used for the TGA methods described in the previous two sections.

4.4.3 Blank experiments

Blank experiments were performed for both TGA methods, using the same experimental procedure but without application of TMPD-MIB or paint. In the case of the bare gypsum board for TMPD-MIB concentration estimations, cores of unpainted gypsum board were also sectioned and processed following Method 2, in order to account for the evaporation of water in the gypsum. The weight loss of the cores from the unpainted gypsum core was uniform throughout the thickness of the gypsum core.

Chapter 5

Experimental Data

5.1 Introduction

In this chapter, experiments that follow the methods presented in Chapter 4 are used to estimate input parameters for the 2LM and to better understand the differences that PVC and paint components has on emission rates and fate of TMPD-MIB after paint application. Mass transfer coefficients for TMPD-MIB are presented in Section 5.2, paint drying and PVC effects on emission rates are presented in Section 5.3. Additionally, TGA experimental results are presented in Section 5.4. Experimental results of TMPD-MIB fate after a paint event are presented in Section 5.5. Finally, conditions of the small environmental chamber experiments obtained by (Lin 2006) are assessed in Section 5.6 in order to assure data consistency for validation of the two layer model as later presented in Chapter 6.

5.2 TMPD-MIB mass transfer coefficient

Experiments with TexM applied on aluminum and gypsum board were performed to estimate the TMPD-MIB mass transfer coefficient. Gypsum board was used with and without paper backing, following the TGA method for pure substance application. This approach was used to isolate the material effects that paper backing has on the overall TMPD-MIB mass transfer coefficient. Figure 5.1 shows the first thirty minutes of a curve of normalized mass loss of TMPD-MIB after application of TexM on aluminum. Integration of the area under the curve of the percent mass loss of TexM for the first ten minutes accounted for 99.9% of the initial amount of methanol applied. This indicates the methanol completely evaporated after ten minutes. The fast initial decay in Figure 5.1 is due to the 80% methanol of TexM that evaporated entirely during the initial minutes after application. This fast decay was followed by the slow evaporation of TMPD-MIB. Linear regressions of the weighing data from one to five hours (not shown) were used to calculate the rate of evaporation of TMPD-MIB. All regressions resulted in coefficients of determination $R^2 > 0.98$.

The obtained evaporation rates measured at 28 ^{o}C are summarized in Table 5.1. Although the evaporation rate of TMPD-MIB after application on gypsum board was expected to be slower than the evaporation rate from aluminum, this was not noticeable. TMPD-MIB evaporation rates normalized by material area were consistent, irregardless of the material applied to, as shown in Table 5.1.

An alternative explanation for this behavior can be found by looking at the TMPD-MIB octanol-air partition coefficient (k_{oa}) which is a useful parameter for predicting the partitioning behavior between air and environmental matrices such as

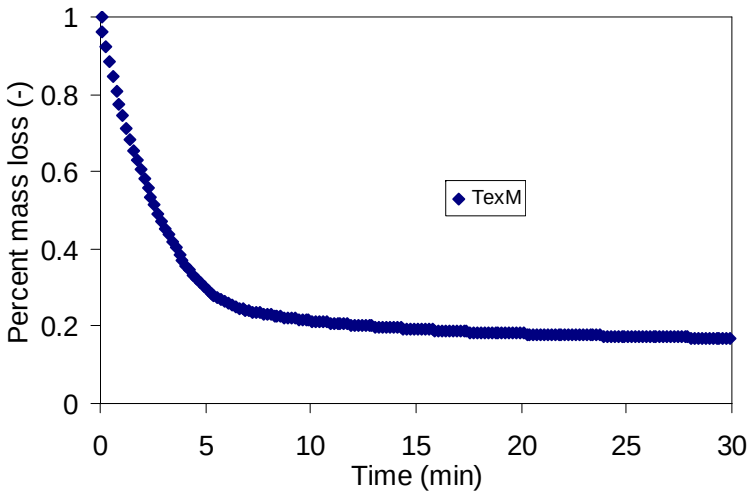

Figure 5.1: Evaporation of methanol and TMPD-MIB from aluminum.

Table 5.1: Summary of the measured TMPD-MIB evaporation rates

Material	TexM	Semi-gloss Paint	Flat Paint
	$\left[\frac{g}{hm^2}\right]$	$\left[\frac{g}{hm^2}\right]$	$\left[\frac{g}{hm^2}\right]$
Aluminum	3.20 ± 0.08	0.04 ± 0.02	0.05 ± 0.02
GB only	3.13 ± 0.06	0.11 ± 0.03	0.08 ± 0.03
GB+paper	2.95 ± 0.08	0.03 ± 0.02	0.07 ± 0.02
Paper	2.73 ± 0.09	0.04 ± 0.02	0.04 ± 0.02

soil, vegetation and aerosol particles (Meylan and Howard 2005). The octanol-air partition coefficient has also been recently used for determining time scales for SVOC uptake in sorptive compartments indoors. Weschler and Nazaroff (2008) defined the time scale for achieving equilibrium sorption (τ) as:

$$\tau = \frac{k_{oa} X}{v_d} \tag{5.1}$$

where,

k_{oa} is the octanol air partition coefficient $[-]$,

X is the organic sorbing substrate thickness$[m]$,

v_d is the SVOC mass transfer coefficient $\left[\frac{m}{h}\right]$

At present, an experimentally determined k_{oa} is not available for TMPD-MIB, but this can be estimated from the octanol-water partition coefficient (k_{ow}) and the Henry's law constant (H). This estimation is shown in Table 5.2 along with other TMPD-MIB properties. Using log k_{ow} of 8.95, v_d=3 $\frac{m}{h}$ as an estimate for the mass-transfer coefficient of a typical SVOC (Weschler and Nazaroff 2008), and X=0.3 nm for an estimated thickness of 10 mg of TMPD-MIB applied on a 6 mm round aluminum sample. The obtained characteristic time was 0.1 h, which is a very fast rate for achieving equilibrium partitioning. This indicates a fast sorption that can compete with pollutant removal from air by means of ventilation strategies, and therefore can partially explain why the evaporation rates were unaffected by sorptive material properties.

Table 5.2: TMPD-MIB properties

Empirical Formula	MW[a] $\left[\frac{g}{mol}\right]$	P_{vp}[a] @ 20°C $[mmHg]$	T_b[a] $[°C]$	H[b] @ 25°C $\left[\frac{atm \quad m^3}{mol}\right]$	$\log(k_{ow})$[b] [–]	$\log(k_{oa})$[c] [–]
$C_{12}H_{24}O_3$	216.32	0.01	254	8.21×10^{-8}	3.47	8.95

[a] Reference: (Eastman 2008).
[b] Reference: (SRC 2009).
[c] Estimated as $k_{oa} = \frac{k_{ow}(RT)}{H}$ in accordance to (Meylan and Howard 2005)

Mass transfer coefficients for TMPD-MIB were estimated using data from Table 5.1 and Appendix Equations G.1-G.4. The calculated mass transfer coefficients ranged from 5.7-6.6 $\frac{m}{h}$. In comparison, these values were larger than the ozone mass transfer coefficient values (2.2-5.2 $\frac{m}{h}$) obtained for indoor environments by Morrison et al. (2003). However, the differences in the mass transfer coefficients found, might be explained due to differences in air speed and source dimensions of the TGA experiments.

The obtained rates for TMPD-MIB emitted after paint application were nearly two orders of magnitude smaller than the rates obtained for pure TMPD-MIB application. These slower rates are the result of retardation due to transport diffusion out of a dried pigment/polymer film. For the semi-gloss and the flat paints, the TMPD-MIB evaporation rates can be found in the last two columns of Table 5.1. With these rates , the estimation of the mass transfer coefficient results in values in the range of 0.06 to 0.41 $\frac{m}{h}$. Therefore the 2LM model mass transfer coefficient of TMPD-MIB can be adjusted to account for differences between the TGA experiments and the experimental data obtained by (Lin 2006).

5.3 Paint drying and PVC

The isothermal TGA results of the aluminum paint drying experiments, followed Method 1 for paint application during a drying period of 24 hours as shown in Figure 5.2. Experiments were performed with three replicates, but only two sets were plotted to ease the visual inspection of Figure 5.2. The compositions of the paints used in these experiments are summarized in Table 4.1. The three paints contained different amounts of PVC, with the flat paint and the eggshell containing higher amounts of PVC than the high gloss paint. The reproducibility of the experiments and the percentage of mass loss during the wet phase (t<30 min) resulted in a correlation coefficient >0.99 for the three different paints.

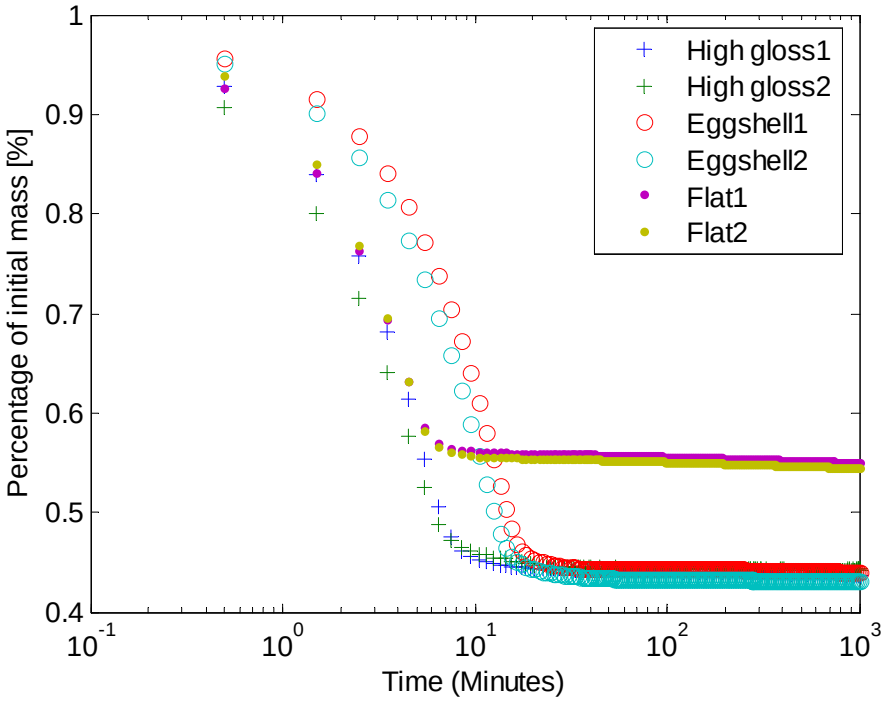

Figure 5.2: Percentage of paint mass remaining in aluminum.

No differences were found in the drying of the paints with respect of the amount of polymer in the paint formulation. All paints were found to lose water at a constant rate of 0.698 $\frac{kg}{hm^2}$. The evaporation rate of the water from the paint was 0.83 times the evaporation rate of pure water when tested under the same conditions (water applied to aluminium). This result agrees very well with Croll (1986) findings, whose research concluded that water evaporated from latex paint at a constant rate of 0.85 the rate of pure water evaporation.

After the water has left the paint, estimates of the TMPD-MIB evaporation rates were made for each paint. These estimates were obtained after by calculating the slopes of the curves shown in Figure 5.2 when water is no longer present in the film (i.e., after t > 1 hour). The obtained values resulted in evaporation rates that varied from 0.03-0.05 $\frac{mg}{hm^2}$. These rates are in the same range of values as the rates found for the semi-gloss paint studied in section 5.2. In the present study, water evaporation rates were similar for all the analyzed paints. Although experiments with more paints is necessary to make generalizations, the findings of this study are in agreement with Lin (2006) who found that recovery of TMPD-MIB in air for an HPVC paint was greater than that of an LPVC paint.

5.4 Internal distribution of TMPD-MIB in gypsum board

The distribution profile of TMPD-MIB inside the material was estimated following the method for concentration profile in porous substrate (TGA and GC) described in section 4.3. Figure 5.3 shows the change in the fraction of initial mass remaining in

the gypsum board as a function of temperature increase. The mass loss of the slice of a gypsum core was assumed to be proportional to the loss of TMPD-MIB present in the gypsum slice. It was also assumed that the gypsum sample was homogeneous and that water loss was the same for all the sliced gypsum samples. Differences between samples were established by comparing results from the weighing experiments from slices of painted and unpainted gypsum board.

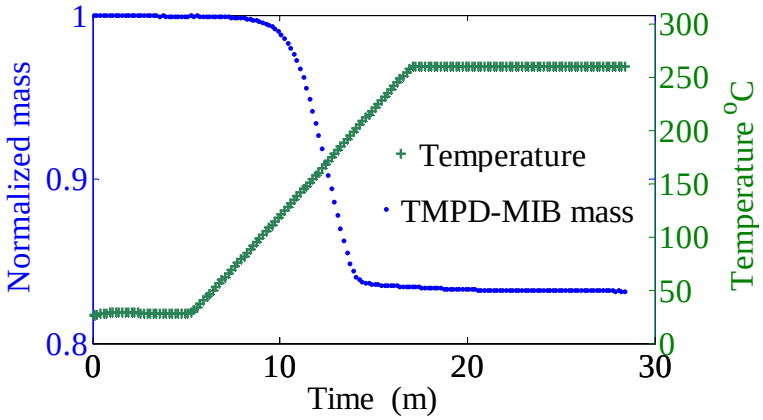

Figure 5.3: Gypsum mass loss with temperature increase.

Figure 5.4 summarizes the results for the unpainted gypsum (blank), and for gypsum painted with the semi-gloss and flat paints. Additionally, a 10:1 magnification of the vertical axis was provided for each of the cases to highlight the fraction of initial mass remaining for each core at the end of the temperature ramp. The results of Figure 5.4 are labeled using the same notation described in Figure 4.4 in which top and bottom are the outer sides of the gypsum that are attached to paper backing. The fraction of mass remaining in the gypsum samples was recorded for 30 minutes as the temperature increased. Figure 5.4 shows the results for the unpainted gypsum (blank), and for gypsum painted with the semi-gloss and flat paints.

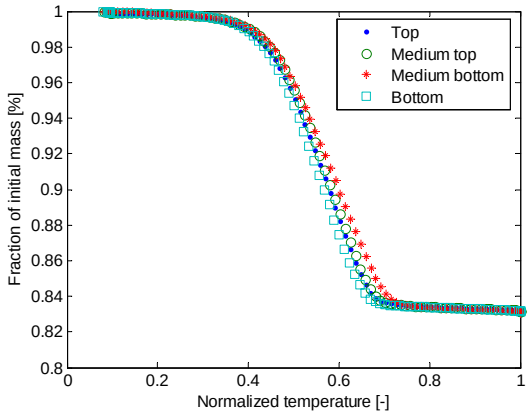

(a) Unpainted gypsum (blank)

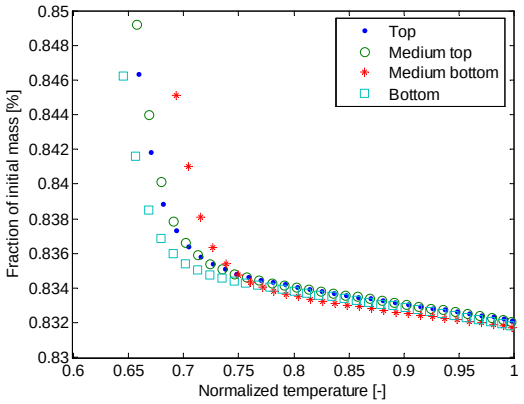

(b) Magnified unpainted gypsum (blank)

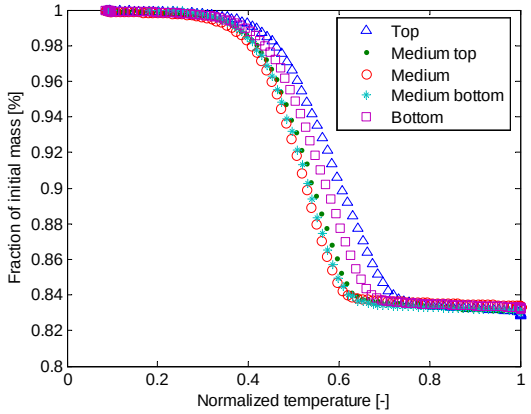

(c) Gypsum painted with semi-gloss paint

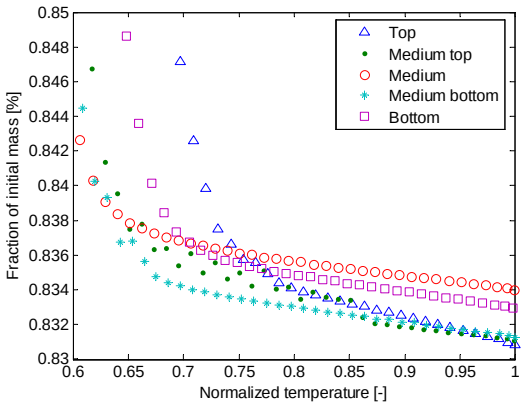

(d) Magnified gypsum painted with semi-gloss

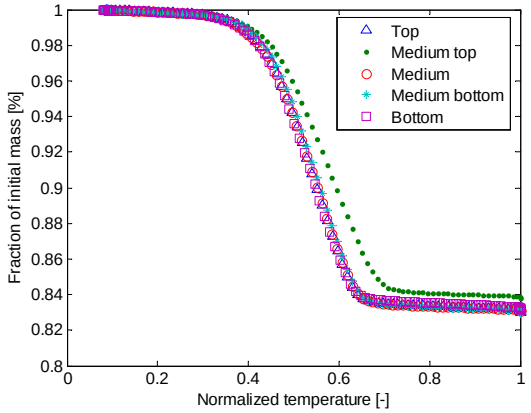

(e) Gypsum painted with flat paint

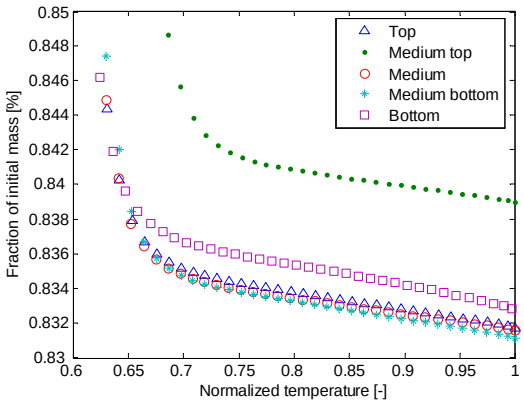

(f) Magnified gypsum painted with flat paint

Figure 5.4: Gypsum mass fraction after temperature increase.

The results obtained from the blank experiments shown in Figures 5.4(a) and 5.4(b) suggest that the gypsum board tested can be considered uniform since the temperature increase affected the samples equally, and no significant variations on mass loss throughout the depth of the gypsum core were detected. Results for the samples painted with semi-gloss paint from Figure 5.4(c) and 5.4(d), show that the fraction of initial mass varied from sample to sample. This indicates that the uniform trend that was obtained for the blank experiment was affected by the addition of the paint. The scattered results suggest a higher reduction of mass for the top and medium layers of the gypsum probably due to the presence of TMPD-MIB in this layer. However, since this was a gravimetrical method, it is indistinguishable if this differences are due to the presence of TMPD-MIB, or other paint components that might migrate from the paint layer into the gypsum.

It is interesting to note that the results obtained for the flat paint were dissimilar to those from the semi-gloss paint, as shown in Figures 5.4(e) and 5.4(f). The results for the gypsum painted with the flat paint were more uniform as it was for the blank experiment, except for the sample located at the medium top of the core sample. This deviation was unexpected since a larger than average mass remained in this layer. Subsequent duplicate experiments also resulted in a higher than average mass at the end of the temperature ramp. A reason for this abnormal behavior could be partially explained since the flat paint contains more pigment and water than the semi-gloss paint, therefore small TiO_2 or solid filler particles could have permeated from the paint layer through the paper and into the gypsum during the wet phase of the paint drying. This increment in the mass of the layer will reduce the volatile content available for evaporation and thus increasing the fraction of initial mass left

in the medium top layer.

5.5 Paint and material recoveries of TMPD-MIB

The differences that PVC content and thickness of the paint layer have on the emissions and fate of TMPD-MIB after paint application on gypsum board were estimated with paint experiments followed Method 2. The thicknesses of the paints used, and recovery results for both paint and material are summarized in Table 5.3. TMPD-MIB distribution after a week of the paint event revealed a higher amount trapped in the semi-gloss paint layer (56%) compared to that found in the flat paint layer (27%), as summarized in the pie charts of Figure 5.5. These pie charts show the comparison of the recovered amounts of TMPD-MIB for paint and gypsum, as well as the expected air emissions that are the portion that should have been emitted to the air and therefore the total mass reported in the pie charts results in a complete mass closure for TMPD-MIB

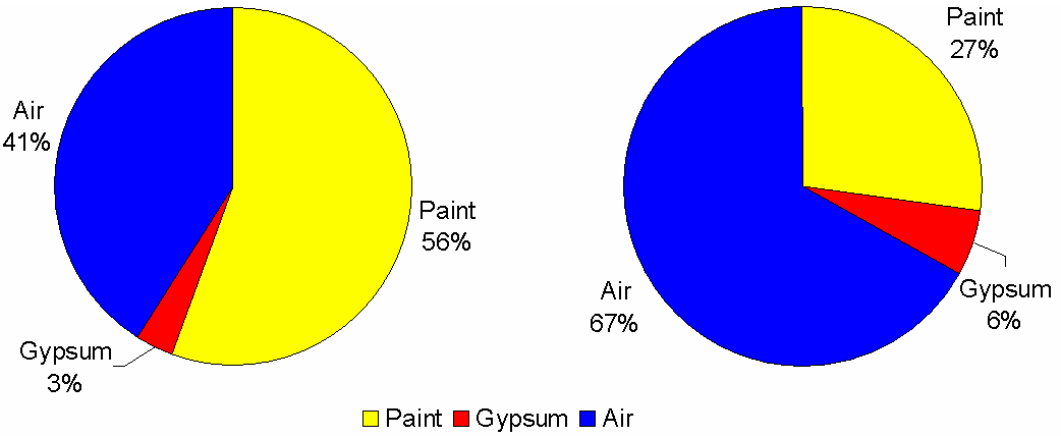

Figure 5.5: TMPD-MIB distribution (after 1 week drying time)

Table 5.3: TMPD-MIB recovery after paint application

Paint type	Thickness μm	Air Drying weeks	Paint Recovery % of initial applied	Gypsum Recovery % of initial applied
Semi-gloss[a]	183	1	55.7	3.1
Flat[b]	160	1	27.4	5.8
Semi-gloss[a]	674	2	71.9	1.1
Flat[b]	266	2	37.9	3.5

[a] PVC of 30, and 1.8% by mass TMPD-MIB.
[b] PVC of 60, and 1.5% by mass TMPD-MIB.

It is interesting to note that the flat paint which contained double the amount of PVC in the semi-gloss paint also nearly doubled the emissions to the air of the semi-gloss paint, while at the same time allowed more TMPD-MIB transport into the material layer. The gypsum material is assumed to be homogeneous, even though its highly interconnected porous structure is hardly uniform, resulting in an overall larger TMPD-MIB diffusion coefficient ($10^{-3}\frac{m^2}{hr}$) compared to that for the paint layer ($10^{-13}\frac{m^2}{hr}$). This significant difference in the transport properties of both layers make the gypsum board a large sink for accumulation of TMPD-MIB transported from the paint layer. The paint layer acts as a barrier for transport of TMPD-MIB out of the gypsum material. This effect can be seen by looking at the higher portion of TMPD-MIB accumulated in the gypsum of the flat paint compared to the semi-gloss paint in Figure 5.5. Therefore, it is highly plausible that the accumulation of TMPD-MIB in the gypsum material is limited by the ease of transport through the paint layer, and not due to other mechanisms like internal sorption.

The TMPD-MIB distribution for the experiments with the thicker set of painted samples that were left to air dry for two weeks can be seen in Figure 5.6. These sam-

ples were painted with as much as three times the amount of paint used in normal applications. However, for practical purposes, is not rare that thicker than usual or multiple paint coats are applied to materials as needed, in order to obtain more paint hiding power.

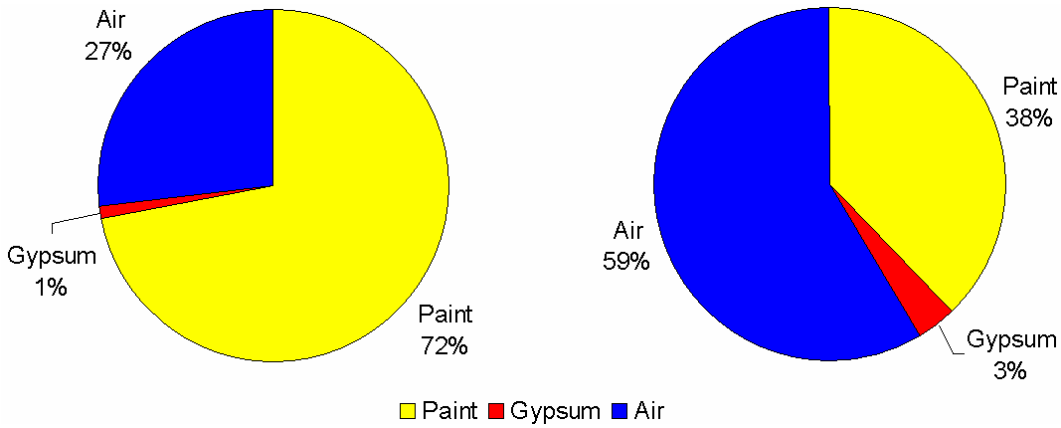

a. Semigloss (674µm) b. Flat (266µm)

Figure 5.6: TMPD-MIB distribution (after 2 weeks drying time)

The objective of these experiments was to isolate paint thickness effects on TMPD-MIB fate. The results obtained indicated that the total amount recovered from the samples with thick paint application increased compared to the samples with thin application. Most importantly, the amount recovered in the gypsum board was reduced as it can be seen from the comparison of Figures 5.5 and 5.6. This reduction clearly shows that as the amount of polymer per area applied is increased, the film formed retains a higher amount of TMPD-MIB.

5.6 Assessment of validation experimental data

Model validation was in part based on previous TMPD-MIB small chamber experiments completed at the University of Texas (Lin 2006, Lin and Corsi 2007). Ex-

perimental data for short and long-term emissions of TMPD-MIB following paint applications were obtained for periods as long as 16 months. Experimental data for gypsum board and simplified HPVC and LPVC latex paints collected in their study was used to estimate parameters such as the diffusion coefficient. TMPD-MIB diffusion coefficient values are not available in the currently published literature. In order to test that conditions in which those experiments were performed resembled a well mixed chamber, their steady state assumption[1] was checked using Computational Fluid Dynamics (CFD). A Digital image of the chamber used in their experiments appears in Figure 5.7.

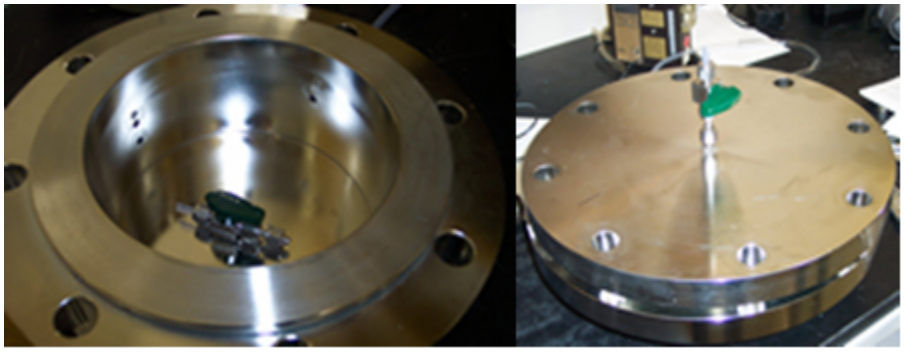

Figure 5.7: Digital image of experimental chamber.

The geometry and mesh used for the simulation of this chamber was constructed in AIRPAK, and is shown in Figure 5.8. CFD simulations of the airflow and mass concentration profile were performed.

Figure 5.9 shows a summary of the vertical velocity and molar concentration profiles inside the chamber at exactly the mid point of the chamber during and after sample collection. In Figure 5.9(a), the air velocity profile is shown for the case in

[1]The samples of Lin and Corsi (2007) were left inside the chamber for some period of time (on average 2 hours) to assure well mixing. The CFD simulations validated their well mixing condition assumption

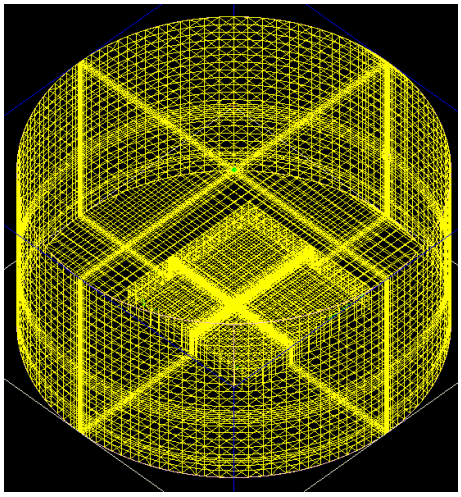

Figure 5.8: Geometry and mesh for CFD simulation.

which the material was emitting at a constant rate and the air exchange rate (ACH) was $1.5\frac{1}{hr}$. The black rectangular area represents the material placed inside the chamber. The steady state airflow distribution takes the form of two ovals in which the maximum air velocity of 1×10^{-3} $\frac{m}{s}$ is comprised by the red region. This oval shape is caused by the inlet (right) and outlet (left) extrusions.

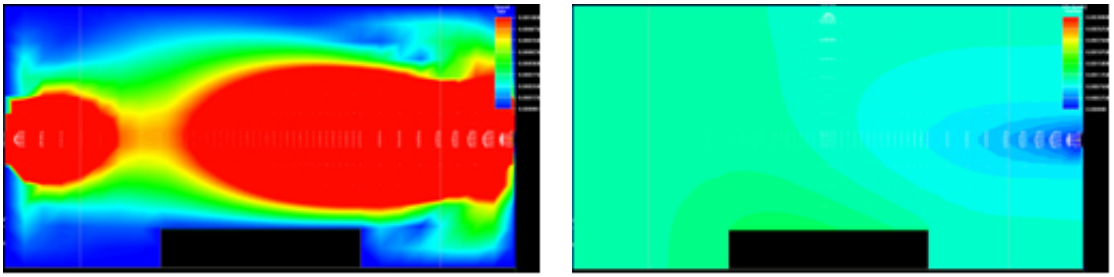

(a) Air velocity profile before sample extraction (b) Concentration profile with constant emission from material before sample extraction

Figure 5.9: CFD simulation of experimental chamber before sample collection.

Figure 5.9(b) shows that the mole fraction of pollutant is slightly higher in the area near the material at a maximum value in green of 0.0015, and the area near the

inlet is the more diluted (blue), while the overall chamber concentration is uniformly distributed. When the sample was taken[2], the outlet on the left side of the chamber was closed and the sample was collected through the top outlet which was previously closed. The results for this simulation appear in Figure 5.10, and the air velocity profile has shifts from that in the previous air flow pattern due to the change in the exhaust point. When the sample was being extracted for 5-25 minutes, the two oval shapes disappeared, but the molar concentration profile keeps the same shape that it had before the sample extraction with only a slightly more uniform concentration reflected in the lighter colors surrounding the material as shown in Figure 5.10(b). Uniform mixing of both airflow and pollutant concentration was verified via CFD simulations.

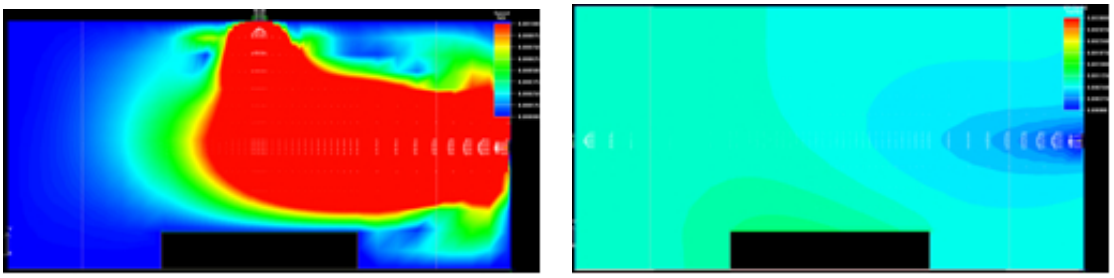

(a) Air velocity profile during sample extraction (b) Concentration profile with constant emission from material during sample extraction

Figure 5.10: CFD simulation of experimental chamber during sample collection.

After the performed CFD simulations, it was concluded that the experimental method used in (Lin 2006) was adequate and therefore the experimental data obtained did not have any biases due to non-uniformities of airflow distribution inside the chamber, making the TMPD-MIB experimental data collected useful for validation

[2]When sample was extracted, a port in the upper part of the chamber was used to collect the sample during approximately 5-25 minutes

and comparison with the predictions of the 2LM. Some portion of Lin's experimental data was used for model validation will be presented in Chapter 6, while a different set of his data was used for model prediction, and results are given in Chapter 7.

Chapter 6

Model Validation

6.1 Introduction

In this chapter, validation of the model was evaluated by different methods. Comparison with an analytical solution is presented in Section 6.2, comparison of the 2LM previous publish models appears in Section 6.3. Validation with experimental data from (Lin 2006) is given in Section 6.4.

6.2 Analytical solution

An analytical solution appropriate for a constant paint film L_2 was used to initially calibrate the numerical solution of the proposed two-layer model. The surface flux out from the paint into the air is given by:

$$j_A(t)\Big|_{z=b} = D_{eff_{L1}} \sum_{n=1}^{\infty} \frac{1}{N(\beta_n)} I_o(\beta_n) \frac{\partial \Psi_{L_1}}{\partial z} exp\left[-(\beta_n^2 t)\right] \tag{6.1}$$

Where $\Psi_{L_1}(\beta_n, z)$ and β_n are the eigenfunctions and eigenvalues, respectively. Their values are found using the system's boundary conditions. A more detailed description of the analytical solution for a two-layer composite system can be found in Appendix B. This analytical solution works particularly well for long-term approximations (i.e. as time goes to infinity) due to the nature of the solution. The number of eigenvalues used for the solution is typically selected as 50. However, this number has to be increased (increasing computation time) in order to obtain a better approximation. This solution is also constrained by the fact that the diffusion coefficient is constant as the paint film dries, and therefore was used to compare with the results of the 2LM (Case I). Such constraint of the analytical solution is not present for the numerical solution of the 2LM, where both the thickness and diffusion coefficient can be varied to account for changes in the drying of the film as obtained for Case II.

6.2.1 Analytical solution sensitivity

A sensitivity analysis of the analytical solution was necessary since the solution will be dependent on the number of eigenvalues used. The typical number of eigenvalues used for the chosen analytical solution is 50. However, the analytical solution was found to be affected by the number of eigenvalues used in the simulation. In Figure 6.1, these differences are apparent. The emissions increase as the number of eigenvalues is increased, particularly in the initial phase for time less than 30 hours. However, it was found that after 400 eigenvalues, further increases in the number of eigenvalues used did not result in emission changes. Selection of at least 200 eigenvalues was needed in order to obtain similar results to the 2LM.

Close to time zero, the differences between the 2LM and the analytical solution can be as large as 60% depending on the number of eigenvalues selected for the

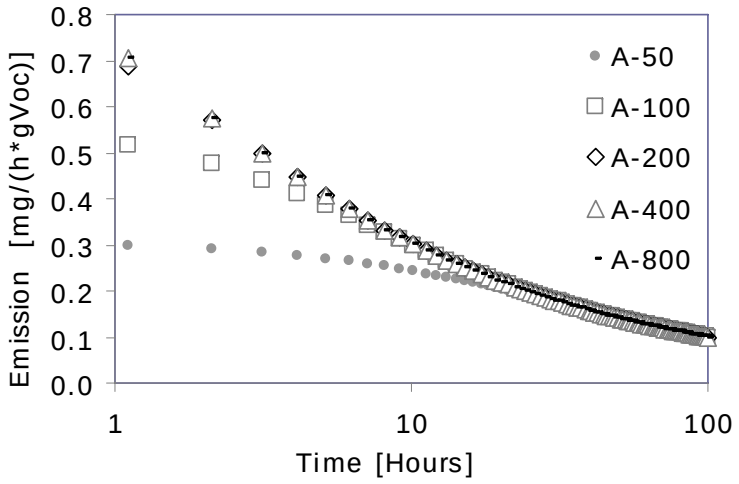

Figure 6.1: Analytical solution changes with number of eigenvalues used.

solution. The numerical integration of these differences is compared in Table 6.1. When compared with the case of largest number of eigenvalues, the 2LM is within 6% of the results of the analytical solution for the times between 0 and 12 hours, resulting in a root mean square error of only 1.7%. In the overall time scale for the simulation, after hour 12, the numerical integration of all the cases yields 0.19 except for the case of 50 eigenvalues. The 2LM shows an overall good fit to the analytical solution, and slightly under predicts the emissions at short times when compared to the case of analytical solution with 400 and 800 eigenvalues.

Table 6.1: Numerical integration of emissions (mg/g).

Time	Numerical	Analytical				
	2LM	50 Eigenv.	100 Eigenv.	200 Eigenv.	400 Eigenv.	800 Eigenv.
0-12	0.66	0.06	0.27	0.59	0.70	0.70
12-100	0.19	0.14	0.19	0.19	0.19	0.19
Total	0.84	0.20	0.46	0.78	0.89	0.89

The logarithmic scale for time in Figure 6.1 highlights the differences particularly for the initial period of the simulation. The differences in the emissions from Figure 6.1 affect the final vertical concentration profile for both the paint and the material layer. These differences reflect inherent errors associated with each solution method. The analytical solution uses a range of significant eigenvalues to approximate the infinite summation from Equation 6.1. The analytical solution works better as time goes to infinity, as shown in Figure 6.1. Further exploration of Equation 6.1 reveals that the exponential term of the solution becomes negligible as time goes to infinity. After time equals 30 hours, both trends for the analytical and 2LM solution match irregardless the number of eigenvalues (> 50) selected for the analytical solution.

6.2.2 Model comparison with analytical solution

The sensitivity analysis from Section 6.2.1 revealed that a large number of eigenvalues is needed in order to obtain an accurate solution at the beginning of the simulation period. Therefore 400 eigenvalues were used to make comparisons between analytical and 2LM solutions. An initial validation of the model was made using the following input parameters: diffusion coefficients for both layers, mass transfer coefficient, mass of the paint, density of paint, area of application and mass fraction of compound. Simulation parameters for the 2LM are listed in Table 6.2, using $\Delta t = 0.1h$, and 800 nodes for the paint layer.

The results of the 2LM compared favorably to the analytical solution as shown in Figure 6.2. Minor differences during the initial simulation period did not affect the overall trend in emissions for long times as expected.

Table 6.2: Simulation parameters.

Parameter[c]		Value
Diffusion coefficient (paint layer)	[m^2 h^{-1}]	10^{-11} to 10^{-13}
Diffusion coefficient (material layer)	[m^2 h^{-1}]	7×10^{-3}
Mass transfer coefficient (TMPD-MIB)	[m h^{-1}]	0.21
Paint density[a]	[g mL^{-1}]	1.25
Mass fraction of TMPD-MIB[a]	[−]	0.015
Area of application	[m^2]	64×10^{-4}
Mass of paint applied [b]	[g]	1

[a] Paint characteristics of a Semi-gloss paint used by (Lin and Corsi 2007).
[b] Hypothetical mass applied to obtain a typical wet paint film of 150 μm.

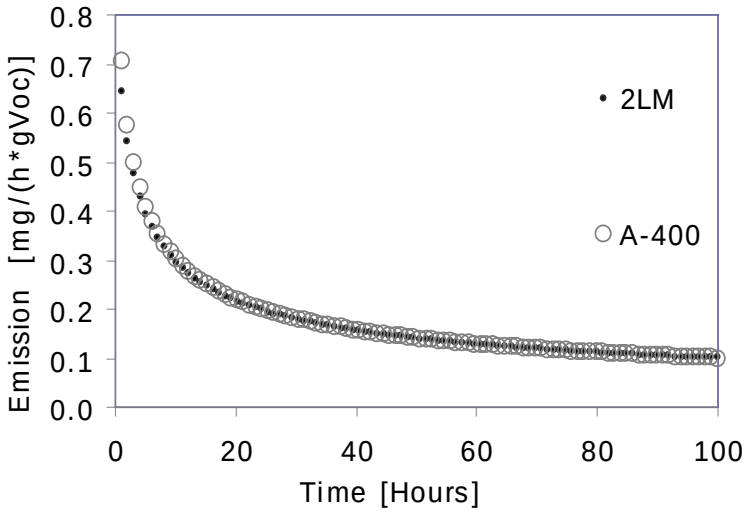

Figure 6.2: Comparison of 2LM and analytical solution with 400 eigenvalues.

6.3 Comparison with published models

Two of the most widely used models to predict emissions from latex paints (Chang and Guo 1992, Sparks et al. 1999) were used for comparison with the 2LM. The experimental data used for comparison of the models was a 277 μm HPVC paint film

obtained by Lin (2006) with characteristics summarized in Table 6.5. Parameters for each model were calculated, and results of the compared models are shown in Figure 6.3.

The first model was developed by Chang and Guo (1992), takes into consideration wet and dry-stage emissions in a simple empirical model. This model can be regarded as a second-order decay model which is obtained from a mass balance in which double-exponential decay parameters are fitted to experimental data. The VOC emissions can be calculated using Equation 6.2 as follows:

$$R(t) = R1 + R2 = R_{10}e^{-k_1 t} + R_{20}e^{-k_2 t} \tag{6.2}$$

where R_1 and R_2 are the area specific emission rates in $\frac{mg}{m^2 h}$, and k_1 and k_2 are the emission rate decay constants of phase 1 and 2 in h^{-1}. Model parameters for the Chang and Guo model were calculated by non-linear regression. The Matlab source code used for this model can be found in Appendix D. The results of the non-linear regression and parameters obtained are summarized in Table 6.3.

A second model developed by Sparks et al. (1999) was used for comparison. This is a very highly cited model for predictions of VOCs from latex paints. Based on experimental data and the mechanistic behavior observed in previous latex paint experiments, Lin (2006) believed that the model introduced by Sparks et al. (1999) was best suited for future analyses based on the fact that it attempts to capture both short-term evaporation and long-term diffusion in a mechanistic fashion. This

Table 6.3: Chang and Guo model parameters obtained for best fit to an LPVC paint.

Parameter	Value
R_{10}	2.51
R_{20}	0.06
k_1	0.0329
k_2	0.0001
R^2	0.98
rmse	0.06

model is based on the assumption that short term emissions are gas-phase-limited, while long-term emissions are source-phase limited (diffusion limited). The combined model has three parts: the VB model (Tichenor et al. 1993) for gas-phase limited emissions, a diffusion term developed by (Hanna and Drivas 1993), and the adjusting term $\left(1-\frac{M_v}{M_{vo}}\right)^2$ for the transition region. The VOC emissions can be calculated with Equation 6.3 as follows:

$$R(t) = k_m\left(C_{vo}\frac{M_v}{M_{vo}} - C\right) + \left(1-\frac{M_v}{M_{vo}}\right)^2 f_{D1}M_D t^{-\frac{1}{2}} \tag{6.3}$$

where R(t) is the emission rate at time t in $\frac{mg}{m^2h}$, k_m is a gas-phase mass transfer coefficient in $\frac{m}{h}$, C_{vo} is the vapor pressure expressed in concentration of a VOC in $\frac{mg}{m^3}$, M_v is the emittable mass for evaporation at time t in $\frac{mg}{m2}$, M_{vo} is the initial emittable mass for evaporation in $\frac{mg}{m^2}$, C is the chamber concentration at time t in $\frac{mg}{m^3}$, f_{D1} is an empirical factor in $h^{\frac{1}{2}}$, and M_D is the emittable mass for diffusion at time t in $\frac{mg}{m^2}$. The only parameters that need to be estimated from the chamber data are C_{vo}, M_{vo}, and f_{D1}. These parameters can be estimated by solving the mass balance equations

of the chamber.

$$\frac{dC}{dt} = -NC + LR(t) \tag{6.4}$$

$$\frac{dM_v}{dt} = -k_m \left(\frac{C_{vo} M_v}{M_{vo}} - C \right) \tag{6.5}$$

$$\frac{dM_D}{dt} = -\left(1 - \frac{M_v}{M_{vo}}\right)^2 f_{D1} M_D t^{\frac{1}{2}} \tag{6.6}$$

where N is the ACH, L is the chamber loading (area of the source/volume of the chamber). The initial conditions are: M_{T0}=2500 $\frac{mg}{m^2}$ (16 mg of TMPD-MIB applied on a material of $64 \times 10^{-4} m^2$), M_v=M_{vo}, and M_D=M_{Do}=M_{To}-M_{vo}. Parameters for the Sparks model were obtained by solving Equations 6.3-6.6. The Matlab source code used for solving this model equations can be found in Appendix E. The parameters used in this model are summarized in Table 6.4.

Table 6.4: Sparks model parameters obtained for best fit to an LPVC paint.

Parameter	Value
C_{vo}	25
M_{vo}	180
f_{D1}	0.00044
k_m [a]	0.2
rmse	0.15

[a] Estimated from (Lin 2006) experiments.

The results for the 2LM prediction together with the experiment results and model predictions from the other models is shown in Figure **??**. The results of Chang & Guo's model were the closest to the experimental data, and resulted in a RMSE=0.06. However, as noted above, their empirical model lacks a mechanistic approach. Furthermore, this model slightly over predicts the emissions at intermediate

times while agreeing well during the initial 100 hours as well as from 500-4000 hours. Inspection of the parameters obtained, reveals that the ratio of the time constants k_1 (0.0329) and k_2 (0.0001)is 329. This large ratio indicates that k_2 is dominant and therefore the double exponential could be replaced with a single exponential model.

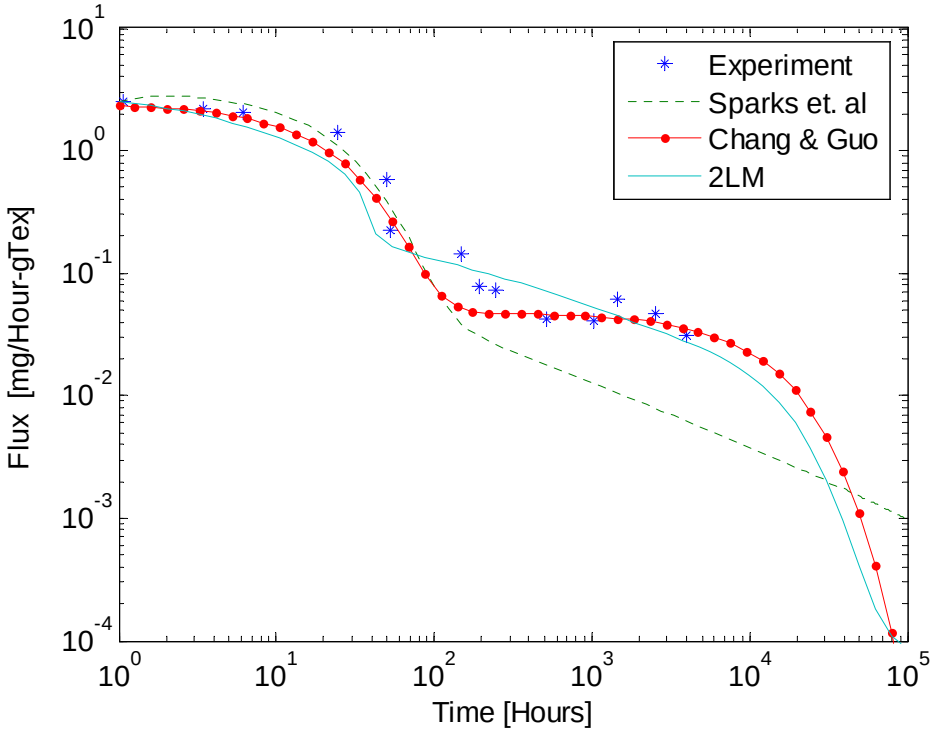

Figure 6.3: TMPD emission comparison of different models.

On the other hand, the Sparks model worked well for short-term emissions, but deviated from the experimental results shortly after the dried period started (after 50 hours). This deviation is caused by the term $f_{D1}M_D t^{\frac{1}{2}}$ which is constrained to the M_D value that depends on the initial condition M_{To}. Since the term f_{D1} obtained was small, the TMPD-MIB emissions were under-predicted from hour 50-4000, and therefore could not be very reliable for long term predictions of TMPD-MIB. The estimation of at least three parameters is required for each sample analyzed.

The approach taken in the 2LM is semi-mechanistic in the sense that it requires the fitting of a single parameter (diffusion coefficient of paint layer). Once the estimation of this parameter is made via fitting to experimental data, the same diffusion coefficient can be used to predict emissions of the same type of paint applied with different paint thicknesses. Furthermore, this parameter was found to be correlated with PVC content of the paint, but further experiments are required to be able to derive a mathematical expression that can be used to independently estimate the paint diffusion coefficient. The RMSE for the 2LM prediction was 0.08, and details of this prediction will be further discussed in the following sections. The overall results of the 2LM agreed fairly well with experimental data for short and long term emission predictions.

A prediction with the three models was estimated up to 100,000 hours or 11.4 years. While both Chang and Guo exponential model, and the 2LM behave as a three time phase models, the Sparks model continues decaying with a two time phase approach. At the end of the simulation period the three models predict emissions within an order of magnitude of each other. However, Sparks model under predicts as mentioned above. It is unclear whether a three phase behavior is present in the experimental data, particularly since Lin's experimental data contained a fractional uncertainty of 35% as time increased.

6.4 Experimental data from small chamber experiments

6.4.1 Parameters

The mass transfer coefficient (kc) for water was estimated to be 0.72 $\frac{m}{h}$ based on experimental conditions described by Lin (2006). The TMPD-MIB mass transfer coefficient, ka, was estimated by the square root of the ratio of the molecular weight of water vapor and TMPD-MIB, yielding a value of 0.21 $\frac{m}{h}$ for ka, using :

$$k_c = k_a \sqrt{\frac{Mw_T}{Mw_{wv}}} \tag{6.7}$$

A value of 7×10^{-3} $\frac{m^2}{h}$ was used for the TMPD-MIB effective diffusion coefficient for gypsum board (D_{AL2}). This value was estimated from the sulfur hexafluoride diffusion coefficient in gypsum board reported by Corsi et al. (2005), using the square root factor shown in Equation 6.7. Paint characteristics are summarized in Table 6.5. The two paint formulations shown in Table 6.5 contain different amounts of TMPD-MIB, water, polymer, pigment, and therefore PVC.

HPVC paints are generally characterized as being more "flat." HPVC paints contain more fillers and the film formed is not as homogeneous as that for LPVC paint. The rate of diffusion of TMPD-MIB in latex paint presumably depends upon the ease with which latex polymer chains can exchange positions with the TMPD-MIB penetrant molecules. There are not only limitations of theoretical models for predicting diffusion coefficients for latex paints but also experimental values for the

Table 6.5: Paint characteristics.

Paint Parameter[c]	Low PVC paint	High PVC paint
Water content(%)	20	48
Pigment content(%)	8	15
Polymer content(%)	69 [a]	36 [b]
PVC(%)	18	42
Density (g mL^{-1})	1.254	1.329
TMPD-MIB mass fraction (-)	0.0154	0.0067

[a] Acronal 296d with 50 % solids content.
[b] Flexbond 325 with 55 % solids content.
[c] As reported by (Lin 2006)

diffusion coefficient are very scattered. Additionally, retardation factors of TMPD-MIB transport in latex paint are not available in the published literature. A back calculation of these two parameters was obtained using a best fit of the model described herein to experimental data for latex paint applied on gypsum board. The fit was obtained such that the root mean squared error (RMSE) as calculated with Equation[1] 6.8

$$RMSE = \sqrt{\sum_{i=1}^{i=X} \frac{e_i}{X}} \tag{6.8}$$

$$e_i = (Em_i - Ee_i)^2 \tag{6.9}$$

Where

X is total number of experimental data points,

Em_i is the model prediction (emission factor) data point,

Ee_i is the experiment (emission factor) data point.

[1]The emission factor (Ee_i), was obtained from the experimental data from (Lin 2006). The fminsearch function from Matlab was used in the error minimization.

6.4.2 Constant diffusion coefficient (Case I)

Typical single coating paint film thicknesses are in the range of 100-150 μm. For this reason, experimental data for samples with a film thickness of 134 μm for an LPVC paint and 139 μm for an HPVC paint were selected for estimation of the diffusion coefficient. Best fit results are presented for a Case I, where the diffusion coefficient D_{L1} is assumed to be constant. Results for LPVC and HPVC paints appear in Figures 6.4 and 6.5, respectively.

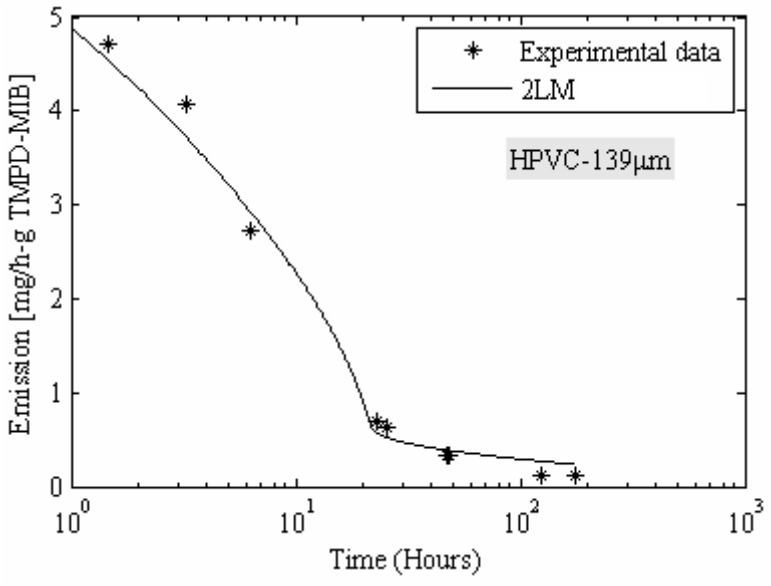

Figure 6.4: Best fit results for LPVC (Case I).

The emission factor expressed in $\frac{mg}{h-g}$ were in all cases normalized by the initial amount of TMPD-MIB applied in order to better account for differences in the TMPD-MIB content of the paint mixtures. Differences in TMPD-MIB emissions of the two types of paints are apparent in Figures 6.4 and 6.5. TMPD-MIB emissions from HPVC paint decay faster than from LPVC paint. The diffusion coefficient (D_{L1})

was found to be on the same order of magnitude for both paints, while the retardation factor was nearly an order of magnitude greater for the LPVC paint. This might be explained by the larger amount of polymer present in LPVC paints. Although the coefficient of determination (R^2) was above 0.90 for both types of paint, the root mean square error (RMSE) was lower for the LPVC than for the HPVC paint. This might be due to the fact that LPVC paint behaves more uniformly as the paint film dries, while the HPVC paint is more prone to cracks and irregularities due to its physical composition.

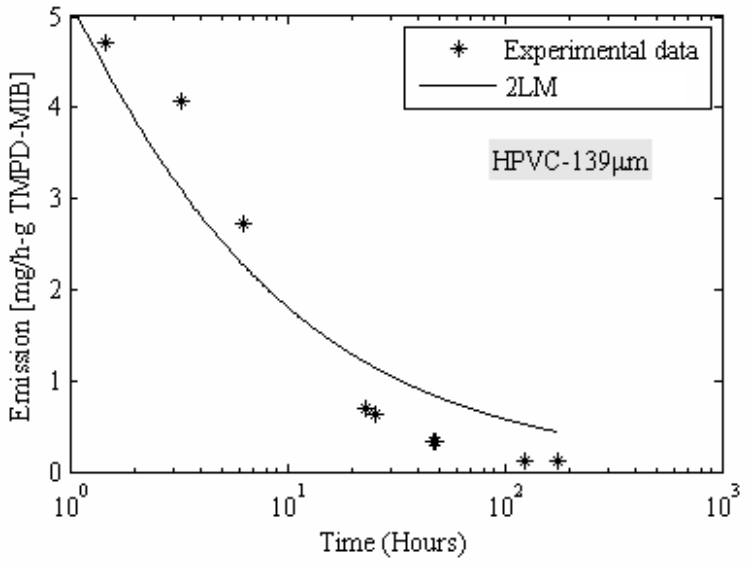

Figure 6.5: Best fit results for HPVC (Case I).

The polymers of the paints used in this research are the result of the copolymerization of two monomers. Both paints used butyl acrylate, but their second monomer is different. The LPVC paint used styrene, and the HPVC paint used vinyl acetate. Physical characteristics between these two compounds are very different even though their molecular weights are comparable. Their octanol-water partition coefficient are

very different. For example, the log kow for vinyl acetate is 0.67, nearly five times smaller than that of styrene (2.95). The solubilities in water are also nearly two orders of magnitude larger for vinyl acetate compared to the value for styrene, and the vapor pressure of 89.1 mm Hg of vinyl acetate is also higher than the 5 mm Hg for styrene. These physical properties can make differences in the binding of the paint, affecting the transport mechanisms of TMPD-MIB in the latex paint.

6.4.3 Variable diffusion coefficient (Case II)

Best fit results are presented for a Case II, where the diffusion coefficient is assumed to vary linearly as a function of the time required for the water to completely evaporate from the paint film. The rate of water depletion from the liquid paint is used to develop an estimate of the water evaporation time t_{evap} using Equation 3.16 in conjunction with a linear function that represents the dynamic behavior of the diffusion coefficient as shown in Equations 3.17 and 3.18. The fit obtained with case II for the LPVC paint can be seen in Figure 6.6.

For this case, the diffusion coefficient of the LPVC paint decreased linearly from 1.5×10^{-5} to 3×10^{-3} $\frac{m^2}{h}$ with a t_{evap} of 7.3 hours, resulting in an RMSE of 4.2, lower than the RMSE of 8.6 for Case I. In contrast, the best fit for the HPVC paint (Figure 6.7) resulted in a slower linear decay for the diffusion coefficient from 1.6×10^{-6} to 1.6×10^{-5} $\frac{m^2}{h}$ with a t_{evap} of 21.6 hours. For this case, the R^2 increased to 0.99 from 0.90 in case I, and reduced the RMSE from 51.8 to 15.9.

The higher water content of the HPVC paint leads to more rapid changes in film properties. For Case II, the inclusion diffusion coefficient is proportional to water content of the film and leads to improved estimates of TMPD-MIB emissions

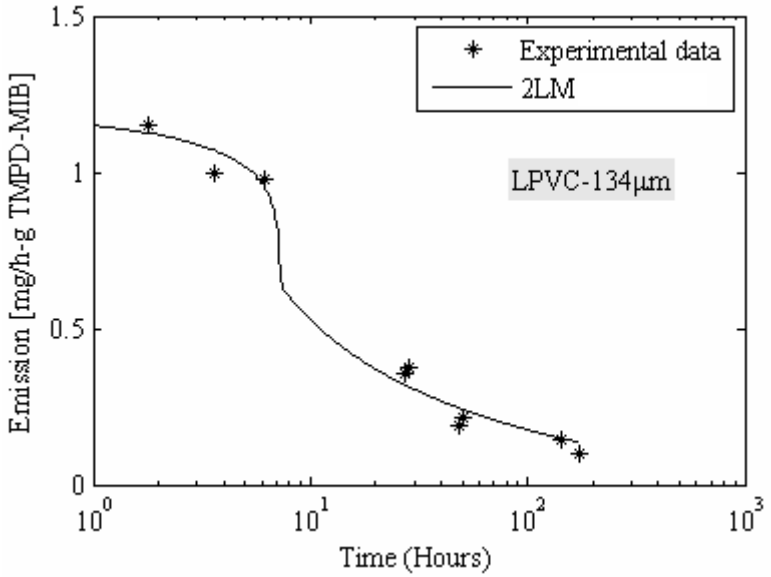

Figure 6.6: Best fit results for LPVC (Case II).

particularly in the initial emissions period. As can be seen from Figure 6.7, the predicted emission in the initial drying period for TMPD-MIB are reduced due to the decrease in the diffusion coefficient of the paint while the water is evaporating ($t < t_{evap}$), resulting in a better fit to the experimental data set in comparison to Case I from Figure 6.5. A summary of the diffusion coefficients obtained as well as the goodness of fit is provided in Table 6.6.

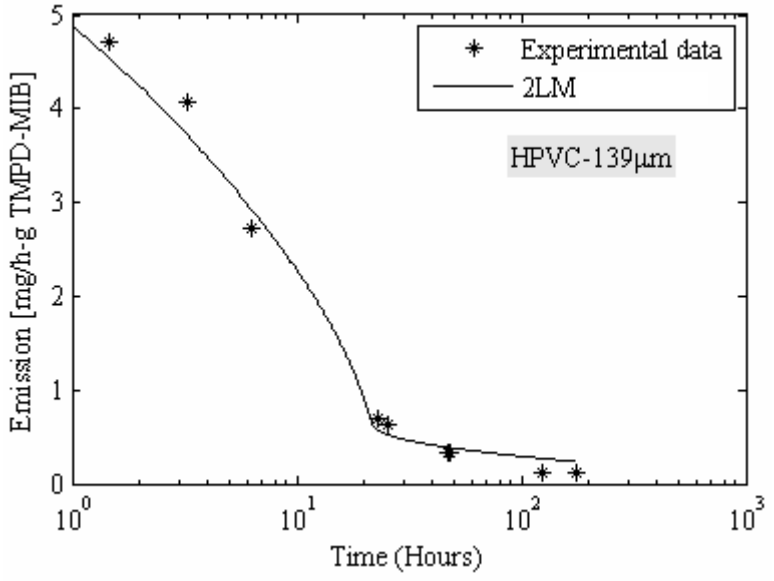

Figure 6.7: Best fit results for HPVC (Case II).

Table 6.6: Parameters obtained from best fit.

Film size $[\mu m]$	D_{L_1} $[m^2h^{-1}]$	R -	$\frac{D_{L_1}}{R}$ $[m^2h^{-1}]$	t_{evap} $[h]$	R^2
134LPVC-I	1.2×10^{-7}	4.5×10^5	2.7×10^{-13}	[b] 7.3	0.95
139HPVC-I	1.9×10^{-7}	9.1×10^4	2.1×10^{-12}	[b] 21.6	0.90
134LPVC-II	[a] $1.5 - 0.03 \times 10^{-5}$	1.3×10^6	$115 - 0.23 \times 10^{-13}$	7.3	0.99
139HPVC-II	[a] $1.6 - 0.16 \times 10^{-6}$	2.1×10^5	$7.6 - 0.76 \times 10^{-12}$	21.6	0.99

[a] Range corresponds to initial and final diffusion coefficient.
[b] Water evaporation time not needed for constant diffusion coefficient case.

Chapter 7

Model Results

7.1 Introduction

In this chapter, the predictive capability of the 2LM is presented. Parameters estimated from the independent data set of paint experiments conducted by Lin (2006) were used in the model to predict emissions. The predictions of emissions and concentration profiles and the comparison of the experimental data with the model prediction are presented in this section.

7.2 Model prediction

The diffusion coefficients for the HPVC and LPVC paints obtained from Section 6.4.1 are used to predict long term emissions of TMPD-MIB for differing thickness of HPVC and LPVC paints. The thickness for the new set of painted samples was 273 μm and 277 μm for LPVC and HPVC paints, respectively. These thicknesses are nearly double the thickness associated with experiments used for parameter estimation. The diffusion coefficients for LPVC and HPVC from Table 6.6 were used. As

it was shown above, Case II captured the physical mechanisms of TMPD-MIB transport for both types of paint. Therefore for the remainder of this chapter, results from Case II were used to show the predictive capabilities of the 2LM. Figure 7.1 shows the results of TMPD-MIB emissions predicted up to 10 000 hours for the LPVC paint, and Figure 7.2 shows the results for up to 4 000 hours for the HPVC paint.

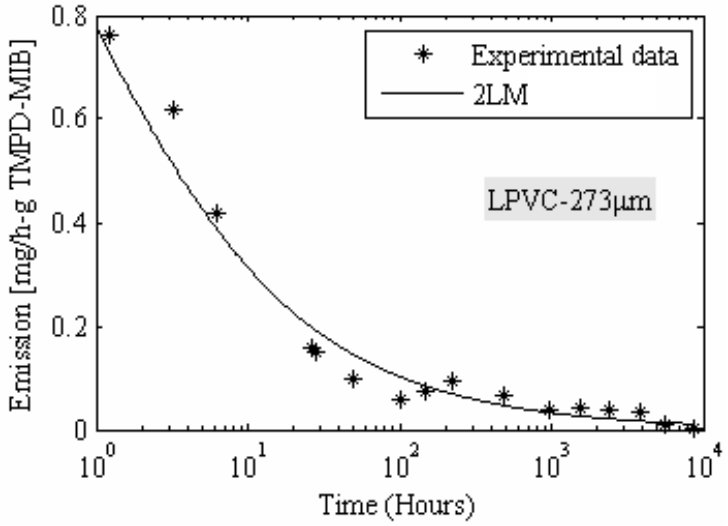

Figure 7.1: Emissions of TMPD-MIB for LPVC paint.

For the LPVC paint, the RMSE was 6.0, and that for the HPVC paint was 16.2. A summary of these results can be found in Table 7.1. Both the experimental data and model predictions indicate two important trends in TMPD-MIB emissions. First, although the mass of TMPD-MIB applied with the HPVC paint was only about one-half that of LPVC paint, its initial normalized emission rate was nearly four times that of LPVC paint (actual emissions from HPVC paint is roughly twice that from LPVC paint). After approximately 150 hours the converse trend occurs, and emission rates from the HPVC become smaller than the rates of the LPVC, presumably since less mass of TMPD-MIB is left in the HPVC paint compared to the LPVC paint.

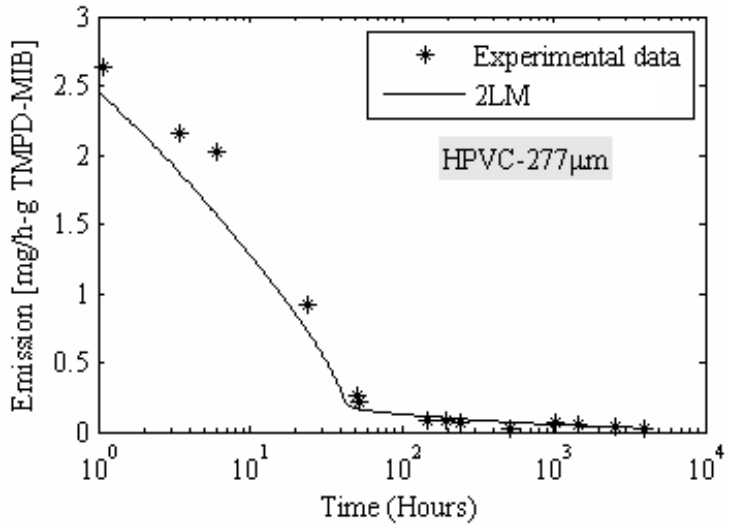

Figure 7.2: Emissions of TMPD-MIB for HPVC paint with a thick paint layer.

Table 7.1: Prediction errors and coefficient of determination.

Film size $[\mu m]$	Case	t_{evap} $[h]$	RMSE -	R^2
273 (LPVC)	II	14.9	6.0	0.93
277 (HPVC)	II	43.1	16.2	0.97

These results suggest the importance of pigment volume concentration on TMPD-MIB emission dynamics, particularly during the transition from a wet to dry film.

Second, model predictions are consistent with experimental results in suggesting that there are long-term emissions of TMPD-MIB from dry paint films. In fact, integration of the modeled emission curve for a typical LPVC paint thickness suggests that only 54% of the initial TMPD-MIB mass applied is emitted after 10,000 hours (1.14 years). This prediction was consistent with experimental findings reported by Lin and Corsi (2007) for an LPVC paint with a 134 m paint film thickness.

7.2.1 TMPD-MIB Concentration profile

The 2LM was used to predict the concentration profile of TMPD-MIB inside both the paint film and the material. Simulations of the concentration profile were obtained for 10, 100, 1 000 and 10 000 hours after the paint event. No significant differences were found in the TMPD-MIB concentration profile for the either paint layer in the initial period after paint application up to 100 hours. The vertical concentration profile (paint and material layers) at different times is shown for the 273 μm and the 277 μm LPVC paints in Figure 7.3. The peak concentration for the paint layer is higher for the LPVC paint (1.95×10^7 $\frac{mg}{m^3}$) compared to the peak concentration for the HPVC paint (9×10^6 $\frac{mg}{m^3}$). The differences in the peak concentration is due to the larger fraction of TMPD-MIB that the LPVC paint contains compared to the HPVC paint.

The paint layer remains almost unchanged for the paint profile during the first hundred hours. However, the TMPD-MIB peak concentration profile occurs near the middle of the paint layer. As time increases, the concentration profile for TMPD-MIB results in a less pronounced peak as shown in Figures 7.3(a) and 7.3(c). A comparison between the two paint layers of the LPVC and HPVC paints, reveals a higher peak concentration for the LPVC paint particularly at 10 000 hours.

The large difference between the magnitude of the diffusion coefficient for paint and material layers results in a uniform concentration profile for the material layer for both paints as shown in Figures 7.3(b) and 7.3(b). Furthermore, there is an increase in the accumulated TMPD-MIB over time in the material layer. These increases are due to the slow migration of TMPD-MIB from the paint layer into the material.

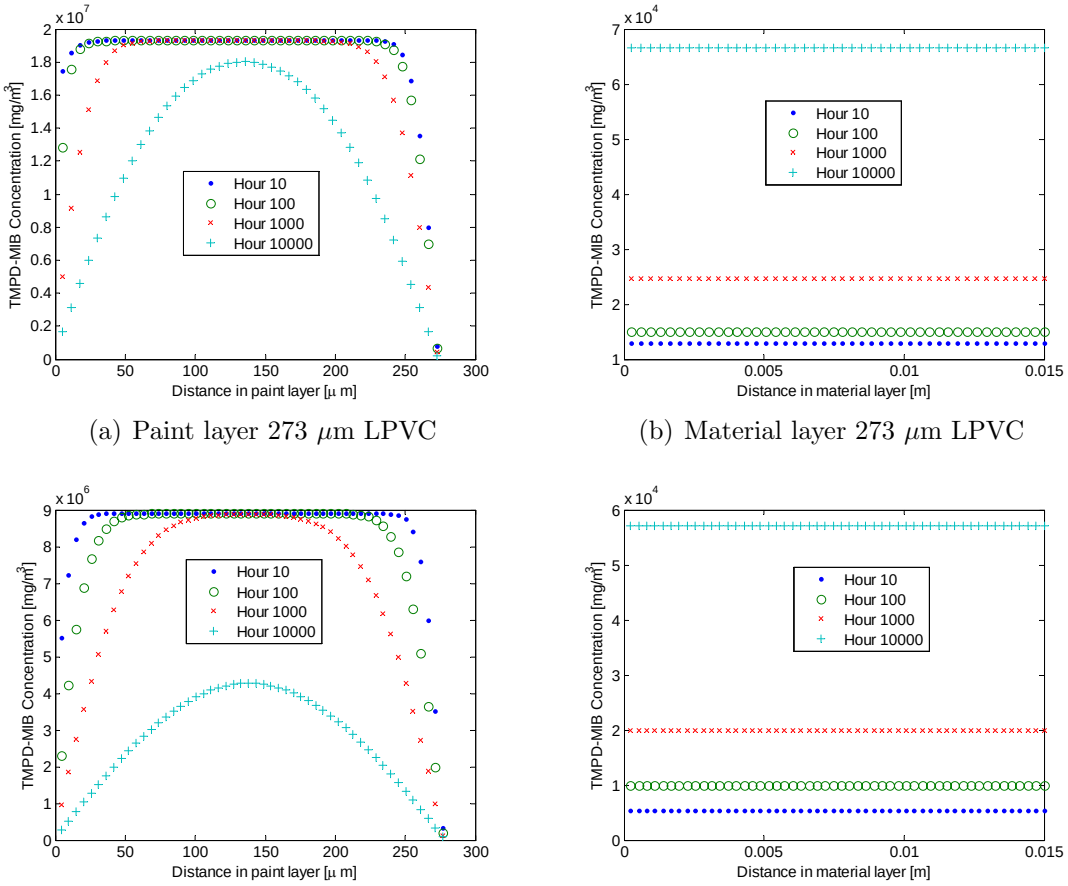

(a) Paint layer 273 μm LPVC

(b) Material layer 273 μm LPVC

(c) Paint layer 277 μm HPVC

(d) Material layer 277 μm HPVC

Figure 7.3: Concentration profile in paint and material layers at different times.

7.2.2 Effects of air velocity on paint emissions

The air velocity over the material surface affects the convective mass transfer coefficient, where the higher the velocity the greater the mass transfer coefficient. The impact of air velocity on the emission rate was analyzed through a parametric study. The short term ($t < 150$) emission rates of TMPD-MIB at four different air velocities are shown in Figure 7.4. The value for the TMPD-MIB mass transfer coefficient was varied over three orders of magnitude, to 100 ka.

Predicted emissions were compared with the experimental base case for the 134 μm LPVC paint experiment reported by Lin and Corsi (2007).

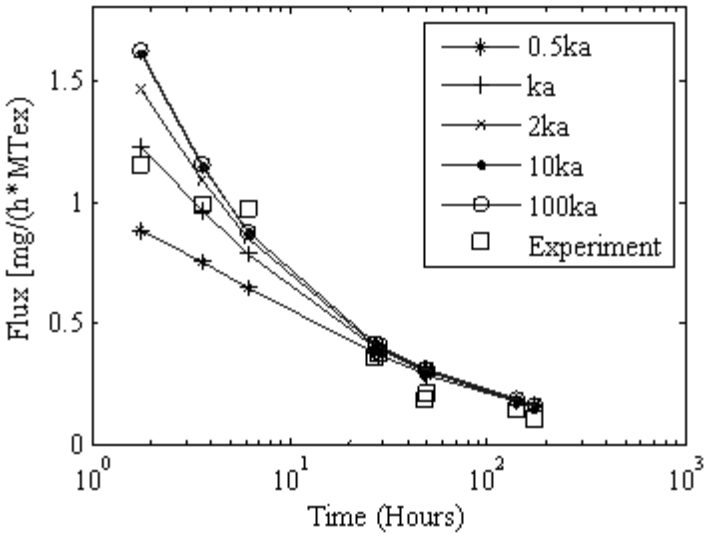

Figure 7.4: Effects of air speed on TMPD-MIB emissions.

As the mass transfer coefficient increases, the emission rate increases up to a point of 10-fold increase in ka for $t < 150$ hrs. Results at 100-fold increase are identical to those at 10-fold increase, indicating that above 10 times ka, the mass transfer coefficient is so large that emissions no longer have any dependence on gas-side mass transfer processes. In fact, four times ka results in a convergence to 95% of the one hundred-fold ka emissions curve. Therefore for ka values greater than 0.84 m h^{-1}, the rate limiting factor is diffusion rather than gas-side mass transfer. At times greater than 150 hrs, the dependency of emissions on the mass transfer coefficient diminishes dramatically, suggesting that emissions from the dry film are dominated by diffusion processes within the film and substrate and not above the film on the air side.

7.3 TMPD-MIB internal distribution (model prediction and experiment comparison)

The 2LM was compared against the experimental data collected in this research as shown in 5.5. For the paints used in the experiments, the following input parameters were determined and used for the model: The TMPD-MIB and water mass transfer coefficients (0.06 to 0.41 $\frac{m}{h}$) were obtained from the evaporation experiments described in section 5.2, the effective diffusion coefficient for gypsum board was the same as previously determined. The diffusion coefficient for the paint layer was obtained from the best fit to the experimental data. The diffusion coefficients obtained for the paints summarized in table 6.6 can not be used in this case, because both paints have different PVC concentration, and therefore the diffusion coefficient of TMPD-MIB changes. With the determined diffusion coefficient for the paints used in the experiment, the prediction of the model can be compared to the experimental data. Experimental data was obtained for thicker painted samples and the remaining TMPD-MIB mass after two week was compared to the model predictions for mass remaining, as shown in Figure 7.5.

The solid bars represent the experimental results, while the striped bars display the model results. There was a good agreement between the model predictions and the experimental data, particularly for the air predictions. The mean absolute error was less than 5% for all the cases. The results from the predictions were closer to the experiment in the flat paint. This behavior might be due to the type of diffusion coefficient used for this type of paint. Another posibility for the differences between the model results and the semi-gloss paint results might be due to the thicker than

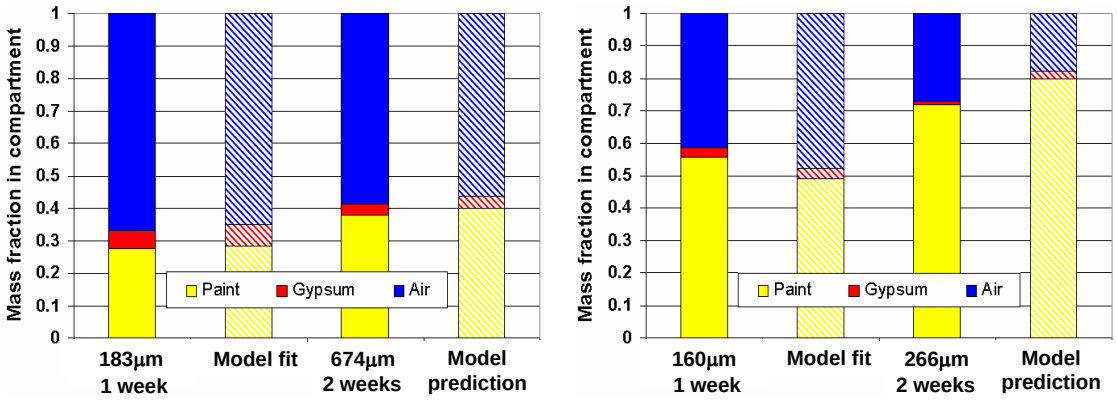

(a) Semi-gloss paint

(b) Flat paint

Figure 7.5: Model compartment results.

normal paint layer used which might have overly increased the amount of polymer per area present in the film.

The mass of TMPD-MIB remaining in both paint and material layers changes with time as it is emitted into the air. For this reason, it was expected to obtain a distribution profile of TMPD-MIB in the material that tends to be uniform as time goes to infinity. Results from the 2LM simulation for a semi-gloss paint are shown in Figure 7.6. In this figure, the normalized mass of TMPD-MIB at different depths in the gypsum for three different times is shown. The horizontal scale in this figure is the depth in the gypsum board, where zero corresponds to the upper layer of gypsum that is in contact with the paint layer.

As it can be seen from this figure, the model predicts a nearly uniform concentration of TMPD-MIB even for t=10h, taking into account that the vertical scale in this figure has been magnified ten times. This result suggest that after one week from the paint event, the concentration profile of TMPD-MIB inside the gypsum will

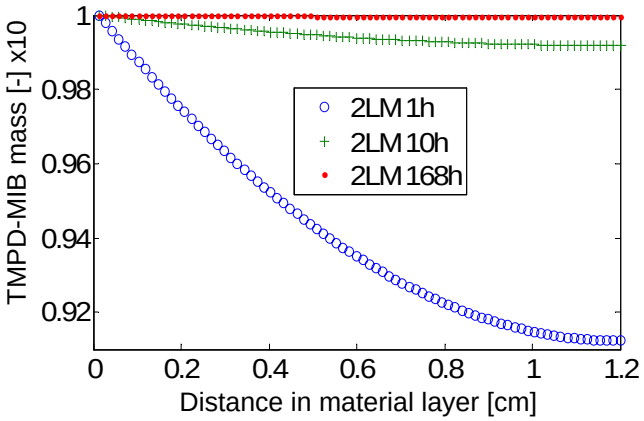

Figure 7.6: TMPD-MIB mass distribution in gypsum variation with time

be uniform throughout as shown in Figure 7.6. Experimental results for the Flat paint after 168 hours were compared to the model prediction, and the agreement of the model with the experiment is shown in Figure 7.7. No appreciable differences between the semi-gloss paint and the flat paint were obtained. Magnifying results of this case can be seen in Figure 7.8 for the semi-gloss paint, where small deviations from the model are visible. These small differences did not have a clear pattern or bias towards accumulation of TMPD-MIB at any particular depth of the gypsum.

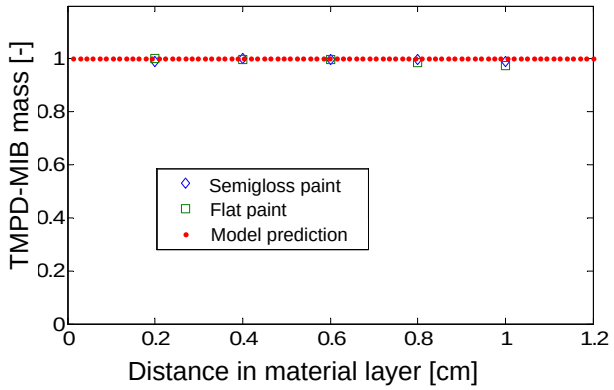

Figure 7.7: Mass distribution profile comparison for different paints

The model predicted an uniform concentration profile even at short times. This

behavior could be explained by the highly interconnected porous structure from the gypsum board. Soon after the paint event, water could facilitate the transport of TMPD-MIB into the gypsum, and therefore a uniform distribution of TMPD-MIB could be obtained even at short periods of time after paint application.

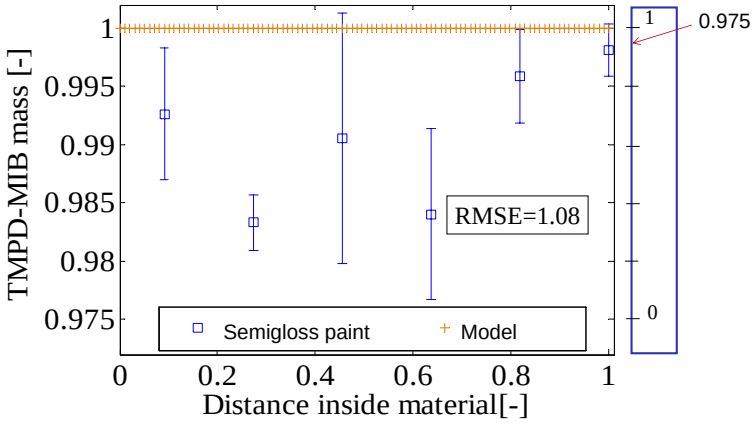

Figure 7.8: TMPD-MIB mass distribution in gypsum for a semi-gloss paint

However, the experimental data that has been used to validate the 2LM was an indirect way to estimate TMPD-MIB, since estimates were derived from a gravimetric method rather than direct TMPD-MIB measurements. Although no VOC distribution data inside porous materials like gypsum is available in the currently published literature, efforts have been made in the present research to gain a better understanding of the transport of VOCs like TMPD-MIB inside porous materials by indirectly estimating the amount of TMPD-MIB in gypsum sections at different depths.

Chapter 8

Conclusions and Future Work

A summary with the highlights from the present work are briefly discussed in this chapter. Conclusions from the present work will be presented in section 8.1, the implications of the findings and usefulness of the developed model are discussed in section 8.2. Recommendations and future work to continue the modeling and research of VOC emissions from latex paints are outlined in 8.3.

8.1 Conclusions

A one dimensional diffusion two layer model was developed for prediction of VOCs emitted from Latex paints. The model was compared to the results of an analytical solution for simplified boundary conditions. The model described herein was validated with TMPD-MIB small chamber experiments, and it was successfully used to predict emissions of TMPD-MIB from paints with different PVC and thickness.

A major contribution from this research is that the entire wet and dry emission processes for TMPD-MIB transport was found likely to be dominated by diffusion

processes. Variations of the mass transfer coefficient past the typical values found in indoor environments did not result in appreciable effects, and therefore, emissions of TMPD-MIB were found to be unaffected by changes in the mass transfer coefficient. This finding was obtained while varying the TMPD-MIB mass transfer coefficient in the range of expected mass transfer values for indoor environments. Therefore, it was determined that a detailed gas-phase analysis of mass transport for TMPD-MIB would therefore have negligible effects in the overall evaporation rate.

Modeling results indicate that the diffusion coefficient of TMPD-MIB in the paint layer does not depend on the thickness of the wet paint film, but it depends on the PVC of the paint. The complex interactions that pigment and polymer have with TMPD-MIB are in itself a topic of intense research and continue to be not very well understood. However, the findings from this research further support the idea that emissions of TMPD-MIB are dependent on the PVC of the paint. The emissions of coalescing aid agents like TMPD-MIB were shown to be directly proportional to the PVC of the paints studied.

A constant diffusion coefficient as used in the 2LM proved successful for modeling emissions of TMPD-MIB from LPVC paints. However, a constant diffusion coefficient failed to capture the physical mechanisms of the drying film for the HPVC paints which had a higher water content and less homogeneous film than the LPVC paints.

The water content of latex paint was found to be an important parameter with respect to short term emissions of TMPD-MIB. For the set of paints studied, the

higher the water content of the paint the faster the initial release of TMPD-MIB. The inclusion of a linear decrease in the diffusion coefficient of the paint layer to account for water evaporation from the wet film, results in a better prediction of TMPD-MIB emissions. This linear variation reflects the rapidly changing nature of the painted film, and the constant evaporation rate of water that was identified for different paints as they dry.

The TMPD-MIB concentration profile was estimated with the 2LM for both the paint and material layers, and it was indirectly validated for gypsum material via TGA experiments. The TMPD-MIB concentration profile inside the gypsum material was found to be uniform at different depths. These results confirm the predictions of the 2LM, for which the distribution profile was also uniform throughout the material, due to the large differences in the diffusion coefficients of the paint and material layers.

8.2 Implications

Emissions predicted with the proposed model can be used to make better estimates of the contribution that architectural coatings have on ground level ozone formation, particularly for ozone non-attainment areas that face problems reducing ozone levels.

VOC's emitted from paints move outside from indoor environments and contribute in some portion to the ozone formation mechanisms. For this reason is very important to consider PVC as an important parameter of the paint formulation that can influence how fast and for how long emissions of TMPD-MIB will last. In areas with ground level ozone formation problems, the careful selection of paints can there-

fore help reduce VOC peak emissions from uncontrolled fugitive sources from paints, especially for large paint users such as new developments and large scale renovation projects. However, it should also be kept in mind that porous materials like gypsum board will continue to emit TMPD-MIB for very long periods of time if the amount of PVC in the paint is reduced, potentially increasing the exposure for occupants in buildings.

In this study, experiments involving thermo gravimetric analysis (TGA) were conducted to assess the behavior of TMPD-MIB transport from paint to porous substrates like gypsum board, and good agreement with the 2LM predictions were obtained. The slow transport of TMPD-MIB that has been observed after paint application was captured by the 2LM for long periods of time. The proposed 2LM offers a better way to predict the emission of these slow emitting compounds than the typically used exponential decay models. The use of the predictive model could result in better predictions for indoor occupants exposure to TMPD-MIB and other slow emitting VOCs from paint. This in turn, can be used by regulating agencies as a base for calculating the actual VOC's that will be emitted from paint during a period of time, rather than estimating VOC emissions by the total amount originally used in the paint formulation.

Results from this research could be use for modeling of the impact of paint on ozone formation. These impacts could be used by regulatory agencies to provide guidance and develop policies. For example, restricting the use of paints with potential for increasing the peak concentration of ozone during summer months, or limiting the use of certain paints (like the HPVC paints in this study) that could aggravate ozone

concentration level during summer months particularly in non-attainment cities.

8.3 Future work

In order to account for non-homogeneities of the material as well as effects like lateral drying, the 2LM could be improved by implementing the 2D Fick's law equation for each layer. However, the added complexity would require a better understanding of gypsum porosity in different directions, and more experimental data would be required in order to validate the model. Additionally, chemical reactions should be included, in order to model painting of materials like concrete, where hydrolysis reactions reduce the amount of TMPD-MIB.

Paints contain different polymers and additives which are difficult to model and could affect the TMPD-MIB evaporation rate due to internal paint sorption interactions. Since paint formulations from diverse manufacturers are dissimilar, it will be very important to expand the research studies to different paint formulations and varying degrees of PVC in order to obtain a mathematical expression that can be used to calculate the diffusion coefficient for the paint layer. Additionally, future work should seek to validate the 2LM with other paint components like different coalescing aid agents and with other slow evaporating substances used in newer water-borne paint formulations.

Modeling and experimental results indicated the possibility of accurately predicting the fate of TMPD-MIB in gypsum board. However, a more direct method to measure the mass of TMPD-MIB by layers inside the material would be highly

recommended. Analyzing gypsum board by layers via gas chromatography could verify the model results, and quantify the actual amount of VOC stored in gypsum at different depths.

Gypsum board that is not coated with paper should be evaluated. Plastic coatings would be expected to provide a more impermeable layer than paper as well as a more sorptive media. These and other new construction materials should be modeled.

Improvements on the numerical solution can be made in order to increase computation speed. For example, implementation of a higher order differencing scheme should reduce the amount of nodes per layer required to obtain an independent solution.

Finally, future work should also focus on developing a uniform standard method to evaluate emissions from latex paints in such a way that results from different experiments are more comparable, and therefore the variations in the estimation of parameters from different models could be reduced.

Appendix A

Example Calculation for Water Evaporation

Using Equation 3.16, with temperature of 20^oC, using a saturation vapor density $C_{sat} = 17 \times 10^{-3}\ \frac{Kg}{m^3}$, $RH = 60\%$, and $Kc = 0.0025\ m/s$, the time to deplete from an initial thickness of 100 μm to 50 μm

$$t = \frac{50\mu m}{\frac{25 \times 10^{-4} m/s}{1 \times 10^3 \frac{Kg}{m^3}} 17 \times 10^{-3} \frac{Kg}{m^3} (1 - 0.6)} = 2.9 \times 10^3 s$$

Appendix B

Analytical Solution

The system of partial differential equations can be solved using the separation of variables method (Choy and Reible 2000), in which a concentration is assumed to be separable into independent functions of position and time of the form:

$$C_{A,i}(z,t) = \Psi_i(z) \cdot \Gamma(t) \tag{B.1}$$

Substituting Equation B.1into Equations 3.1 and 3.2 the following expression is found:

$$\left(\frac{D_{Aeff,i}}{R_{f,i}}\right) \frac{1}{\Psi_{i,n}(z)} \frac{d^2\Psi_i}{dz^2} = \frac{1}{\Gamma(t)} \frac{d\Gamma}{dt} \tag{B.2}$$

where the left hand side is a function of the space variable, z, and the right had side is a function of the time variable, t. In order for Equation B.2 to be satisfied, the equality has to be equal to a constant that typically is chosen as $-\beta^2$. With the addition of this constant and for the two layer system like the one described in

chapter 3.2, the separation of the two equations results in:

$$\frac{d\Gamma}{dt} = -\beta^2 \cdot \Gamma(t) \tag{B.3}$$

$$\frac{d^2\Psi_1, n}{dz^2} + \frac{\beta n^2}{\frac{D_{Aeff,1}}{R_{f,1}}}\Psi_{1,n}(z) = 0 \qquad for z \in [0, a] \tag{B.4}$$

$$\frac{d^2\Psi_2, n}{dz^2} + \frac{\beta n^2}{\frac{D_{Aeff,2}}{R_{f,2}}}\Psi_{2,n}(z) = 0 \qquad for z \in [0, a] \tag{B.5}$$

where Equation B.3 can be recognized as the temporal problem with an exponential solution, $\Gamma(t) = exp(-\beta^2 t)$ and Equations B.4 and B.5 are known as the spatial problem, which solution will depend on the boundary conditions of the two layer system.

A new set of transformed boundary conditions can be obtained from Equations 3.3-3.5 as:

$$\frac{d\Psi_2}{dz} = 0 \qquad for \quad z = 0 \tag{B.6}$$

$$D_1\frac{d\Psi_1}{dz} = D_2\frac{d\Psi_2}{dz} \qquad at \quad z = a \tag{B.7}$$

$$\Psi_1(z) = \Psi_2(z) \qquad at \quad z = a \tag{B.8}$$

$$\frac{d\Psi_1}{dz} + \left(\frac{ka}{D_{Aeff,1}}\right)\Psi_1(z) = 0 \qquad at \quad z = b \tag{B.9}$$

The general form of these equations will be:

$$\Psi_1(\beta_n, z) = A_{1,n}sin(\frac{\beta_n}{\sqrt{\alpha_1}} \cdot z) + B_{1,n}cos(\frac{\beta_n}{\sqrt{\alpha_1}}) \cdot z) \tag{B.10}$$

$$\Psi_2(\beta_n, z) = A_{2,n}sin(\frac{\beta_n}{\sqrt{\alpha_2}} \cdot z) + B_{1,n}cos(\frac{\beta_n}{\sqrt{\alpha_2}}) \cdot z) \tag{B.11}$$

where $\alpha_i = \frac{D_{Aeff,i}}{R_{f,i}}$ Then,

$$\frac{d\Psi_1}{dz} = \left[\frac{\beta_n}{\sqrt{\alpha_1}} \cdot A_{1,n}\right] cos\left[\frac{\beta_n}{\sqrt{\alpha_1}} \cdot z\right] - \left[\frac{\beta_n}{\sqrt{\alpha_1}} \cdot B_{1,n}\right] sin\left[\frac{\beta_n}{\sqrt{\alpha_1}}\right] \tag{B.12}$$

$$\frac{d\Psi_2}{dz} = \left[\frac{\beta_n}{\sqrt{\alpha_2}} \cdot A_{2,n}\right] cos\left[\frac{\beta_n}{\sqrt{\alpha_2}} \cdot z\right] - \left[\frac{\beta_n}{\sqrt{\alpha_2}} \cdot B_{2,n}\right] sin\left[\frac{\beta_n}{\sqrt{\alpha_2}}\right] \tag{B.13}$$

Using the transformed boundary conditions and solving for the coefficients after simplifying it is obtained:

$$A_{1,n} = -K_D \cdot cos\left(\frac{\beta_n}{\sqrt{\alpha_2}}a\right) sin\left(\frac{\beta_n}{\sqrt{\alpha_1}}a\right) + cos\left(\frac{\beta_n}{\sqrt{\alpha_1}}a\right) sin\left(\frac{\beta_n}{\sqrt{\alpha_2}}a\right) \tag{B.14}$$

$$B_{1,n} = K_D \cdot sin\left(\frac{\beta_n}{\sqrt{\alpha_2}}a\right) sin\left(\frac{\beta_n}{\sqrt{\alpha_1}}a\right) + cos\left(\frac{\beta_n}{\sqrt{\alpha_2}}a\right) cos\left(\frac{\beta_n}{\sqrt{\alpha_1}}a\right) \tag{B.15}$$

$$A_{2,n} = 0 \tag{B.16}$$

$$B_{2,n} = 1 \tag{B.17}$$

where $K_D = -\frac{D1}{D2}\sqrt{\frac{\alpha_2}{\alpha_1}}$, and β_n is obtained by calculating the roots of:

$$\begin{aligned}
&\left[\left(\frac{D_1}{\sqrt{\alpha_1}} + \frac{D_2}{\sqrt{\alpha_2}}\right)\beta_n\right] sin\left(\left[\frac{a}{\sqrt{\alpha_1}} + \frac{b-a}{\sqrt{\alpha_2}}\right]\beta_n\right) + \\
&\left[\left(\frac{D_1}{\sqrt{\alpha_1}} + \frac{D_2}{\sqrt{\alpha_2}}\right)\beta_n\right] sin\left(\left[\frac{a}{\sqrt{\alpha_1}} + \frac{b-a}{\sqrt{\alpha_2}}\right]\beta_n\right) + \\
&\left[-k_a\left(\frac{D_1}{D_2}\sqrt{\frac{\alpha_2}{\alpha_1}} + 1\right)\right] cos\left(\left[\frac{a}{\sqrt{\alpha_1}} - \frac{b-a}{\sqrt{\alpha_2}}\right]\beta_n\right) + \\
&\left[-k_a\left(\frac{D_1}{D_2}\sqrt{\frac{\alpha_2}{\alpha_1}} - 1\right)\right] cos\left(\left[\frac{a}{\sqrt{\alpha_1}} - \frac{b-a}{\sqrt{\alpha_2}}\right]\beta_n\right) = 0
\end{aligned}$$

The complete solution to the system in each layer is obtained by linear superposition of the product of the two solutions (temporal and spatial) such that:

$$C_{A,i}(z,t) = \sum_{n=1}^{\infty} \delta_n \cdot \Psi_i(\beta_n, z) \cdot (\beta_n, t)$$

or

$$C_{A,i}(z,t) = \sum_{n=1}^{\infty} \delta_n \cdot exp\left[-\beta_n^2 t\right] \tag{B.18}$$

where δ_n are constant coefficients that satisfy the initial boundary conditions $C_{A0}(z)$ and can be solved from Equation B.18 when t=0, and using the orthogonality property of eigenfunctions to obtain:

$$\delta_n \cdot N(\beta_n) = I_0(\beta_n) \tag{B.19}$$

where the term $N(\beta_n)$ is known as the normalization integral and is given by:

$$N(\beta_n) = R_{f,1} \int_0^a \left[\Psi_1(\beta_n, z')\right]^2 dz' + \int_a^b \left[\Psi_2(\beta_n, z')\right]^2 dz' \tag{B.20}$$

and the term $I_0(\beta_n)$ is the initialization integral and is given by:

$$I_o(\beta_n) = R_{f,1} \int_0^a \Psi_1(\beta_n, z') \cdot C_{A0}(z') dz' + R_{f,2} \int_a^b \Psi_2(\beta_n, z') \cdot C_{A0}(z') \tag{B.21}$$

Replacing Equation B.19 in B.18 the concentration is obtained as:

$$C_{A,i}(z,t) = \sum_{n=1}^{\infty} \left[exp(-\beta_n^2 t) \cdot \frac{1}{N(\beta_n)} \cdot \Psi_i(\beta_n, z) \cdot I_o(\beta_n) \right] \tag{B.22}$$

And finally, the surface flux can be obtained by differentiating Equation B.22 at z=b to obtain:

$$j_A(t) \Big|_z = b$$

or

$$j_A \Big|_{z=b} = D_{A(eff),1} \sum_{n=1}^{\infty} \left[exp\left[-(\beta_n^2 t)\right] \frac{1}{N(\beta_n)} \frac{\partial \Psi_1}{\partial z} \Big|_{z=b} I_o(\beta_n) \right] \tag{B.23}$$

Appendix C

2LM Coefficient Derivation

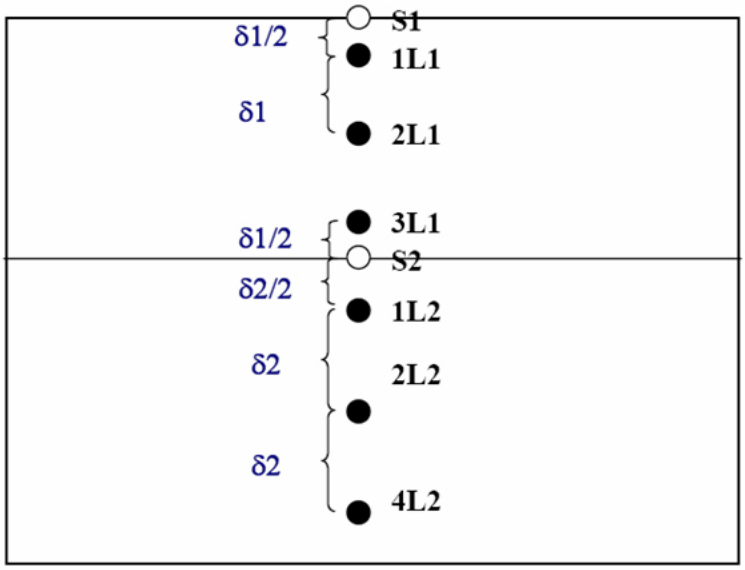

Figure C.1: Full implicit discretization scheme.

For the following equations, an effective diffusion coefficient that accounts for material properties, and also internal layer sorption can be defined as:

$$\left(\frac{D_{Li}}{R_i}\right) = D_{eff_{Li}} = D_1 \tag{C.1}$$

Node C_{s_1}

$$\left(\frac{D_{L1}}{R_1}\right)\frac{\partial C_{L_1}}{\partial z}\Big|_{z=b} = -k_a C_{L_1}\Big|_{z=b} \tag{C.2}$$

Using the node discretization shown in Figure C.1, equation C.2 is transformed to:

$$D_1\frac{C_{S_1} - C_{1L_1}}{\frac{\Delta X_1}{2}} = -k_a C_{S_1} \tag{C.3}$$

Solving for the surface node C_{S_1} equation C.3 becomes:

$$C_{S_1} = \frac{2D_1}{2D_1 + k_a\Delta X_1}C_{1L_1} \tag{C.4}$$

Node C_{1L_1}

$$\frac{\partial C_{L_1}}{\partial t} = D_1\frac{\partial^2 C_{L_1}}{\partial z^2} \tag{C.5}$$

Discretizing this equation arround node C_1L_1 we obtain:

$$\frac{\Delta X_1}{\Delta t}\left(C_{1L_1} - C^0_{1L_1}\right) = D_1\left(\frac{C_{S_1} - C_{1L_1}}{\frac{\Delta X_1}{2}}\right) - D_1\left(\frac{C_{1L_1} - C_{2L_1}}{\Delta X_1}\right) \tag{C.6}$$

Coefficients:

$$\begin{aligned} &C_{S_1}\left(-\frac{2D_1}{\Delta X_1}\right) + \\ &C_{1L_1}\left(\frac{\Delta X_1}{\Delta t} + \frac{3D_1}{\Delta X_1}\right) + \\ &C_{2L_1}\left(\frac{D_1}{\Delta X_1}\right) \qquad\qquad = \left(\frac{\Delta X_1}{\Delta t}\right)C^0_{1L_1} \end{aligned}$$

(4) in (6)

$$C_{1_1}\left(\frac{\Delta X_1}{\Delta t}+\frac{3D_1}{\Delta X_1}-\frac{2D_1}{2D_1+k_a\Delta X_1}\cdot\frac{2D_1}{\Delta X_1}\right)$$
$$+C_{2L_1}\left(-\frac{D_1}{\Delta X_1}\right)=C^0_{1L_1}\left(\frac{\Delta X_1}{\Delta t}\right)$$

Node C_{2L_1}

$$\frac{\Delta X_1}{\Delta t}\left(C_{2L_1}-C^0_{2L_1}\right)=D_1\left(\frac{C_{1L_1}-C_{2L_1}}{\Delta X_1}\right)-D_1\left(\frac{C_{2L_1}-C_{3L_1}}{\Delta X_1}\right) \tag{C.7}$$

Coefficients:

$$\begin{aligned}
&C_{1L_1}\left(-\frac{D_1}{\Delta X_1}\right)+\\
&C_{2L_1}\left(\frac{\Delta X_1}{\Delta t}+\frac{2D_1}{\Delta X_1}\right)+\\
&C_{3L_1}\left(-\frac{D_1}{\Delta X_1}\right) &&=C^0_{2L_1}\left(\frac{\Delta X_1}{\Delta t}\right)
\end{aligned}$$

Node C_{3L_1}

$$\frac{\Delta X_1}{\Delta t}\left(C_{3L_1}-C^0_{3L_1}\right)=D_1\left(\frac{C_{2L_1}-C_{3L_1}}{\Delta X_1}\right)-D_1\left(\frac{C_{3L_1}-C_{3S_2}}{\frac{\Delta X_1}{2}}\right) \tag{C.8}$$

Coefficients:

$$\begin{aligned}
&C_{2L_1}\left(-\frac{D_1}{\Delta X_1}\right)+\\
&C_{3L_1}\left(\frac{\Delta X_1}{\Delta t}+\frac{3D_1}{\Delta X_1}\right)+\\
&C_{S_2}\left(-\frac{2D_1}{\Delta X_1}\right) &&=C^0_{3L_1}\left(\frac{\Delta X_1}{\Delta t}\right)
\end{aligned}$$

Replacing the expression C_{S_2} in terms of the C_{3L_1}, and C_{1L_2}, this equation becomes:

$$C_{2L_1}\left(-\frac{D_1}{\Delta X_1}\right)+C_{3L_1}\left(\frac{\Delta X_1}{\Delta t}+\frac{3D_1}{\Delta X_1}-\frac{2D_1}{\Delta X_1}\cdot\frac{D_1\Delta X_2}{D_1\Delta X_2+D_2\Delta X_1}\right)$$
$$+C_{1L_2}\left(-\frac{2D_1}{\Delta X_1}\cdot\frac{D_2\Delta X_1}{D_1\Delta X_2+D_2\Delta X_1}\right)=C^0_{3L_1}\left(\frac{\Delta X_1}{\Delta t}\right)$$

Node C_{S_2}

$$D_1\left(\frac{C_{3L_1}-C_{S_2}}{\frac{\Delta X_1}{2}}\right)=D_2\left(\frac{C_{S_2}-C_{1L_2}}{\frac{\Delta X_2}{2}}\right)$$

And solving for C_{S_2}

$$C_{S_2}=\frac{D_1\Delta X_2C_{3L_1}+D_2\Delta X_1C_{1L_2}}{D_1\Delta X_2+D_2\Delta X_1}$$

Node C_{1L_2}

$$\frac{\Delta X_2}{\Delta t}\left(C_{1L_2}-C^0_{1L_2}\right)=D_2\left(\frac{C_{S_2}-C_{1L_2}}{\frac{\Delta X_2}{2}}\right)-D_2\left(\frac{C_{1L_2}-C_{2L_2}}{\Delta X_2}\right) \tag{C.9}$$

Coefficients:

$$C_{3L_1}\left(-\frac{2D_2}{\Delta X_2}\cdot\frac{D_1\Delta X_2}{D_1\Delta X_2+D_2\Delta X_1}\right)+$$
$$C_{1L_2}\left(\frac{\Delta X_2}{\Delta t}+\frac{3D_2}{\Delta X_2}-\frac{2D_2}{\Delta X_2}\cdot\frac{D_2\Delta X_1}{D_1\Delta X_2+D_2\Delta X_1}\right)+$$
$$C_{2L_2}\left(-\frac{D_2}{\Delta X_2}\cdot\right)=C^0_{1L_2}\left(\frac{\Delta X_2}{\Delta t}\right)$$

Node C_{2L_2}

$$\frac{\Delta X_2}{\Delta t}\left(C_{2L_2}-C^0_{2L_2}\right)=D_2\left(\frac{C_{1L_2}-C_{2L_2}}{\Delta X_2}\right)-D_2\left(\frac{C_{2L_2}-C_{3L_2}}{\Delta X_2}\right) \tag{C.10}$$

Coefficients:

$$\begin{aligned} &C_{1L_2}\left(-\frac{D_2}{\Delta X_2}\right)+ \\ &C_{2L_2}\left(\frac{\Delta X_2}{\Delta t}+\frac{2D_2}{\Delta X_2}\right)+ \\ &C_{3L_2}\left(-\frac{D_2}{\Delta X_2}\right) \qquad\qquad = C^0_{2L_2}\left(\frac{\Delta X_2}{\Delta t}\right) \end{aligned}$$

Node C_{3L_2}

$$\frac{\Delta X_2}{\Delta t}\left(C_{3L_2}-C^0_{3L_2}\right)=D_2\left(\frac{C_{2L_2}-C_{3L_2}}{\Delta X_2}\right) \tag{C.11}$$

Coefficients:

$$\begin{aligned} &C_{2L_2}\left(-\frac{D_2}{\Delta X_2}\right)+ \\ &C_{3L_2}\left(\frac{\Delta X_2}{\Delta t}+\frac{D_2}{\Delta X_2}\right)=C^0_{3L_2}\left(\frac{\Delta X_2}{\Delta t}\right) \end{aligned}$$

Appendix D

Matlab Source Code for Chang and Guo Model

Matlab version: 7.0.3.365 (R14) with symbolic, and cftool libraries

```
clear all
close all
f= 0.0067;%  0.0154;
Ly1=277e-6;%   131e-6;
%----------------------------Data to calculate Flux from experimental
%concentration data
    load datos.dat  %datos should contain two columns.
    %column 1 is the time, column 2 is the chamber concentration.
    datos=datos
    Area=0.0064;  %m^2   90.25e-4;%
    Vchamber=0.00333; %m^3
    ACH=1.5;      %1/h
    Q=ACH*Vchamber; %m^3/h
%-------------------------------------------------------------

syms R10 R20 k1 k2 C t;
options = fitoptions('exp2');%     General model Exp2:
                             %        f(x) = a*exp(b*x) + c*exp(d*x)
options.algorithm='Levenberg-Marquardt' %other options
    x1=datos(1:length(datos),1);
    y1=datos(1:length(datos),2);
```

```
    volume=Area*Ly1*100^3;
    if (f==0.0154)
        Mpaint=1.254*volume; %LPVC paint
       % pvc='LPVC';
    else
        Mpaint=1.329*volume; %HPVC paint
       % pvc='HPVC';
    end
    Mtex =f*Mpaint  %mass of texanol in grams
   [fitt,gof]= fit(x1,y1,'exp2',options);   %Fits to the concentration
    R10=fitt.a;k1=-fitt.b;R20=fitt.c;k2=-fitt.d;
    C=R10*exp(-k1*t)+R20*exp(-k2*t);   %concentration equation
    here=2
    Flux=(Vchamber*diff(C,t)+ACH*Vchamber*C)/Mtex;  %Flux equation
    x2=logspace(0,4);
    FFlux=subs(Flux,x2);
    cc=y1;
    told= circshift(x1,1);told(1)=0;
    cold= circshift(y1,1);cold(1)=0;
    E=(Vchamber*(y1-cold)./(x1-told)+Q*(y1+cold)/2)/(Mpaint*f);
    maxtime=x1(length(x1));
    figure
    plot(fitt,x1,y1,'o')
    title(['Concentration Fit - Paint layer thickness = ',...
        num2str(Ly1*1e6,'%3.0f'),'x10^{-6} m'])
     text(max(x1)/4,max(y1)/2,... %max(Flux2)/2
[num2str(fitt.a,'%5.2f'),' exp',num2str(fitt.b,'%6.4f')...
    '+',num2str(fitt.c,'%5.2f'),' exp',num2str(fitt.d,'%6.4f')],...
'HorizontalAlignment','center','BackgroundColor',[1 1 1]...
    ,'EdgeColor',[0,0,0])
    xlabel('Time [Hours]')
    ylabel('Concetration [mg/m^3]')
    legend('Experiment'...
          ,'Double exponential Fit')
    grid on

    [fitt3,gof3]= fit(x1,E,'exp2',options)
    R10=fitt3.a
    k1=-fitt3.b
    R20=fitt3.c
    k2=-fitt3.d
```

```
    F=R10*exp(-k1*t)+R20*exp(-k2*t);
     figure
    loglog(x1,E,'o',x2,subs(FFlux,x2),'.-')
    title('Emission fit results')
    xlabel('Time [Hours]')
    ylabel('Flux [mg/Hour-g_{Tex}]')
    text(max(x1)/4,max(y1)/10,... %max(Flux2)/2
[num2str(fitt3.a,'%5.2f'),' exp',num2str(fitt3.b,'%6.4f')...
    '+',num2str(fitt3.c,'%5.2f'),' exp',num2str(fitt3.d,'%6.4f')],...
'HorizontalAlignment','center','BackgroundColor',[1 1 1]...
    ,'EdgeColor',[0,0,0])
    legend('Using Discrete approximation of C'...
          ,'Using Double exponential Fit of C')
    grid on
    tt=linspace(1,max(x1),1500);
    t2=tt';
    F2=subs(F,tt)';
    Ftemp=subs(Flux,datos(:,1))
    tflux=datos(:,1);
    save Changuo t2 F2 F tflux Flux
```

Appendix E

Matlab Source Code for Sparks Model

Matlab version: 7.0.3.365 (R14) with symbolic, and cftool libraries

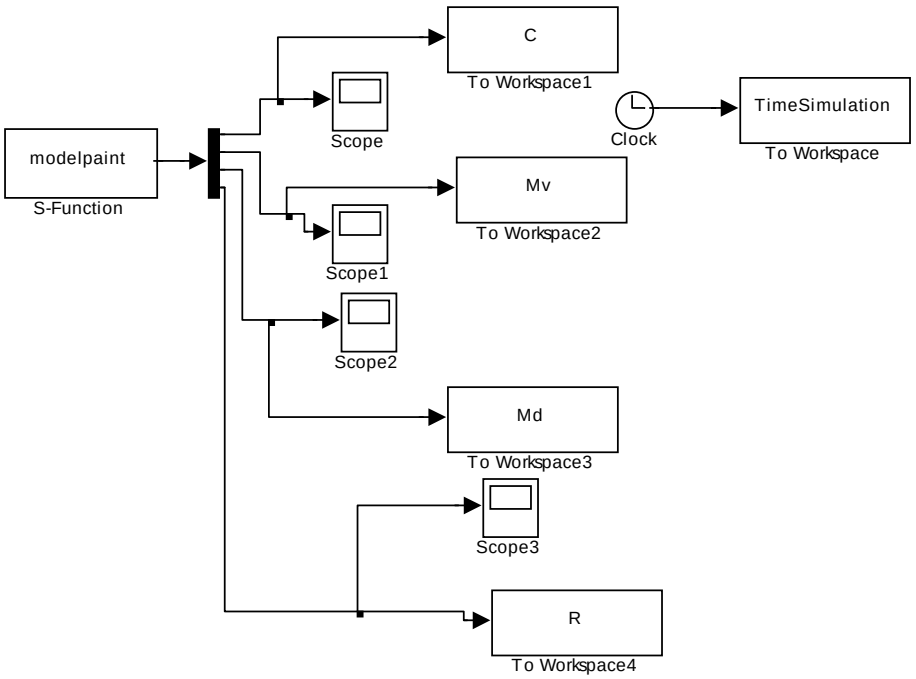

Figure E.1: Matlab Simulink block diagram for Chang and Guo model.

Main program

```
clear all
close all
```

```
clc
A=-1;
Area=[0.0064];
Mto=33.57/64e-4;   %Mto=2575;
Cvo=50;
Mvo=80;
Mdo=Mto-Mvo;
fd1=0.0006;

save COND Cvo Mvo Mdo fd1

sim paint_model
load cdata.dat
load EMISSION
C1=interp1(TimeSimulation,C,cdata(:,1),'cubic')
C2=interp1(TFF,Flux,cdata(:,1),'cubic')
eM=(C1-cdata(:,2)).*(C1-cdata(:,2));

%%%%%%%%%%RMS_errorM=(sqrt((sum(eM)/length(E))))*100
RMS_errorM=(sqrt((sum(eM)/length(eM))))*100
MAPE=sum(abs(cdata(:,2)-C1)./cdata(:,2))/length(cdata)*100
MAPE2=sum(abs(cdata(:,2)-C2)./cdata(:,2))/length(cdata)*100
Totalmass=(Mdo+Mvo)*(8e-2)^2
figure
axis([1 max(TimeSimulation) 0.01 20])
plot(cdata(:,1),cdata(:,2),'s')
Vchamber=0.0033;
Mpaint=1.07;
f=0.0154;
Q=0.0050;
TFlux=linspace(1, max(cdata(:,1)),max(cdata(:,1)))';
%timescale of simulation.  0 to simulation time.
intpC=interp1(TFF,Flux,TimeSimulation,'cubic');
%interpolated Experimental Concentration
told= circshift(TimeSimulation,1);told(1)=0;
cold= circshift(C,1);cold(1)=0;
Ei=
(Vchamber*(C-cold)./(TimeSimulation-told)+Q*(C+cold)/2)/(Mpaint*f)
load Edata.dat
load 2LM,load EXP,load Changuo
%axis([10 max(TimeSimulation) 0 10])
```

```
load EMISSION %TFF Flux
loglog(t,Eexp,'*',t2,F2,'.-')
axis([1 max(TimeSimulation) 1e-3 10])
xlabel('Time [Hours]')
ylabel('TMPD-MIB Emission [mg/Hour-g_{Tex}]')
legend('Experiment','Chang and Guo')
rmse(Eexp,subs(F,t))
```

Model paint

```
function [sys,x0,str,ts] = modelpaint(t,x,u,flag)


switch flag,

  %%%%%%%%%%%%%%%%%%
  % Initialization %
  %%%%%%%%%%%%%%%%%%
  case 0,
    [sys,x0,str,ts]=mdlInitializeSizes;

  %%%%%%%%%%%%%%%
  % Derivatives %
  %%%%%%%%%%%%%%%
  case 1,
    sys=mdlDerivatives(t,x,u);

  %%%%%%%%%%
  % Outputs %
  %%%%%%%%%%
  case 3,
  sys=mdlOutputs(t,x,u);

%%%%%%%%%%%%%%%%%%%
  % Unhandled flags %
  %%%%%%%%%%%%%%%%%%%
  % There are no termination tasks (flag=9) to be handled.
  % Also, there are no continuous or discrete states,
  % so flags 1,2, and 4 are not used, so return an emptyu
  % matrix
  case { 2, 4, 5, 6, 7, 8, 9 }
  sys=[];
```

```
  otherwise
  error(['Unhandled flag = ',num2str(flag)]);

  end

% end sfuntmpl
%
function [sys,x0,str,ts]=mdlInitializeSizes

sizes = simsizes;
sizes.NumContStates  = 3;
sizes.NumDiscStates  = 0;
sizes.NumOutputs     = 4;
sizes.NumInputs      = 0;
sizes.DirFeedthrough = 1;
sizes.NumSampleTimes = 1;   % at least one sample time is needed
sys = simsizes(sizes);
str = [];
ts  = [0 0];
% Cvo=1e9;
% Mvo=15e-3;
% Mdo=1;
load COND
% Cvo;
% Mvo;
% Mdo;
% fd1;
x0=[Cvo;Mvo;Mdo];
save IC Cvo Mvo Mdo fd1
% end mdlInitializeSizes

%
%=============================================================
% mdlDerivatives
% Return the derivatives for the continuous states.
%=============================================================
%
function sys=mdlDerivatives(t,x,u)
 load IC;
 N=1.5;%0.5;
 L=(8e-2)^2/3.3e-3;%(16.3e-2)^2/53e-3;%(8e-2)^2/3.3e-3;
```

```
 Km=.2;
% fd1=0.00084;
 if t~=0
   R=Km*((Cvo*x(2)/Mvo)-x(1))+(1-(x(2)/Mvo))^2*fd1*x(3)*t^(-1/2);
   sys(1)=-N*x(1)+L*R;
   sys(2)=-Km*((Cvo*x(2)/Mvo)-x(1));
   sys(3)=-(1-x(2)/Mvo)^2*fd1*x(3)*t^(-1/2);
 else
     sys=[Cvo;Mvo;Mdo];

 end


% end mdlDerivatives

%
%=============================================================
% mdlOutputs
% Return the block outputs.
%=============================================================
%
function sys=mdlOutputs(t,x,u)
 load IC;
 Km=.2;
 if t==0
     R=0;
 else
     R=Km*((Cvo*x(2)/Mvo)-x(1))+(1-(x(2)/Mvo))^2*fd1*x(3)*t^(-1/2);
 end
 sys(1)=x(1);
 sys(2)=x(2);
 sys(3)=x(3);
 sys(4)=R;



% end mdlOutputs
```

Appendix F

TMPD-MIB and Temperature Rise

Curves for vapor pressure changes with increment on temperature of TMPD-MIB were not found in the current published literature. A set of experiments using Method 1, where TMPD-MIB was applied on aluminum were performed at different isothermal temperatures from 28^{o}C to 110^{o}C. The maximum limit of 110^{o}C was picked for these experiments, since it is of importance to understand the effect of temperature increase on the emissions. In particular, the current EPA method for estimating VOC content of water-based architectural coatings (Method-24) is a method that calls for holding an oven temperature at 110^{o}C for an hour to gravimetrically estimate the VOC content of paint applied on aluminium.

The profile obtained for the emissions as the temperature increases can be seen in Figure F.1. There is a three fold increase in the evaporation rate at 110 ^{o}C versus the one obtained at 28 ^{o}C. This increasing trend in the emissions of TMPD-MIB obeys the typical non-linear increase of vapor pressure with temperature rise according to the Clausius-Clapeyron equation. The resulting power equation that describes the changes in emission with temperature increase is:

$$E(T) = 7 \times 10^{-7} T^{4.53} \tag{F.1}$$

Where,

$E(T)$ is emission rate as a function of temperature $\left[\frac{g}{hm^2}\right]$,

T is Temperature ^{o}C

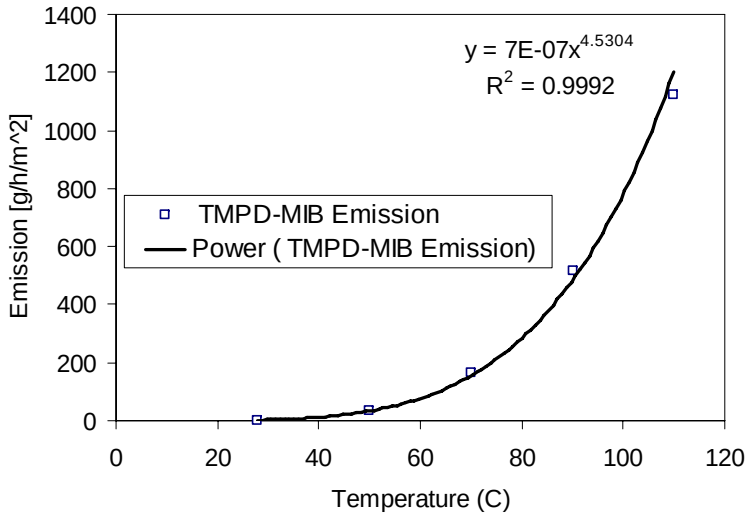

Figure F.1: Emission rate of TMPD-MIB variation with temperature increase.

Appendix G

Mass Transfer Coefficient Calculation Example

The mass transfer coefficient of TMPD-MIB can be calculated using the following equations:

$$N_A = k_G(P_s - P)A \tag{G.1}$$

$$P = \frac{C_i RT}{M_{wi}} \tag{G.2}$$

$$C_i = \frac{E}{Q} \tag{G.3}$$

$$k_c = k_G RT \tag{G.4}$$

Where,

N_A is emission rate $\left[\frac{mol}{h}\right]$,

k_G is a mass transfer coefficient $\left[\frac{mol}{m^2 hPa}\right]$,

P_s is TMPD-MIB saturation pressure $[Pa]$,

P is TMPD-MIB pressure at room conditions$[Pa]$,

C_i is TMPD-MIB concentration $\left[\frac{g}{m^3}\right]$,

A is sample area $[m^2]$,

R is the universal gas constant $\left[\frac{m^3 Pa}{Kmol}\right]$,

T is temperature $[K]$,

E is TMPD-MIB emission rate $\left[\frac{g}{h}\right]$,

Q is ventilation rate $\left[\frac{m^3}{h}\right]$.

Example calculation

The saturation vapor pressure of TMPD-MIB is 1.3Pa at 20^{o}C (ICSC:0629). With this vapor pressure and Equation F.1, a prediction of the vapor pressure results in 6Pa at 28 ^{o} C. The TMPD-MIB pressure can be calculated using Equation G.3, and replacing in the ideal gas law or Equation G.2 using: Q=40 mL/min (Q=0.0024 m^3/h). Assuming an emission rate of TMPD-MIB of 90 $\frac{\mu g}{h}$ emitting from a source with an area of 2.83×10^{-5} m^2 then N_A $\left[\frac{mol}{h}\right]$ can be calculated given that molecular weight of TMPD-MIB is Mw_{Tex}=216.32 $\frac{g}{mol}$as $N_A = 4.17 \times 10^{-7}$ $\frac{mol}{h}$, and then k_G $\left[\frac{mol}{m^2 Pah}\right]$ is 0.00237, and finally using Equation G.4 the mass transfer coefficient k_C is 5.91 $\frac{m}{h}$

Appendix H

Matlab Source Code Analytical Solution

```
%This program requires the Symbolic toolbox to calculation of solution
clear all
hold on
%INPUT PARAMETERS
%==========================
Diffusion_Material=1.2e-6;  %m^2/s; %MATERIAL diffusion coefficient
Diffusion_Paint=1.73e-15/4; %m^2/s;    %PAINT diffusion coefficient
Material_Thickness=1.5E-2;  %m
Paint_Thickness=180e-6;     %m
VOC_Fraction=0.0154;        %[-]
Deltat=1;                   %h
Material_Area=0.0064;       %m^2
Retardation_Material=1;     %retardation factor 1
Retardation_Paint=1;        %retardation factor 2
Paint_density=1.254;
Simulation_Time=10;
Number_of_Eigenvalues=120;
%==========================
l1=Material_Thickness;
l2=Paint_Thickness;
D1=Diffusion_Material;
D2=Diffusion_Paint;
```

```
R1=Retardation_Material;    %retardation factor 1
R2=Retardation_Paint;       %retardation factor 2
f=VOC_Fraction;
Area=Material_Area;
volume=Area*l2*100^3;
simtime=Simulation_Time;    %simulation in hours
%Calculation of Mass in the paint given density of paint
Mpaint=Paint_density*volume;
in_c=1e9*f*Mpaint/volume;   %Initial Compound concentration
a=l1;
b=a+l2;
j=1;
time=1:1:(simtime);
TFlux=linspace(Deltat, simtime,simtime)'; %timescale of simulation.
w=eigv;
%*****************************************
Surfaceflux=
fanalytic(D1,D2,R1,R2,simtime,a,b,in_c,Mpaint,f,Area,time,w);
  figure (2)
  grid on
  title('B.C.(R1=R2=1, D1=1e-6,D2=1e-15) ')
  xlabel('Hours')
  ylabel('Flux [mg/(h*MTex)')
  semilogx(time,Surfaceflux)
  legend('Analytical solution','Experimental data')
  hold on
%=================================================================
function [Surfaceflux]=
fanalytic(D1,D2,R1,R2,simultime,a1,b1,in_c,Mpaint,f,Area,time,w)
Mtex=Mpaint*f;
D(1)=D1*3600;%D(1)=7e-7;  %difussion coeff ly1      m
D(2)=D2*3600;%D(2)=2.047e-11; %diffusion coeff ly2   m
R(1)=R1;%R(1)=25;     %retardation factor 1
R(2)=R2;%R(2)=100;    %retardation factor 2
a=a1;%0.0150;
b=b1;%0.0151;
ka=0.0002*3600;   %m^2/s
coef=[b,in_c;a,0;0,0];
hours=simultime;%hours=1000;
syms z;
%Range of significance for eigenvalues.
```

```
%Both the concentration and flux
%equations require an infinite number of eigenvalues Bn: n=1,2,3...
%however as the negative square of the igenvalues is present in the
%exponential term, the significance of each eigenvalue decreases
with increasing n.
%Generally setting Bmax to 20 or 30 times the period of the smallest
%coefficient in the transcendental function sine and cosine terms is
%sufficient for a range of significant eigenvalues.
%Calculate System Eigenvalues
alpha=D./R
gamma=sqrt(D.*R);
C(1)=gamma(1)+gamma(2);
C(2)=a/sqrt(alpha(1))+(b-a)/sqrt(alpha(2));
C(3)=gamma(1)-gamma(2);
C(4)=a/sqrt(alpha(1))-((b-a)/sqrt(alpha(2)));
C(5)=ka*(gamma(1)/gamma(2)-1);
C(6)=a/sqrt(alpha(1))-(b-a)/sqrt(alpha(2));
C(7)=-ka*(gamma(1)/gamma(2)+1);
C(8)=a/sqrt(alpha(1))+(b-a)/sqrt(alpha(2));
C;
f=fbeta(C,3);
%Bmax=w*pi/(min(abs([C(2) C(4) C(6) C(8)])))
Bmax=w*pi/(min([abs(C(2)) abs(C(4)) abs(C(6)) abs(C(8))]));
for i=1:2
    nb_sub=floor(Bmax*abs(C(2*i))/pi);
    for j=0:nb_sub-1
        bnd_sub1(j+1)=(j+0.5)*pi/abs(C(2*i));
    end
end
for i=3:4
    nb_sub=floor(Bmax*abs(C(2*i))/pi);
    for j=1:nb_sub
        bnd_sub2(j)=j*pi/abs(C(2*i));
    end
end
bnds=sort([0 bnd_sub1 bnd_sub2]);
j=1;
for i=1: size(bnds,2)-1
    if (fbeta(C,bnds(i))*fbeta(C,bnds(i+1))<=0)
        Beta(j)=bisection(bnds(i),bnds(i+1),C);
        j=j+1;
```

```
    end
end
bisection_end=1
A(1,:)=0;
B(1,:)=1;
for n=1:size(Beta,2)  %j-1
k1=Beta(n)*a/sqrt(alpha(1));
k2=Beta(n)*a/sqrt(alpha(2));
A(2,n)=-gamma(1)/gamma(2)*cos(k2)*sin(k1)+cos(k1)*sin(k2);
B(2,n)=gamma(1)/gamma(2)*sin(k2)*sin(k1)+cos(k2)*cos(k1);
Psi(1)=(A(1,n)*sin(sqrt(R(1)/D(1))*z*Beta(n))+B(1,n)*
cos(sqrt(R(1)/D(1))*z*Beta(n)))^2; %definition of function Psi1
Psi(2)=(A(2,n)*sin(sqrt(R(2)/D(2))*z*Beta(n))+B(2,n)*
cos(sqrt(R(2)/D(2))*z*Beta(n)))^2; %definition of function Psi2
Normint(n)=R(1)*double(int(Psi(1),0,a))+R(2)*
double(int(Psi(2),a,b)); %integration
end
beta_end=1
  for n=1:size(Beta,2)
      suma=0;
   for k=1:size(coef,2)-1
       i=layer(coef(k,1),a,b);
       Psi(1,n)=(A(1,n)*sin(sqrt(R(1)/D(1))*z*
       Beta(n))+B(1,n)*cos(sqrt(R(1)/D(1))*z*Beta(n)));
       %definition of function Psi1
       Psi(2,n)=(A(2,n)*sin(sqrt(R(2)/D(2))*z*
       Beta(n))+B(2,n)*cos(sqrt(R(2)/D(2))*z*Beta(n)));
       %definition of function Psi2
       suma=suma+R(i)*double(int(coef(k,2)*Psi(i,n),
                            coef(k+1,1),coef(k,1)));
   end
   Initint(n)=suma;
  end
 for t=1:hours
      suma=0;
     for n=1:size(Beta,2)
         k3=sqrt(R(2)/D(2))*Beta(n);
         dPsi2(n)=k3*(A(2,n)*cos(k3*b)-(B(2,n)*sin(k3*b)));
         suma=suma+(exp(-time(t)*(Beta(n))^2)*Initint(n)*
                  dPsi2(n)/Normint(n));
     end
```

```
     Surfaceflux(t)=-D(2)*suma;
 end
 fluxcalc=1
 Surfaceflux=Surfaceflux*Area/Mtex;  %Flux Normalized mass
%=============================================================
function Rooti=bisection(a,b,x)
format long
eps_abs = 1e-5;%1e-5;
eps_step = 1e-9;%1e-9;
%a = 0.0;
%b = 2.0;
while (b - a >= eps_step || ( abs( fbeta(a,x) ) >=
             eps_abs && abs( fbeta(b,x) )  >= eps_abs ) )
    c = (a + b)/2;
    if ( fbeta(c,x) == 0 )
       break;
    elseif ( fbeta(a,x)*fbeta(c,x) < 0 )
       b = c;
    else
       a = c;
    end
end
Rooti=c;
%-------------------------------------------------------
function result=fbeta(x,b)
  %  x are the coefficients
    %  b the value to evaluate the function at.
result=x(1)*b*sin(x(2)*b)+x(3)*b*sin(x(4)*b)+x(5)*
                           cos(x(6)*b)+x(7)*cos(x(8)*b);
%-------------------------------------------------------
function result=layer(z,a,b)
%  x are the coefficients
    %  bet the value to evaluate the function at.
    if (a<z)&(z<=b)
        result=2;
    else
        result=1;
    end
%-------------------------------------------------------
```

Appendix I

Matlab Source Code: Two Layer Model (2LM)

Matlab version: 7.0.3.365 (R14) with symbolic, and cftool libraries

```
clear all
close all
%Input data
%=====================================================
w1=[1.57e-06,214493,0.10;];     %case 1 use [D1 R1] or case 2 use
%[D1 R1 p]
                                %where D1= Diffusion coefficient paint
                                %layer, R1= retardation factor
                                %p is percentage decrease of D1
w2=[4.3E-3 1];                  %[m^2/h diffusion coeff, ret factor
L=[139e-6 1.5E-2];              %[m] length of Layers one and two
Area=[0.0064];                  %[m]  area of painted material
f=[0.0067];                     %[-]  fraction of compound painted
Case=[2];                       %[-]  0 for normal use 1 for case2
ka=[0.21];                      %[m/h]VOC mass transfer coefficient
kw=[0.72];                      %[m/h]water mass transfer coeff
Nodes=[10 10];                  %[-]  number of nodes layers one and two
Vchamber=[0.00333];             %[m^3]Chamber volume
ACH=[1.5];                      %[1/h] Air exchange rate of chamber
Ncalc=[1];                      %[-]Flag : 1 to calculate nodes 0 for
                                %normal execution
Deltat=1;                       %Deltat: timestep for simulation [h]
load data.dat                   %[h] [mg/m^3] Text file that includes
%the chamber concentration obtained in experiments.  This concentration
```

```
%values are used to calculate the Emission from the
%paint into the air.  These emissions can be compared to the results of
%the Two layer model (2LM). Column 1 contains the time [h], and Column 2
%contains VOC concentration in the air [mg/m^3].
%=====================================================
Q=ACH*Vchamber;                 %[m^3/h]
t=data(:,1);            %Saving the time scale from experimental dataset
t1=round(data(:,1));    % Rounding the time scale
%=============================================
%Calculation of number of nodes for simulation
%=============================================
[N Out]=fnodecalc(w1,w2,L,Area,f,Case,ka,kw,Nodes,data,Ncalc,Deltat);
%=====================================================
%Solution of the system of equations for a mesh of NxN
%_____________________________________________________
Ncalc=0;    %Flag changed for nomal execution
[Masspaint Massgyp Massp Massm Mpaint MM]=...
                  f2LM(w1,w2,L,Area,f,Case,ka,kw,[N N],data,Ncalc,Deltat);
%outputs:
%Masspaint: Array of mass of compound in paint for all times    [mg]
       %Massgyp: Array of mass of compound in material for all times [mg]
       %Massp:  mass in the paint at final simulation time    [mg]
       %Massm:  mass in the material at final simulation time [mg]
       %Mpaint: mass of paint applied [g]
%Mpaint is the mass of paint applied in [g]
%Emission calculation (2LM)
Mtex=Mpaint*f*1000;     %Mass of Texanol applied in  [mg]
%(f is Texanol mass fraction)
Flux=(diff(Mtex-MM)*1000/Mtex/Deltat)';
cc=data(:,2);
TFF=linspace(Deltat,max(t1),max(t1)/Deltat)'; %timescale of simulation
                                              %to plot dM/dt
TFF(1)=[];    %deletes the first time step, flux starts at 2Deltat
TFlux=linspace(1, max(t1),max(t1))'; %timescale of simulation.
intpC=interp1(t,cc',TFlux,'cubic');%interpolated Experimental Conc.
told= circshift(TFlux,1);told(1)=0;
cold= circshift(intpC,1);cold(1)=0;
Ei=(Vchamber*(intpC-cold)./(TFlux-told)+Q*(intpC+cold)/2)/(Mpaint*f);
Eexp=interp1(TFlux,Ei,t);
%==================================
nt=round(t);    %To plot only exactly the same number of plots as
```

```
                %experimental data available
for i=1:length(nt)-1
Emodel(i)=Flux(nt(i)/Deltat);
end
Emodel(i+1)=Flux(length(Flux));
Emodel=Emodel';
%___________________________________
figure
semilogx(t,Eexp,'s',TFF,Flux,'.')
grid on
  title('Comparison of 2LM with Experimental data')
  xlabel('Hours')
  ylabel('Flux [mg/(h*gTex)')
  legend('Emission (Experiment)','Emission (2LM model)')
eM=(Emodel-Eexp).*(Emodel-Eexp);
RMS_errorM=(sqrt((sum(eM)/length(Eexp))))*100; %Root mean square error
MSE=sum(eM)/length(Eexp)*100;  %mean Square error
R_2=1-sum((Eexp-Emodel).*(Eexp-Emodel))/sum((Eexp-mean(Eexp)).*  ...
    (Eexp-mean(Eexp))); %Coeff of Det R^2
min=RMS_errorM;
N;
Simulation_Terminated=1
%=====================================================================
function [N Out]
=fnodecalc(w1,w2,L,Area,f,Mode,ka,kw,Nodes,data,Ncalc,Deltat)
Massp=1;Massm=1; errmp=10;errmn=10;
r=0;
while (errmp>.1) | (errmn>.1)
 r=r+1;
 Masspold=Massp;    %saving the old value of mass to calc. error in
                    %approximation
 Massmold=Massm;    %for both layers
 %Nodes=Nodes+10;    %increment of 10 on the number of nodes
 Nodes(1)=Nodes(1)+10;
 %f2LM is the main subroutine that solves the system of equations for
 %the two layer model. Outputs selected are the sum of the mass for
 [Masspaint Massgyp Massp Massm Mpaint]
 =f2LM(w1,w2,L,Area,f,Mode,ka,kw,Nodes,data,Ncalc,Deltat);
 Massp=Masspaint(length(Masspaint));
 Massm=Massgyp(length(Massgyp));
 Out(r,1)=Nodes(1); %Output of number of nodes for paint layer;
```

```
 Out(r,2)=Nodes(2); %Output of number of nodes for material layer
 Out(r,3)=Massp;    %Output of total mass in paint layer;
 Out(r,4)=Massm;    %Output of total mass in material layer
 errmp=abs(Masspold-Massp)/Masspold*100;
 errmn=abs(Massmold-Massm)/Massmold*100;
end
 N=Out(length(Out));
 %=====================================================================
function [Mp,Mm, Massp, Massm, Mpaint, MM] =
f2LM(w1,w2,L,Area,f,Case,ka,kw,N,data,Ncalc,Deltat)
D1=w1(1);   %1.8492e-10;%*8;%3.849e-13;%0.73e-15*3600/1.8;%2.047e-11;
             %diffusion coeff   m  paint layer m^2/h
D2=w2(1);
Ly1=L(1);%Ly1=313e-6;  % Size of paint layer [m]
Ly2=L(2);%Ly2=15e-3;   % Size of material layer [m]
R1=w1(2);%118.5;     %retardation factor 1
R2=w2(2);    %retardation factor 2
volume=Area*Ly1*100^3;
RH=0.7; %Relative Humidity
if (f==0.0154)
    Mpaint=1.254*volume;  %density =1.254 g/cc
    twater=1.254*Ly1*.16/(kw/1000*17e-3*(1-RH));
else
    Mpaint=1.329*volume;
    twater=(1.329*Ly1*0.43)/(kw/1000*17e-3*(1-RH));
end
if (f==0.0095)
    Mpaint=1.442*volume;
    twater=(1.254*Ly1*0.16)/(kw/1000*17e-3*(1-RH));
end
Mtex=f*Mpaint*1000;  %initial mass of texanol applied in mg.
InitialC_L1=1e9*f*Mpaint/volume; %Initial condition
%.C: concentration of Texanol in paint[mg/m^3]
InitialC_L2=0;%I.C: Concentration of Texanol material layer [mg/m^3]
Nodes_Ly1=N(1); %Number of Nodes for Paint layer
Nodes_Ly2=N(2); %Number of Nodes for Material layer
simultime= max(data(:,1));%maximum experimental data point
t=data(:,1);  %Saving the time scale from experimental dataset
t1=round(data(:,1));% Rounding the time scale
%Deltat=.01;      %Delta t for simulation [s]hours.
if (Ncalc==1 )
```

```
  simultime=data(1,1);
end
time=1:1:(simultime);
%=========================================================
Nodes=Nodes_Ly1+Nodes_Ly2; %Total number of Nodes
DeltaX1=Ly1/(Nodes_Ly1) ;   %Definition of DeltaX1 [m]
DeltaX2=Ly2/(Nodes_Ly2) ;   %Definition of DeltaX2 [m]
%Redefinition of some variables
b=Ly1+Ly2;%distance from bottom
a=Ly2; % b-a is size of paint layer
Npaint=Nodes_Ly1;
Nmat=Nodes_Ly2;
%Calculation of Water evaporation time
%=========================================================
%kw=0.72; %water mass transfer coefficient [m/h]
%=========================================================
%-------------------------------------------------------------------
%Coefficients Independent Vector initialization
%-------------------------------------------------------------------
p=.5;   %leave as 0.5 for uniform concentration in the paint layer
Na=Nodes_Ly1*.5;
Nb=Nodes_Ly1*.5;
for j=1:Na % Set initial condition for layer 1
    C(j,2)=InitialC_L1*Nodes_Ly1*p/Na;%/Nodes_Ly1;
end
for j=Na+1:Nodes_Ly1  % Set initial condition for layer 1
    C(j,2)=InitialC_L1*Nodes_Ly1*(1-p)/Nb;%/Nodes_Ly1;
end
for j=Nodes_Ly1+1:Nodes  %Set initial condition for layer 2
    C(j,2)=InitialC_L2;%/Nodes_Ly2;
    dv(j)=Area*DeltaX2;
end
% Main loop to solve the system of eqns for t=0 until simultime
initial_Concentration=C(:,2);
count=1;  %counter to setup for time display and saving of results
if Case==2
    diff1=D1;
    fdiff1=diff1*w1(3);
end
for i=1:(simultime/Deltat)
 if Case==2
```

```
    if (i*Deltat) <= twater
    D1=((fdiff1-diff1)/twater*(i*Deltat)+diff1);
    else
    D1=fdiff1;
    end
  end
 DeltaX1=Ly1/(Nodes_Ly1) ;   %Definition of DeltaX1 [m]
 DeltaV=Area*DeltaX1;
 %==========Coefficients=============================
alpha1=Deltat*(D1/R1)/(DeltaX1^2);
alpha2=Deltat*(D2/R2)/(DeltaX2^2);
kcs=2*D1/(2*D1+ka*DeltaX1);
m1=(D1/R1)*DeltaX2/((D1/R1)*DeltaX2+(D2/R2)*DeltaX1);
m2=(D2/R2)*DeltaX1/((D1/R1)*DeltaX2+(D2/R2)*DeltaX1);
Deltam=(DeltaX1+DeltaX2)/2;
Den1=.5*(Deltam+DeltaX2)*Deltam*DeltaX1;
Den2=.5*(Deltam+DeltaX2)*Deltam*DeltaX2;
%Node 1
  a(1)=0;
  b(1)=-3*alpha1-1+(2*alpha1*kcs);
  c(1)=alpha1;
 %Internal nodes layer 1
 for j=2:Nodes_Ly1-1
    a(j)=alpha1;
    b(j)=-1-(2*alpha1);
    c(j)=alpha1;
 end
%last node of layer 1
 j=j+1;
    a(j)=alpha1;
    b(j)=-1-3*alpha1+(2*alpha1*m1);
    c(j)=2*alpha1*m2;
%First node layer 2
j=j+1;
     a(j)=2*alpha2*m1;
     b(j)=-1-3*alpha2+2*alpha2*m2;
     c(j)=alpha2;
%internal layer 2
for j=(Nodes_Ly1+2):Nodes-1
    a(j)=alpha2;
    b(j)=-1-2*alpha2;
```

```
    c(j)=alpha2;
end
%Last node Layer 2
a(Nodes)=alpha2;
b(Nodes)=-1-alpha2;
c(Nodes)=0;
%==========Coefficients=================================
 %Free Vector Coefficients Update
 C(:,1)
 =-C(:,2);%/DeltaVp;%*(-1+3*alpha1-kcs*2*alpha1)+C(2,2)*(-alpha1);
 %======== Thomas algorithm
 d=C(:,1);
 n=Nodes;
 btemp=b;
 for k=2:n
    m=a(k)/btemp(k-1);
    btemp(k)=btemp(k)-m*c(k-1);
    d(k)=d(k)-m*d(k-1);
end
x(n)=d(n)/btemp(n);
for k=n-1:-1:1
    x(k)=(d(k)-c(k)*x(k+1))/btemp(k);
end
C(:,2)=x' ;
Cs=kcs*C(1,2);
C1=C(1,2);
FF(i)=-(D1/R1)*2.*(Cs-C1)/(DeltaX1*Mpaint*f)*Area;
MM(i)=Area*(DeltaX1)*sum(x(1:Nodes_Ly1))+Area*(DeltaX2)*
                     sum(x(Nodes_Ly1+1:Nodes));
if (mod(i,1/Deltat)==0) %Selection of timescale every hour
   Mp(i*Deltat)=Area*(DeltaX1)*sum(x(1:Nodes_Ly1));
   Mm(i*Deltat)=Area*(DeltaX2)*sum(x(Nodes_Ly1+1:Nodes));
end
end     %End of main loop
 Massp=Area*(DeltaX1)*sum(x(1:Nodes_Ly1));
 Massm=Area*(DeltaX2)*sum(x(Nodes_Ly1+1:Nodes));
twater;
 %============================================================
```

Bibliography

Axley, J. W. (1995). New mass transport elements and components for the nist iaq model. Technical report, U.S Department of Commerce.

Beverley, K. J., J. H. Clint, and P. D. I. Fletcher (1999). Evaporation rates of pure liquids measured using a gravimetric technique. *Physical Chemistry Chemical Physics 1*(1), 149–153.

Census-Bureau (2008). Current industrial report: MA325F- paints and allied products.

Chang, J. and Z. Guo (1992). Characterization of organic emissions from a wood finishing product wood stain. *Indoor Air 2*(3), 146–153.

Chang, J. C. S., L. E. Sparks, Z. Guo, and R. Fortmann (1998). Evaluation of sink effects on vocs from a latex paint. *Journal of the Air & Waste Management Association 48*(10), 953–958.

Choy, B. and D. Reible (2000). *Diffusion models of environmental transport*. Boca Raton, Florida: CRC Press LLC.

Corsi, R. L., A. Iwasinska, C. Lin, and C. B. (2005). The interaction of volatile organic compounds with gypsum board and plywood. (pp. 1-31). *Prepared for: American Solvents Council of the American Chemistry Council 3*, Austin, TX.

Crank, J. and G. Park (1951). Diffusion in high polymers: some anomalies and their significance. *Trans.Faraday Soc 47*, 1072.

Croll, S. G. (1986). Drying of latex paints. *Journal of Coatings Technology 58*(734), 41–49.

Currie, J. (1970). Movement of gases in soil respiration. *In Sorption and transport processes in soils. SCI Monograph 37*, 152–171.

Davison, G. and D. Skuse (1999). *Advances in additives for water-based coatings*. United Kingdom: The Royal Society of Chemistry.

Decopaint (2000). Study on the potential for reducing emissions of volatile organic compounds (voc). Technical report, University of Amsterdam, Enterprise Ireland, Institute for Environmental management (WIMM).

Dewhurst, J. E., A. S. Drayton-Elder, X. Gao, T. M. Santosusso, C.-f. Tien, and T. L. Wickmann (2001). Property development during film formation of two component waterborne polyurethane using dielectric spectroscopy. In T. P. Urban and M. w. (Eds.), *ACS symposium series 790*, pp. 124–140. Americal Chemical Society.

Eastman (2008). Eastman chemical company, material safety data sheet Texanol® ester alcohol. MSDSANSI/ANSI/EN/150000000148/Version 7.1. Revised on 07/29/2008. Available at: `http://www.Eastman.com`.

Eckersley, S. and A. Rudin (1994). The film formation of acrylic latexes: A comprehensive model of film coalescence. *Journal of applied polymer science 53*, 1139–1147.

Goldschmidt, A. and H.-J. Streitberger (2003). *BASF Handbook on Basics of Coating Technology*. Vincentz Network.

Guo, Z. S., L. E. Sparks, B. A. Tichenor, and J. C. S. Chang (1998). Predicting the emissions of individual vocs from petroleum-based indoor coatings. *Atmospheric Environment 32*(2), 231–237.

Haghighat, F., H. Huang, and C. Lee (2005). Modeling approaches for indoor air voc emissions from dry building materials - a review. *ASHRAE Trans. 111*(part 1), 635–645.

Hanna, S. and P. Drivas (1993). odeling voc emissions and air concentrations from exxon valdez oil spill. *Journal of the Air & Waste Management Association 43*, 298–309.

Hansen, C. M. (1968). A mathematical description of film drying by solvent evaporation. *J. Oil. Col. Chem. Assoc. 51*, 27–43.

Hester, R. and D. Squire (1997). Rheology of waterborne coatings. *Journal of Coatings Technology 69*(864), 109–114.

Holl, Y., J. Keddie, P. McDonald, and W. Winnik (2001). Drying modes of polymer colloids. In T. P. Urban and M. W. (Eds.), *ACS Symposium series 790*, Film Formation in Coatings. Mechanisms, Properties and Morphology, Washington, USA, pp. 2–26. Americal Chemical Society.

Huang, H. Y. and F. Haghighat (2002). Modeling of volatile organic compounds emission from dry building materials. *Building and Environment 37*(11), 1127–1138.

ICSC:0629. Texanol®. PCS: International Programme on Chemical Safety. Available online at http://www.inchem.org/documents/icsc/icsc/eics0629.htm. Accessed on August 2009.

Kiil, S. (2006). Drying of latex films and coatings: Reconsidering the fundamental mechanisms. *Progress in Organic Coatings 57*(3), 236–250.

Kirsch, S., A. Pfau, T. Frechen, W. Schrof, P. Pfohler, and D. Francke (2001). Scrub resistance of highly pigmented paints: A study on abrasion mechanisms of different scrub techniques. *Progress in Organic Coatings 43*(1-3), 99–110.

Li, F., J. L. Niu, and L. Z. Zhang (2006). A physically-based model for prediction of vocs emissions from paint applied to an absorptive substrate. *Building and Environment 41*(10), 1317–1325.

Lin, C.-C. (2006). *Emissions of 2,2,4-trimethyl-1,3-pentanediol monoisobutyrate from latex paint.* Ph. D. thesis, University of Texas at Austin, Civil, Architectural, and Environmental Engineering.

Lin, C. C. and R. L. Corsi (2007). Texanol® ester alcohol emissions from latex paints: Temporal variations and multi-component recoveries. *Atmospheric Environment 41*(15), 3225–3234.

Marrion, A. (2004). *The chemistry and physics of coatings* (Second ed.). Cambridge, UK: The Royal Society of Chemistry.

Method-24. EPA reference method: Determination of volatile matter content, density, volume solids and weight solids of surface coatings. in CFR 40, Part 60, Appendix A.

Meylan, W. M. and P. H. Howard (2005). Estimating octanol-air partition coefficients with octanol-water partition coefficients and henry's law constants. *Chemosphere 61*, 640–644.

Morrison, G. C., Z. Ping, D. J. Wiseman, M. Ongwandee, H. Chang, J. Portman, and S. Regmi (2003). Rapid measurement of indoor mass-transfer coefficients. *Atmospheric Environment 37*(39-40), 5611 – 5619.

Sheetz, D. P. (1965). Formation of films by drying of latex. *Journal of Applied Polymer Science 9*(11), 3759–3773.

Silva, G. V., M. Vasconcelos, A. M. Santos, and E. O. Fernandes (2003). Comparison of the substrate effect on voc emissions from water based varnish and latex paint. *Environmental Science and Pollution Research 10*(4), 209–216.

Sparks, L. E., Z. Guo, J. C. Chang, and B. A. Tichenor (1999). Volatile organic compound emissions from latex paint - part 1. chamber experiments and source model development. *Indoor Air-International Journal of Indoor Air Quality and Climate 9*(1), 10–17.

SRC (2009). Interactive physprop database. Last accessed on October 10th 2009. `http://www.srcinc.com/what-we-do/databaseforms.aspx?id=386`.

Steward, P. A., J. Hearn, and M. C. Wilkinson (2000). An overview of polymer latex film formation and properties. *Advances in Colloid and Interface Science 86*(3), 195–267.

Swan, P. (2005). An introduction to coalescing aids and eastman film forming technologies. In *36th International conference on Coatings Technology.*, pp. 265–278. Sec, Czech Republic.

Tiarks, F., T. Frechen, S. Kirsch, J. Leuninger, M. Melan, A. Pfau, F. Richter, B. Schuler, and C. L. Zhao (2003). Formulation effects on the distribution of pigment particles in paints. *Progress in Organic Coatings 48*(2-4), 140–152.

Tichenor, B. A., Z. Guo, and L. E. Sparks (1993). Fundamental mass transfer model for indoor air emissions from surface coatings. *Indoor Air 3*(4), 263–268.

Vahdat, N. (1991). Estimation of diffusion coefficient for solute-polymer systems. *Journal of Applied Polymer Science 42*, 3165–3171.

Vanderhoff, J., H. Tarkowski, M. Jenkins, and E. Bradford (1966). Theoretical consideration of the interfacial forces involved in the coalescence of latex particles. *Journal of Macromolecular Chemistry 1*(2), 361–397.

Walker, F. H. (2001). Fundamentals of polymer chemistry: I. *Journal of Coatings Technology 73*(912), 75–79.

Weschler, C. J. and W. W. Nazaroff (2008). Semivolatile organic compounds in indoor environments. *Atmospheric Environment 42*(40), 9018 – 9040.

Xu, Y. and Y. Zhang (2003a). An improved mass transfer based model for analyzing voc emissions from building materials. *Atmospheric Environment 37*(18), 2497–2505.

Xu, Y. and Y. Zhang (2003b). An improved mass transfer based model for analyzing voc emissions from building materials. *Atmospheric Environment 37*(18), 2497–2505.

Yang, X., Q. Chen, J. Zeng, J. S. Zhang, and C. Y. Shaw (2001). A mass transfer model for simulating volatile organic compound emissions from 'wet' coating materials applied to absorptive substrates. *International Journal of Heat and Mass Transfer 44*(9), 1803–1815.

Yang, X., Q. Chen, J. S. Zhang, R. Magee, J. Zeng, and C. Y. Shaw (2001). Numerical simulation of voc emissions from dry materials. *Building and Environment 36*(10), 1099–1107.

Zhang, L. Z. and J. L. Niu (2003). Mass transfer of volatile organic compounds from painting material in a standard field and laboratory emission cell. *International Journal of Heat and Mass Transfer 46*(13), 2415–2423.

Vita

Leonardo A. Ramirez was born in Bucaramanga, Colombia. He received his Bachelors in Electrical Engineering from Universidad Javeriana in November 2000. In January 2002 he entered the State University of New York at Stony Brook and received a Masters of Science in Electrical Engineering in May 2003. During the following two years he worked for an emission testing company. In September of 2005 he started his doctoral studies at The University of Texas, where he continuously worked as a teaching assistant. He accepted a research position at the California Air Resources Board in November 2009.

Permanent Address: Leo.Ramirez@gmail.com

This dissertation was typeset with LaTeX 2_ε[1] by the author.

[1] LaTeX 2_ε is an extension of LaTeX. LaTeX is a collection of macros for TeX. TeX is a trademark of the American Mathematical Society. The macros used in formatting this dissertation were written by Dinesh Das, Department of Computer Sciences, The University of Texas at Austin, and extended by Bert Kay, James A. Bednar, and Ayman El-Khashab.